University of the
Witwatersrand, Johannesburg

Doctoral Thesis

Degradation Analysis of Metal Oxide Varistors under Harmonic Distortion Conditions

Author: Pitshou Ntambu Bokoro

Supervisor: Prof. I.R Jandrell

A thesis submitted in fulfilment of the requirements
for the degree Doctor of Philosophy

in Electrical Engineering

May 2016

Declaration of Authorship

I, Pitshou Bokoro, declare that this thesis titled, 'Degradation Analysis of Metal Oxide Varistors under Harmonic Distortion Conditions' and the work presented in it are my own. I confirm that:

- This thesis has never previously been submitted for a degree or any other qualification at this University or any other institution.
- Where I have consulted the published work of others, this is clearly attributed.
- Where I have quoted from the work of others, the source is always given. With the exception of such quotations, this thesis is entirely my own work.

Signed: Pitshou Bokoro

Date: May 2016

UNIVERSITY OF THE WITWATERSRAND, JOHANNESBURG

Abstract

Doctor of Philosophy

Degradation Analysis of Metal Oxide Varistors under Harmonic Distortion Conditions

by Pitshou Bokoro

Modern electrical networks provide an opportunity for inevitable interaction between metal oxide arresters and power system harmonics. Therefore, these arrester devices are continuously exposed to the combined effect of distorted system voltage and environmental thermal stresses. Recent studies supported by field experiments have shown significant rise in the leakage current through these surge arrester devices when exposed to ac voltage with harmonics. However, the major shortcoming in the current knowledge and applications of varistor arresters resides on the reliability and the electrical stability of these overvoltage protection units, when subjected to long-term and continuous distorted ac voltage and thermal stresses from the environment.

Commercially-sourced ZnO arresters of similar size and electrical properties are tested using standard ac accelerated degradation procedure or electro-thermal ageing test; the $V-I$ characteristic measurement and the high-frequency impulse tests. The times to degradation, the coefficient of non-linearity, the reference voltages, as well as the clamping voltage measured are used to analyse the reliability and the electrical stability of the metal oxide-based arrester samples. The resistive component of the leakage current is extracted from the measured total leakage current. The three-parameter Weibull probability model is invoked in order to analyse the degradation phenomenon.

The results obtained indicate that for respective increase of 4.4%, 3.1% and 5.7% in the 3^{rd}, the 5^{th} and the 7^{th} harmonic content, the resistive current is increased by 92.67%. The mean life of the arrester samples is reduced by 40.91%, and the probability of accelerated time to degradation is found to be 58.93%. The accelerated loss of stability is proven by 81.71% reduction in the coefficient of non-linearity and 43.75% drop in the reference voltage, which both indicate the shift of the $V-I$ characteristic curve towards the high conduction region.

Acknowledgements

The author would like to acknowledge the financial support from the High Voltage Engineering Research Group of the University of the Witwatersrand and the contribution of the Centre for Telecommunications of the University of Johannesburg.

Contents

List of Figures

List of Tables

Abbreviations

ATP	**A**lternative **T**ransient **P**rogram
AVR	**A**pplied **V**oltage **R**atio
CDF	**C**umulative **D**ensity **F**unction
CoO	**Co**balt **O**xide
Cr_2O_3	**C**hromium **D**ioxide
CSV	**C**omma **S**eparated
Er_2O_3	**E**rbium **O**xide
GDT	**G**as **D**ischarge **T**ube
IEEE	**I**nstitute of **E**lectrical and **E**lectronics **E**ngineers
FFT	**F**ast **F**ourier **T**ransform
MCOV	**M**aximum **C**ontinuous **O**perating **V**oltage
MOV	**M**etal **O**xide **V**aristor
MSCM	**M**odified **S**hifted **C**urrent **M**ethod
MTTF	**M**ean **T**ime **T**o **F**ailure
ML	**M**ean **L**ife
Nd_2O_3	**N**eodymium **O**xide
PDF	**P**robability **D**ensity **F**unction
PEA	**P**ulse **E**lectro **A**coustic
PrO	**P**raseodymium **O**xides
PWM	**P**ulse **W**idth **M**odulation
SPD	**S**urge **P**rotective **D**evices
THC	**T**hird **H**armonic **C**urrent
THRC	**T**hird **H**armonic **R**esistive **C**urrent
TSC	**T**hermally **S**timulated **C**urrent
VSI	**V**oltage **S**ource **I**nverters

$\mathbf{Y_2O_3}$	**Y**ttrium **O**xide
ZnO	**Z**inc **O**xide

Symbols

α	coefficient of non-linearity	-
β	shape parameter	-
δ_{xy}	life reduction factor	%
γ	location parameter	hrs
θ	scale parameter	hrs
$\eta(x_i, y_i)$	correlation function	-
$C(x_i, y_i)$	C - intercept function	-
E_{1mA}	breakdown field	V/cm^2
$F(i, n)$	percentage cumulative degradation	%
$F(t)$	cumulative density function	-
$f(t, \beta, \theta, \gamma)$	probability density failure	-
$h(t)$	degradation-rate function	-
I_L	total leakage current	mA
I_R	resistive component of leakage current	μA
$i(t)$	instantaneous current	mA
$m(x_i, y_i)$	slope function	-
$Pr\,[t_x \geq t_y]$	probability of reduced lifetime	-
t_i	extrapolated degradation time	hrs
t_m	measured degradation time	seconds
t_p	time at which p% of varistor will be degraded	hrs
W_R	resistive power losses	W
$\chi^2_{0.01}$	chi-square distribution	-
z	likelihood test statistic	-

To the one above all without whom nothing is possible.

To my wife Arlette and twin boys Emmanuel and Nathanael for their continued love and support.

To Prof. Jandrell for his visionary leadership, words of wisdom and unwavering support.

To Dr. Hove for his participation in this project.

To Dr. Paul for advices and encouragements.

To all that may have assisted in any way possible...

Chapter 1

Introduction

1.1 Background Theory

Modern electrical or power systems increasingly experience harmonic-distortion as a result of continuous growth in the use of non-linear loads [1, 2]. Power system harmonics have since been reported to be one of the fastest rising power quality disturbances encountered in recent years [3, 4]. On the other end, overvoltage protection in electrical systems nowadays consists of essential practice given the high cost of equipment involved, as well as for the purpose of ensuring service reliability.

Over the last three decades, metal oxide varistors (MOVs) have proven to be quite a popular and efficient protection option available against lightning or switching surges. The effectiveness of varistor arresters could mainly be attributed to the following qualities: non-linear current-voltage ($V - I$) characteristic; high energy absorption capabilities; and relatively fast surge clamping mechanism [5, 6].

However, the long-term stability of MOVs, which is critical to the performance of these surge protective devices (SPD), remains somewhat dependent on the environmental (electrical or physical) conditions in which these devices may be subjected to operate under. The loss of stability often referred to as degradation or ageing is reported to be one of the most common causes of MOV failure [7, 8].

Electrical Degradation results from long-term operation of varistor devices under ac or dc voltage[9, 10], as well as from high magnitude of surge currents discharged through these protection units [11, 12]. The degradation phenomenon is manifested in terms of measurable changes in electrical (decrease in the coefficient of non-linearity, decrease in the reference voltage, increase in the degradation rate, $V - I$ shift, increased clamping voltage...) or physical properties (reduced double schottky barrier...) of varistor arresters [13, 14].

The prevalence of harmonic-producing loads or power electronics equipment in modern electrical circuits has paved the way to the inevitable operation of MOV-based arresters in ac circuits and systems with distorted voltage. Therefore, the performance reliability and the stability of MOVs operating under the above described condition is worthy of investigation.

1.2 Problem Statement

Recent studies conducted in this field suggested that harmonic distortion in the applied voltage to MOV-based arresters cause the third harmonic current (THC) component of the leakage current to increase, and thus introducing errors in the THC-based condition assessment of these devices. Although the influence of voltage harmonics on the accelerated loss of stability or degradation of MOV-based arresters is intuitively not expected, field experience suggest that similar MOV units will unexpectedly fail at different times and for several well documented causes. The one cause of accelerated failure that has not been considered or explored in this field is the long-term effect of voltage and current harmonics on performance reliability and electrical stability, and hence the useful life of MOV-based surge arrester units. Since the continuous operation of MOV units under fundamental ac voltage and temperature results in the decrease of the Schottky barrier interface or the intergranular regions. It is therefore important to establish whether or not harmonic voltage components embedded on the applied voltage, and temperature will on the long run significantly increase the pace or reduce the time at which the Schottky barrier is overcome, and consequently accelerating the electrical degradation process. Thus the following fundamental research question: Will voltage and/or current harmonics accelerate the degradation of MOVs under long-term distorted ac supply?

1.3 Scope of the Study

This study firstly entails the physical implementation of accelerated degradation test of low voltage ZnO-based surge arresters, at elevated voltage and temperature with and without an injection of harmonic voltage components from an external source of harmonics. Secondly, the scope of this study extends to the statistical analysis and comparison of the following parameters: the mean time to degradation (or mean life) based on the reliability function and the probability of reduced time to degradation or failure between two Weibull probability distributions; the frequency or rate of degradation based on the failure rate functions; the electrical stability of these ZnO overvoltage components based on the non-linear coefficient, the reference voltage and the shift in the $V - I$ characteristic curve; the high-frequency protection voltage based on the clamping voltage; the resistive component of the total leakage current before and after injection of harmonics. Therefore, this study is aimed at attaining the following broad and specific objectives:

1.3.1 Broad Objective

The broad objective of this research study is to analyse the probability of accelerated degradation of MOV-based surge arresters under long-term distorted ac voltage supply conditions.

1.3.2 Specific Objectives

The specific objectives of this study consist of the following:

1. To evaluate the non-linearity coefficient of MOV samples subjected to accelerated with and without harmonic-distortion.
2. To analyse the degradation rate of MOV samples subjected to accelerated ac degradation with and without harmonic-distortion.
3. To examine the behaviour of the clamping voltage of MOV samples subjected to accelerated degradation with and without harmonic-distortion.

1.4 Significance of Accelerated Degradation under Harmonic-Distortion

Over the last three decades, MOV-based surge arresters have been effectively used to mitigate or reduce the risk of insulation failure in power systems, as a result of high amplitude induced voltage and currents that may originate from switching or lightning surges. Therefore, production stalling and subsequent economical and financial implications that may arise as a result of insulation breakdown in power systems depend somehow on the health condition and performance of MOV-based surge arresters under both steady-state and transient operation conditions.

Just as MOVs are important components in electrical networks, power electronics devices consist of efficient and cost-effective means of providing control and switching of electrical loads in power systems. However, the drawback in this switching technique remains the flow of non-linear currents which interact with the system impedance, and thus causing the system voltage to be distorted. Under inevitable harmonic-distortion conditions, risk prevention of insulation failure in power systems requires in-depth knowledge and understanding of the reliability of MOV-based surge arresters operating under distorted system voltage.

Accelerated electrical degradation of MOV arresters subjected to distorted ac system voltage at standard operating temperature shall therefore imply the probability of reduced life expectancy or time to degradation, and significant loss of electrical stability of these overvoltage devices. The probability of reduced life expectancy measures the reliability of these devices and the shift of the $V - I$ characteristic curve indicates the loss of electrical stability.

The practically implemented electrical degradation of MOV-based surge arresters under the influence of temperature and voltage, such as undertaken in this study, provides the best possible and available representation technique of arrester's useful life deterioration under continuous ac or dc conduction. Therefore, accelerated degradation can be logically evaluated in terms of statistical comparison of the average or mean time to electrical degradation and the average rise in the resistive current component of two populations of ZnO arrester devices. Fundamentally, the mean time to electrical degradation and the increase in the resistive leakage current for ZnO arresters imply the following physical significances:

1.4.1 The Time to decrease the Schottky Barrier Height

The mean time to electrical degradation is associated to the time corresponding to increased number of charge carriers in the varistor microstructure, sufficient to overcome the intergranular regions and thus leading to the decrease in the schottky barrier height.

1.4.2 The Biasing Effect of Voltage Harmonics

The rise in the resistive current component through ZnO devices when harmonics are present in the voltage stress has been well documented in the literature. The relatively shorter life expectancy of ZnO arresters when subjected to distorted ac voltage stress, such as observed in this study, has paved the way for the fundamental understanding of the effect of voltage harmonics on the varistor microstructure. Therefore, the time to degradation, the electrical stability and other electrical measurements observed in this study consist of reasonable manifestation of the physical changes that may have taken place in the microstructure of ZnO arrester populations. The reduction in the time to the occurrence of the described physical changes in the microstructure of ZnO arresters poses a significant threat to the reliability of power systems, as the shorter the time to degradation, the quicker the electrical degradation process.

1.5 Overview of the Study

Chapter 1 introduces the relevance of MOV-based overvoltage protection and harmonic-distortion in modern power systems. The potential risk of accelerated degradation associated with varistor-based SPDs subjected to long-term and continuous operation under harmonic-distortion conditions is highlighted. The extent at which, the underlined problem in this study is approached, is discussed in this chapter. Before concluding on this chapter, the pertinence and the significance as well as the layout of this report are discussed.

The second chapter of this study commences with a survey of major causes, aggravating factors and typical symptoms of electrical degradation or ageing associated with MOV arresters. A review of problematic interaction between varistor SPDs and power system harmonics is also undertaken, followed by the physics or mechanisms of electrical degradation. **Chapter 2** concludes on the following:

- The inaccuracies and lack of practical implementation for many of the techniques suggested in a bid to extract the resistive component of the total leakage current;
- The application of the accelerated degradation test, at elevated voltage and temperature, as a viable technique to simulate electrical degradation of MOV-based surge arresters;
- The appropriate application of the Weibull probability distribution in the analysis of electrical degradation or failure;
- The gap in the knowledge of the effect of voltage harmonics on the acceleration of electrical degradation of varistor arresters.

Chapter 3 presents a description of the varistor samples used, the experimental works undertaken and the measurement conditions of the electrical parameters required in this study. The performance conditions of the $V-I$ characteristic test and the high-frequency test, before and after degradation are indicated. The set-up of the accelerated degradation procedure as well as the systematic measurement of the degradation or failure times and the leakage current are also discussed. This chapter paves the way to the analysis of electrical degradation based on the measurements obtained.

Chapter 4 introduces the application of the Weibull probability distribution on the analysis of the degradation times. The assessment and determination of the average values of the $V - I$ characteristic, the coefficient of non-linearity, the reference voltages and the clamping voltages. This chapter concludes on the following:

- The comparative behaviour of the PDF and CDF patterns of the degraded ZnO arrester populations;
- The probability of accelerated time to degradation for arrester populations subjected to harmonic distortion;
- The accelerated rate or frequency of degradation for arrester populations subjected to harmonic distortion;
- The accelerated loss of stability for arrester populations subjected to harmonic distortion.
- The Influence of degradation under distorted voltage on the clamping voltage behaviour.

Chapter 5 investigates the impact of voltage harmonic content in the applied stress on the resistive component of the total leakage current, and consequently on electrical degradation of MOV-based surge arresters. This chapter concludes on the contribution of voltage harmonics to the net biasing voltage effect, which results on the resistive current being increased, hence the electrical degradation of MOV arresters. The fundamental and the third harmonic resistive current (THRC) are proven to be the most dominant current components in the resistive current. The fundamental concept of accelerated electrical degradation with respect to the microstructure behaviour of ZnO devices is also discussed.

Chapter 6 concludes the study on the basis of the results obtained and discussed in chapters 4 and 5. The recommendations pertaining to further research opportunities in this field of study are also provided.

1.6 Conclusion

The efficient and reliable coexistence between power electronics devices and MOV-based surge arresters in modern power systems, justifies the basis of further knowledge on probable accelerated electrical degradation, of these overvoltage protective units, under harmonic-distortion conditions. Therefore, the performance reliability and the electrical stability of MOV-based arresters subjected to continuous operation under harmonic-distortion and environmental temperature are important contribution to the current knowledge and applications of ZnO arrester devices.

Chapter 2

Literature Review

2.1 Introduction

In this section, a survey of studies pertaining to the fundamental causes and multiple symptoms or characteristics of electrical degradation or ageing, as applicable to MOV-based surge arresters, is undertaken. The state of knowledge associated to the interaction between varistor arresters and power system harmonics is equally discussed. A brief description of statistical and probabilistic approaches to electrical degradation analysis is also highlighted, followed by a review of the major theories and principles that support the mechanisms or physics of electrical degradation in MOV arresters.

2.2 Electrical Degradation of Varistor Arresters: Causes and Symptoms

Electrical degradation of varistor arresters is generally caused by the discharge of high-amplitude surge or impulse currents and by long-term exposure to continuous ac or dc current conduction [9]–[12]. Environmental conditions such as heat, humidity or radiation, are reported to be contributing factors or favouring agents to the degradation phenomenon [10, 13, 14]. Therefore, electrical degradation or ageing fundamentally requires a trigger action, which is generally known as the primary cause, to which accelerating or aggravating factors is usually associated. The electrical characteristics or symptoms associated to electrical degradation in MOVs are inevitably studied in conjunction with the standard developed techniques of artificially inducing or causing this form of degradation phenomenon.

2.2.1 High Amplitude Surge Currents

High amplitude surge currents generally result from switching and lightning transients. The following studies made use of standard lightning impulse wave generators to induce degradation on MOV arresters:

1. Sargent, Dunlop and Darveniza [11] used standard 8/20μs impulse, at rated surge current of zinc oxide varistor samples involved, to study the effects of both single and multiple surge currents on the degradation of metal oxide arresters. The following observations are made:

    - Both single and multiple pulses are capable of causing changes in electrical, physical and the microstructure of the MOVs.
    - Severe degradation is encountered in case of multiple pulse currents being discharged through the MOV arresters.

    This work seems to be focussed on the amplitude and number of pulse currents as the major factor responsible for physical and electrical changes observed, as well as for the development of additional phases and the formation of localised hot spots in the microstructure of the MOV samples. However, for similar number and magnitude of pulse currents applied at a constant time between successive activation, different degrees of MOV defects or rather degradation observed could be attributed to several other factors clearly not considered in this study.

2. De Salles, Martinez and de Queiroz [10] applied a set of standard 8/20μs impulse currents to similar MOV arresters at the following environmental or surface temperature conditions: room temperature or 20^o C; 60^o C and 80^o C. The amplitude of the surge currents used are of the following values: 10 kA, 15 kA, 20 kA and 30 kA. The electrical ageing of the arrester devices was monitored on the basis of measured changes in the watt losses, which best fitted the logistic probability distribution. The Boxplot Minitab statistical software tool was invoked to evaluate the confidence intervals and the mean values of the measured parameter under different surface temperature conditions considered in this study. The following observations are made:

    - Similar watt loss pattern is noted at amplitudes close (10 kA and 15 kA) to the rated surge current discharge of the samples at the temperature of 80^o C and for the same number of impulses.
    - Increasingly higher watt loss pattern is observed at much higher amplitudes (20 kA and 30 kA) to the rated current discharge of the samples at the temperature of 80^o C and for the same number of impulses.

- For each pulse amplitude discharged through the samples, the highest watt loss for 10 kA and 30 kA amplitude is measured at the highest surface temperature.

These findings seem to confirm that the amplitude level of the surge current, discharged through MOV devices, is the main trigger of electrical degradation. However, the major benefit of this work resides on the fact that it tends to complete the work presented in [11], in the sense that the contributing effect of environmental temperature condition, in which arrester devices are subjected to, is demonstrated to be an aggravating factor to the ageing process.

3. Vasic et al [15] subjected two different types of varistors, amongst other available overvoltage protection units, to a thousand $8/20\mu$s impulses. Varistor samples used in this study consisted of: 10 mm and 14 mm diameter size, with rated ac value of 230 V for each. The rated surge current withstand capabilities were 2.5 kA and 4.5 kA, respectively. The degradation process is measured on the basis of the change in the voltage-current ($V - I$) characteristic curve, the voltage-resistance ($V - R$) characteristic curve and the varistor breakdown or reference voltage (V_{1mA}). These measurements are obtained after every hundred pulse currents. A Statistical analysis was conducted on the obtained data and the following conclusions are drawn up:

   - An increase in varistor activation results in an increase of the varistor resistance and the breakdown voltage value.
   - The $V-I$ characteristic of varistor seems to drift towards the high conduction region as the number of activation increases.
   - The rate at which the $V-I$ characteristic drifts towards the high conduction region appears to be quite low, and this could be translated in a small change of the coefficient of non-linearity (α).

   The major contribution of this study is founded on the fact that previous pulse current discharges do not necessarily cause drastic change of the non-linearity coefficient of MOV devices. Furthermore, high varistor resistance and breakdown voltage observed could be attributed to polarisation phenomenon, which in many cases is described as a manifestation stage of degradation [16, 17]. However, the pulse currents used in this study are rated amplitude transient currents, which sum up this work as an attempt to investigate the effects of several cumulative pulse currents of rated amplitude discharged on MOV arresters. The contributing effect of temperature is completely overlooked on the basis that it is likely to be pronounced when degradation results from dc or ac continuous conduction.

4. Nahm [18] investigated the ageing characteristics of Er_2O_3 doped $PrO_{1.83} - ZnO$ varistors with the aid of a multi-surge current generator, capable of producing standard 8/20 μs impulse currents in various amplitudes. The content of the Er_2O_3 additives used in the study was 0.5 mol% and 2.0 mol%. The time between three successive impulses of similar magnitude was two minutes, whereas ten minutes transition time are conceided each time a higher magnitude triggering is conducted. At respective content of Er_2O_3, the following quantities are measured before and after surge degradation at various amplitude levels: the current-density curve $(E - J)$; the breakdown field (E_{1mA/cm^2}); the non-linear coefficient at different $(V - I)$ curve regions; the clamping voltage (V_c); and the clamp voltage ratio $(k_c = V_c/V_{1mA})$. The following observations are made:

   - $PrO_{1.83} - ZnO$ varistor samples doped with 0.5 mol% of Er_2O_3 exhibited small variation of the E–J characteristics in the breakdown region, whereas those doped with 2.0 mol% of Er_2O_3 exhibited large variation in the breakdown region.
   - $PrO_{1.83} - ZnO$ varistors with 0.5 mol% content of Er_2O_3 show small variation in the $\%\Delta E_{1mA/cm^2}$ and $\%\Delta\alpha$ as opposed to those with 2.0 mol% content.
   - The clamping voltage of $PrO_{1.83} - ZnO$ varistors doped with 0.5 mol% content of Er_2O_3 increased in the range of 272–324 V/mm for surge currents of 5–50 A, and 544–640 V/mm for surge currents of 0.4–1.8 kA. For 2.0 mol% content of Er_2O_3, The clamping voltage increased in the range of 365–510 V/mm for surge currents of 5–50 A, and 670–930 V/mm for surge currents of 0.4-1.8 kA.
   - The clamp voltage ratio of $PrO_{1.83} - ZnO$ varistors doped with 0.5 mol% content of Er_2O_3 increased in the range of 1.65–1.97 for surge currents of 5–50 A, and 2.22–3.17 for surge currents of 0.4–1.8 kA. For 2.0 mol% content of Er_2O_3, the clamp voltage ratio increased in the range of 1.56–1.84 for surge currents of 5–50 A, and 1.92–3.13 for surge currents of 0.4–1.8 kA.

   For the purpose of Nahm's study, an impulse generator is used to induce degradation and to subsequently observe the clamping characteristics of the varistor devices. A dc wave generator was also used to monitor the stability characteristics of arresters involved. The findings obtained in this study showed that $PrO_{1.83} - ZnO$ varistors doped with 0.5 mol% content of Er_2O_3 prove to be more stable than those doped with 2.0 mol% content of Er_2O_3. The high clamping characteristic is associated with high content of Er_2O_3 in $PrO_{1.83} - ZnO$ varistors. Therefore, it clearly emerges out of this study that the stability and clamping characteristics of MOV arresters are important performance parameters of MOV-based arresters. Furthermore, excellent stability behaviour of MOVs may not necessarily be associated to good clamping characteristics.

5. Tsukamoto [19] investigated the degradation mechanism of MOV surge arresters as a result of 4/10 μs, 8/20 μs and 10/350 μs impulse waves. The change in the varistor voltage point (ΔV_{1mA}) recorded after impulse application was therefore measured against the impulse charge transfer. The impulse current distribution across the edge and centre parts of varistor samples was conducted using the spot electrode method. Therefore varistor arresters having a diameter between 32-74 mm and a height between 3-36 mm were used in this study. The following findings are obtained:

   - For a 10/350 μs single shot the change in the varistor voltage started to occur at the charge transfer of 0.2 C/cm^2 and rapidly changed to -10 % above 0.35 C/cm^2.
   - For a 4/10 μs and 8/20 μs, the change in the varistor voltage is recorded at much lower charge transfer of 0.03 C/cm^2 and reached -10 % above 0.1 C/cm^2.
   - The spot electrode method showed that for steep waveforms such as the 4/10 μs and 8/20 μs, the drop in varistor voltage is high on the edge. This implies higher impulse current distribution on the edge of MOV samples.
   - The change in varistor voltage in terms of the number of shots indicated that for a positive applied impulse, the varistor voltage is continuously decreased until saturation is reached (no change despite increase in number of shots). For a negative applied impulse, the varistor voltage continuously increases. These phenomena could be attributed to the reported increase of interstitial zinc ion concentration near grain boundary and the damage of the bismuth oxide in grain boundary which causes reduction of resistance.

   The most important contribution of this work rests on the high decrease of varistor voltage mostly across the edge as a result of higher steep impulse wave current distribution in this region of MOV arresters. This finding basically attempts to provide fundamental understanding of the degradation mechanism as a result of high-frequency and high amplitude surge currents.

2.2.2 Continuous ac or dc Current Conduction

Continuous ac or dc current conduction result from long-term exposure of MOV arresters to dc or/and power-frequency voltages. The following studies made use of dc or 50 Hz ac sine wave voltage generators to induce degradation on varistor arresters:

1. Eda, Iga and Matsuoka [9] used laboratory prepared ZnO samples of 14 mm diameter and 1.8 mm thickness to study the effect of dc and ac voltage bias, and that of temperature biasing on thermal runaway or degradation. The $V-I$ characteristics of the arresters is measured using a dc constant current supply ranging from 1μA to 1 mA. The capacitance and dielectric properties are measured at 1 V_{RMS} at frequency range of 500 Hz to 1 MHz using a capacitance bridge, and the bias voltage for capacitance dependence was assessed at 1 kHz in the range of 0 to 100 V/mm. The thermally stimulated current (TSC) is measured in quartz tube by changing the ambient temperature at a rate of 0.333^{o}K/s with no bias voltage. The following are observed:

    - Asymmetrical change in the $V-I$ characteristic of ZnO ceramics is caused by applied dc bias.
    - Symmetrical change in the $V-I$ characteristic of ZnO ceramics is caused by applied ac bias.
    - A decrease in the capacitance and an increase in the dielectric loss in the low-frequency region after dc and ac biasing.
    - A TSC is observed in ZnO ceramics after dc biasing.
    - Both asymmetrical and symmetrical changes in the $V-I$ characteristic of ZnO ceramics can be attributed to the deformation of the schottky barrier.

    The $V-I$ characteristic, the capacitance and the dielectric loss are used in this study as basic degradation symptoms of MOV devices subjected dc and ac continuous conduction. Therefore, the findings obtained suggest that dc or ac conduction can each effectively cause varistor arresters to reach degradation or end of life. However, the degradation symptoms or characteristics produced are mainly dependant on the nature and the time of biasing voltage applied to MOV arresters. The operating temperature appears to be an important factor in this process.

2. Zhou, Zhang and Gong [20] studied the degradation phenomena of low voltage ZnO varistors caused by dc biasing on the basis of the $V-I$ characteristic and the capacitance-voltage ($C-V$) measurement. The ZnO samples are therefore subjected to dc bias at the temperature of 140 ^{o}C for 120 hours of operation. The

magnitude of the dc bias was set at 0.75 V_{1mA}. The $V - I$ characteristic is used to analyse the stability of ZnO varistors against dc bias, and the $C - V$ relationship served to estimate the barrier height and the depletion width before and after dc degradation. The complex-capacitance plane analysis is also invoked to investigate the impact of dc degradation on deep bulk traps of low-voltage ZnO varistors. The following observations are made:

- The change in $V - I$ characteristic implies an increase in the leakage current and a decrease in the reference voltage after degradation.
- The leakage current increases with the biasing time, and this could be interpreted as stability measurement of ZnO devices against biasing, as suggested in [21]. The following relationship is therefore applied:

$$I_L = I_{L_0} + k \cdot t^{1/2} \tag{2.1}$$

  Where: I_L is the leakage current at biasing time t, I_{L_0} is the leakage current at $t = 0$, k is the coefficient of stability or the degradation rate expressed in μA/h.
- The decrease in the barrier height and the depletion width after degradation could be explained in terms of the defect structure model proposed in [22, 23].
- The properties of the deep bulk traps change after degradation, and the decrease in the relaxation time is due to the fact that trapped electrons are easily released from the deep bulk trap.

These findings confirm the observations made in [9], as far as dc biasing and the schottcky barrier are concerned. While the $V - I$ characteristic as well as the leakage current are proven to be important measuring parameters which reveal the stability of MOV arresters. The biasing time and the magnitude of the bias voltage, together with the operating temperature consist of major triggering and aggravating factors of dc degradation process, respectively.

3. Nahm [24] applied dc bias or stress to investigate the effect of Er_2O_3 additives on the microstructure, and consequently the electrical properties and the degradation behaviour of $ZnO - Pr_6O_{11} - CoO - Cr_2O_3 - Y_2O_3 - Er_2O_3$. The electric field-current density $(E - J)$ characteristics, the breakdown field E_{1mA/cm^2} and the leakage current density at 0.8 E_{1mA/cm^2} are systematically measured to achieve the objectives of this study. The non-linearity coefficient is also assessed within the following range of the current density: 1.0 mA/cm^2 - 10 mA/cm^2. The following relationship is applied:

$$\alpha = \frac{1}{logE_2 - logE_1} \tag{2.2}$$

Where: E_1 and E_2 are electric fields at leakage current density of 1.0 mA/cm^2 and 10 mA/cm^2, respectively. The dc stress applied consisted of four continuous conditions: $0.85E_{1mA}/115^o$C/24h; $0.90E_{1mA}/120^o$C/24h; $0.95E_{1mA}/125^o$C/24h and $0.95E_{1mA}/150^o$C/24h. The degradation rate was determined using equation 2.1. The following results are obtained:

- The addition of Er_2O_3 content shift the $E - J$ characteristic curve towards the lower field strength.
- The breakdown field increases with an addition of Er_2O_3 content to the varistor ceramic microstructure. This could be attributed to the decrease in the average grain size.
- The non-linearity coefficient increases with an increase of Er_2O_3 content.
- Excellent stability is observed at 1.0 mol % content of Er_2O_3.

These findings demonstrate the improved stability of varistor devices as a result of Er_2O_3 oxide additives doping. Therefore the higher the breakdown field and the coefficient of non-linearity, the lower the leakage current and the coefficient of stability or degradation rate. Furthermore, since the $(V - I)$ characteristic change in the slope is temperature dependant[25], the measure of the stability coefficient of a varistor device is always measured at specific operating temperature.

4. Wang, Tang and Yao [26] used ac degradation characteristics to test the effect of mol % content of Nd_2O_3 additives on the electrical properties of low-voltage Zinc Oxide varistor ceramics. Therefore varistor ceramics with 0; 0.03; 0.06; 0.09 and 0.12 mol % content of Nd_2O_3 are degraded with continuous ac stress of 1.0 V_{1mA} magnitude, at 125^oC for 24 hours. The $V - I$ characteristic, the non-linearity coefficient α, the varistor voltage V_{1mA} and the coefficient of stability k are thus evaluated. The $C - V$ characteristic is also used to determine the barrier height and the depletion width. The following findings are made:

   - The $V - I$ characteristic of varistor ceramics with Nd_2O_3 content show more linear response in the breakdown region.
   - The varistor voltage increases with an increase in Nd_2O_3 content. This can be attributed to the decrease in the average grain size.
   - The non-linearity coefficient increases with an increase of Nd_2O_3 content.
   - The leakage current decreases with an increase in Nd_2O_3 content.

- The coefficient of stability decreases with an increase in Nd_2O_3 content.

The major contribution of this study lies on the improved stability of MOV arresters when the content of Nd_2O_3 additives is increased. However, the shortcoming is that the effect of Nd_2O_3 additives on the clamping characteristics is not known.

5. He et al [27] studied the influence of Y_2O_3 on ac degradation or ageing characteristics of high voltage gradient ZnO varistors. These varistor devices are subjected to continuous ac stress of $0.85V_{1mA}$ at 135^{o}C for a duration of 168 hours. The Y_2O_3 doping content was as follows: 0.00 mol %; 0.50 mol %; 0.75 mol % and 1.00 mol %. The $E - J$ characteristic curve, the breakdown field and the non-linear coefficient, before and after ac stress, are measured for varistors with and without Y_2O_3 content. Similarly, the leakage current measured at $0.75E_{1mA}$ before and after the stress are used to assess the coefficient of stability. The $C - V$ characteristic curve and the double barrier schottcky parameters were also determined. The following findings were observed:

   - The most obvious increase in the breakdown field is observed in samples with 1.00 mol % content of Y_2O_3- doped varistor devices.
   - The leakage currents for all the samples at different content of Y_2O_3 increased after ac stress. However, the most significant increase is observed for 0.50 mol % of Y_2O_3.
   - The lowest coefficient of stability is found to be 0.081μA $/h$, which is higher than that of the samples with 0.00 mol %, and is associated to samples doped with 0.75 mol % of Y_2O_3 content.
   - The barrier height reduction after ac degradation is quite pronounced for samples doped with Y_2O_3 content or high voltage gradient samples, with the largest variation being recorded at 0.50 mol% content of Y_2O_3.

   These findings indicate that high voltage gradient varistor samples, produced by doping of traditional varistors with different mol % content of Y_2O_3 additives, are not stable given their relatively high degradation rates. Therefore, this study evaluated the benefit of producing high voltage gradient varistor arresters on the basis of operational stability under continuous 50 Hz ac voltage stress. However, the reasons behind the negative impact of the oxide additives, used in this work, are not clearly revealed in this study.

2.3 Power System Harmonics and Varistor Arresters

The increasing demand of high efficiency converters and other power electronic components, for improved control and switching of modern electrical and electronic systems or equipment, has paved the way for the continued presence of distorted voltage and currents in circuits involving these devices. The interaction between MOVs and power quality problems, such as harmonics, is becoming more and more pronounced in modern power systems [28]. Therefore, the use of MOV-based arresters for overvoltage protection of non-linear devices inevitably implies direct exposure to distorted voltages and currents. The current state of knowledge pertaining to the interaction between MOV arresters and power system harmonic disturbances, is centred on measurement errors associated to leakage current-based condition assessment of varistor devices operating in circuits with distorted voltage:

2.3.1 Leakage Current - based Condition Assessment

Leakage current measurements are the most commonly applied technique mostly used in the field [14, 29], to assess the health condition of arresters. However, when the supply voltage contains harmonic-distortion, this method suffers considerable shortcomings. The following studies describe the various aspects of this assessment methodology:

1. Hinrichsen [30] used a computer program to simulate the characteristics of both resistive and third harmonic components of the total leakage current, obtained under continuous operating voltage and temperature, in order to study the high risk of measurement errors and therefore misinterpretations of results, that could be associated to on-line monitoring of gapless arresters in ac transmission or distribution circuits. The following findings are made:

    - Electrical ageing or degradation of MOV arresters can be detected by measuring the resistive component or power losses. A phase-correct voltage signal is required for this purpose or some compensation circuit to do away with the capacitive current component.
    - The third harmonic component (THC) displays similar voltage dependence to the resistive component of the total leakage current. Despite its low amplitude, the THC can be used as an indirect measurement of the resistive current. This characteristic forms the basis of its prominent use in the indirect method of health assessment of MOV-based arresters.
    - The THC to resistive current ratio changes with temperature and the presence of third harmonic in the voltage causes the THC to increase.

- For a 3% third harmonic with phase angles between 0^o to 360^o superimposed in the applied voltage across a MOV arrester, the highest measurement error in the THC is found to be between 120^o and 270^o.
- Adequate stability verification procedures during development and running production should be encouraged over a high risk of measurement errors and costly on-line monitoring.

These findings highlight the technical challenges related to practical implementation of leakage current measurement based on-line monitoring of MOV arresters in ac transmission and distribution circuits. However, the long-term stability of varistor arresters, is such an important factor to the reliability of the protected system, and should be monitored either permanently on-line or off-line at regular time intervals. Stability verification during production, such as suggested in this work, does not mean that the MOV devices will not undergo degradation. Furthermore, environmental factors in which arresters may be operating could fundamentally be different from the conditions during production tests.

2. Yan, Wen and Yi [31] incorporated both compensation and harmonics analysis methods into a computer-based numerical harmonics approach. In this technique, an analogue-digital (A/D) card leakage current monitor, which basically consisted of a surge counter with a built-in current transformer, is implemented to measure the MOV leakage current. This measured current signal is then digitally processed to offset all capacitive harmonic components present in the leakage current. The resistive harmonic components thus extracted are used to determine the total resistive current of the arrester. Therefore, the leakage current, the peak resistive current and the power loss of MOV arresters were measured under the following range of applied voltage: 0.6 kV to 2.3 kV. The following findings were observed:

- The resistive component of the leakage current is very small (about 2%) of the leakage current, and can quickly rise with an increase of the applied voltage. This quantity can indeed provide the working condition of arresters.
- Higher order resistive currents tend to increase while the fundamental component remains low when MOV arresters are either electrically or/and thermally degraded.
- Numerical harmonics analysis method provide overall monitoring of MOV arresters since the energy absorbed and degradation are measured.

The observations made in this work confirmed the need for monitoring resistive current of MOV since the characteristics of this current component provide good indication of arresters' condition. However, the numerical harmonics analysis appears to be theoretically sound but quite difficult and expensive technique to physically implement on line. It requires sophisticated capacitive compensation circuits in order to eliminate capacitive current components, and some digital signal processing (DSP) methods capable of evaluating higher order resistive harmonic components.

3. Jaroszewski, Kostyla and Wieczorek [32] simulated varistor equivalent circuit in the Matlab software environment in order to study the effect of voltage harmonics content on the leakage current-based diagnosis technique. Therefore, for a number of simulation runs consisting of several magnitudes of the supply voltage and odd harmonic voltage components, the following findings were made:

    - The THC is found to be present in the current response of varistors irrespective of the applied voltage being higher or lower than the varistor maximum continuous operating voltage (MCOV).
    - The THC is visibly noticed in the varistor current spectrum when higher order harmonics are present in the applied voltage of lower magnitude than the varistor MCOV.
    - Significant increase of the THC is observed when the harmonics content in the supply voltage increase.
    - High current conduction through varistor devices result from operation under supply voltage of magnitude higher than the varistor MCOV.
    - Higher harmonics present in the supply voltage may cause measurement errors and therefore misdiagnosis of the actual condition of varistor arresters, since an increase of the THC cannot necessarily be associated to ageing of varistor blocks.

    The findings resulting from this work consist of an important foundation for condition monitoring and performance analysis of MOV arresters, operating in ac distorted transmission or distribution circuits. Harmonics in the system voltage are identified to be negatively influencing leakage-based condition assessment of varistor devices. However, this work did not attempt to quantify such an influence of harmonics on the monitoring of arresters.

4. Karawita and Raghuveer [33] used the generally constant phase shift between the capacitive and the resistive components of the total leakage current to investigate the effectiveness of the phase shift criteria-based diagnosis of MOV arresters. In this method, the phase shift (ϕ_{c_1,t_1}) between the fundamental component of the capacitive and that of the total leakage current is increased from zero until the peak value of the fundamental capacitive current ($\widehat{i}_{c_1}$) is reached. The $\widehat{i}_{c_1}$ is therefore subtracted from the peak value of the fundamental total leakage current ($\widehat{i}_{t_1}$)

to obtain the peak value of the remaining resistive current component ($\widehat{i}_r$). The phase shift between the generated $\widehat{i}_r$ and the $\widehat{i}_{c_1}$ is compared to that obtained using compensation techniques. The phase shift method and compensation techniques were therefore applied to the following samples: one unaged and two aged samples of 10 kV of MCOV; two new station arresters of 36.5 kV MCOV and one new polymeric distribution arrester of 15.3 kV of MCOV. The following findings were made:

- The magnitude of the resistive current generated in this method closely compares with that obtained using compensation technique, and therefore can be used to diagnose the condition of the arrester. This is mostly applicable to one unaged and two aged samples of 10 kV of MCOV, since the mean phase shift was constant.
- Step change in the phase shift, such as observed in the testing of the two new station arresters, renders the use of this technique difficult. For one degree change in the phase shift between $\widehat{i}_r$ and $\widehat{i}_{c_1}$, the percentage error in $\widehat{i}_r$ is 7.8%.
- The presence of harmonics in the applied voltage can possibly affect the peak of the resistive current, and therefore making this diagnostic technique quite problematic.

The findings made in this work suggest that the phase shift technique could be possibly used to diagnose the condition of MOV arresters. However, this method suffers a great deal of inaccuracy in the determination process of the resistive current, as a result of the assumption that all harmonic capacitive currents are embedded in the resistive current component, and the interference of voltage harmonics with the peak value of the resistive current.

5. Abdul-Malek, Yusof and Yousof [34] proposed the modified shifted current method (MSCM)-based algorithm, in order to extract the resistive current component from the measured total leakage current of MOV arresters, and hence to assess the condition of MOVs. The MSCM-based algorithm was therefore implemented in LabView data acquisition software program with functional block diagrams, before being transferred on a metal oxide surge arrester intelligent monitoring system (MOSAIMS). This technique was used to monitor the leakage current of an aged Ohio Brass 12 kV, 5kA MOV arrester. The results obtained were compared to those resulting from conventional compensation techniques conducted on the same arrester sample. The following observations were made:

- The total leakage current obtained from the MSCM technique proves to be dominantly resistive.
- The waveforms obtained from the MSCM show good overlap with those resulting from conventional compensation method. This indicated a good agreement between the two techniques.
- A deviation of about 5% is however observed between the two waveforms (MSCM and compensation techniques), which could be associated to measurement errors and harmonic effects.

The findings described in this work demonstrate the capability of the MSCM technique to successfully subtract the capacitive component, by injecting a quarter cycle shifted leakage current. The extracted resistive current can thus be obtained from field measurement. However, this method just as many others remain prone to noise, harmonics and other interferences.

6. Khodsuz, Mirzaie and Seyyedbarzegar [35] investigated the suitability of the maximum value of the fundamental and third harmonic resistive currents as well as that of the fundamental capacitive current, in the condition monitoring of MOV arresters. Equivalent circuit of surge arrester has been modelled, using the electromagnetic transient program-alternative transient program (EMTP-ATP) software package, in order to study the effects of voltage fluctuations, third harmonic voltage components, overvoltage and ageing on the accuracy of the afore-mentioned current indicators. The signal processing analysis aspect has been achieved using the Matlab package. The following findings were made:

   - For an increase or a decrease of 5% of the nominal voltage, irregular variations of the maximum fundamental and third harmonic resistive currents are observed, whereas a 5% variation is observed in the maximum fundamental capacitive current in both cases of 5% increase or decrease of the nominal voltage. This implies that the fundamental capacitive current is the best indicator of voltage fluctuation.
   - The ratio of the fundamental capacitive current measured during overvoltage condition to normal rated value could be used as an indicating criterion of overvoltage during surge arrester current measurement.
   - The presence of third harmonic voltage in the supply voltage causes the third harmonic resistive current indicator to increase, while the fundamental resistive and capacitive currents are less sensitive to the presence of harmonics in the supply voltage.
   - Both the maximum fundamental and third harmonic resistive currents can be effective in indicating ageing or degradation of MOV arresters.

These findings highlight the effectiveness of the fundamental capacitive current component as an indicator of voltage fluctuations and overvoltages. The sensitivity of the third harmonic resistive current, to the presence of higher voltage harmonics in the supply, is also validated in this work. The fundamental resistive current is also proven to be able to serve as an indicator of degradation along with the third harmonic resistive current.

7. Shulzhenko et al [36] studied the influences of higher-frequency voltage signals, generated in the switching process of single-phase voltage source inverter (VSI) and three-phase full bridge pulse width modulation (PWM) inverter, on the operation of MOV arresters. In the case of single-phase VSI, the installed MOV arresters were subjected to a square wave whose fast Fourier transform (FFT) revealed the presence of high-frequencies ranging from 16.7 kHz-0.5 MHz. For the three-phase PWM inverter, arresters were subjected to a triangular wave containing high-frequencies ranging from 15-60 kHz. The following findings were obtained:

   - In both cases of inverters used, the total power losses are estimated to be less than the maximum average power of the MOV devices in use. The total power losses are estimated using the sum of the watt losses resulting from all the components (fundamental and harmonics). This could be written as follows:

   $$W = W_o + \frac{2}{T}\int_{0}^{\frac{T}{2}} w_i\left(t\right)dt \tag{2.3}$$

     Where: W is the average or resistive power losses, W_o is the dc power loss, T is the period of the switching frequency and $w_i(t)$ is the instantaneous power loss.

   - The capacitive currents obtained at 50 Hz and 13 kHz as well as the $V - I$ characteristics of the MOV arresters could be accurately represented using equivalent circuit model of MOVs.

   - In the long-term operation of MOV arresters, if the higher-frequency voltage signals are high enough as the operating voltage of MOV arresters, resistive current components will dominate the capacitive component and cause thermal instability of the varistor devices.

These findings suggest amongst others that long-term degradation of varistor devices, subjected to ac fundamental embedded with noise frequencies, is possible unless such frequencies (noise) are of high enough magnitude as the operating voltage of these varistors.

2.3.2 Other Reported Effects

Several other claims on the effects of power system harmonics on varistor arresters are discussed in this section:

1. The IEEE C62.48^{TM} [37] relative to the interactions between power system disturbances and SPDs suggests the following:

    - SPDs with inductive and capacitive components may be prone to harmonic-caused failure.
    - SPDs will react to harmonic voltages in a similar fashion they react to any voltage. Therefore, if the threshold voltage of the SPD device is exceeded, conduction may take place which could eventually shorten the life of these SPDs.
    - The response of SPDs to noise will depend on the design of the SPD and the magnitude and frequency of noise pulses.

    These suggestions consist of precautionary measures based on the generally documented effects of power system harmonics on devices with similar components (inductance and capacitance). Furthermore, no analytical study provides evidence of the effect of continuously applied harmonic-distortion, embedded on the fundamental voltage component, on the degradation of SPDs.

2. Macanda and Cantagrel [38] studied the influence of surge arresters on ac distribution networks. Four type 1 ac SPDs, which basically consisted of three air-gap and one gapless arresters, were therefore tested in three-phase, three or four-wire ac circuit configurations. The surge currents applied to these SPDs were 15 x 8/20 μs with a peak value of 25 kA and 5 x 10/350 μs of the following values: 0.1, 0.25, 0.5, 0.75 and 1.0 p.u of the SPD's nominal peak value (25 kA). The gapless or MOV-based arrester was connected in series with a gas discharge tube (GDT) on a three-phase, three-wire circuit. The following observations were made:

    - No follow current was experienced during the entire test sequence related to MOV-based or gapless arrester technology.
    - The MOV-based arrester did not show any bad influence or disturbances on the power quality of the three-phase, three-wire ac circuit.

    This work seems to suggest that bad ac voltage quality resulting from the operation of type 1 ac SPDs during surge conditions are mainly caused by follow currents.

This therefore implies that MOV-based arrester technology cannot create bad interference with ac circuit during surge conditions, in which they are connected, since they are immune of follow currents. However, the focus of this work was specifically oriented on the performance-related issues ac type 1 arresters during surge conditions. The stability of these arresters during power-frequency operation which could, on the long run, impact on the performance of these arresters was completely overlooked.

The gap in the knowledge of ZnO arrester devices operating continuously in electric networks with distorted voltage remains the probability of accelerated electrical degradation or ageing of MOV-based surge arresters.

2.4 Statistical and Probabilistic Analysis of Electrical Degradation

The useful life of MOV arresters is usually defined as the time required for these surge protection components to reach degradation or end of life [9]. Therefore lifetime prediction of MOV arresters is of utmost importance to the reliability of power systems. Since varistor arresters are meant to behave like solid insulators [39], statistical methods recommended to the analysis of insulator's life could therefore be applied to varistor arresters. The following statistical techniques are proposed:

2.4.1 Weibull and Log Normal Statistical Distribution

The following studies demonstrated the common applications of the two or three-parameter Weibull model in the analysis and prediction of the degradation or failure times:

1. Cygan and Laghari [40] conducted a review of the methods and models applied to analyse and predict lifetimes of solid insulators subjected to electrical and thermal stresses. The following findings are reported:

    - The most popular technique to accelerate the ageing or degradation of an insulating material is to subject the material at higher voltage and temperature than normal operating conditions.
    - The Weibull and log normal statistical distributions are most commonly applied to analyse life deterioration of solid insulating materials.

- The cumulative damage theory forms the basis of multi-stress ageing and therefore provides better approximation of the degradation phenomena of electrical insulation.

2. The IEEE 930^{TM} [41] provides fundamental guidelines related to the application of the two or three-parameter Weibull analysis of insulation life data (times to degradation or degradation voltage). The following recommendations are proposed:

   - The percentage cumulative degradation of the Weibull cumulative density function (CDF) is obtained using the Ross approximation's expression [42, 43, 44]:

$$F(i,n) \approx \left(\frac{i-0.44}{n+0.25}\right) \times 100 \tag{2.4}$$

   Where: $F(i,n)$ is the percentage cumulative degradation, $i = 1, 2, ...r$ is the rank number of degradation times and n is the number of samples subjected to accelerated degradation test.

   - The adequacy or the goodness of fit of the CDF obtained is verified using the correlation factor η, which should be higher or equal to the Weibull critical coefficient value, provided in figure 2.1. The correlation factor is given by the following equation:

$$\eta\left(x_i, y_i\right) = \frac{\sum\left(x_i - \overline{x}\right) \cdot \left(y_i - \overline{y}\right)}{\sqrt{\sum\left(x_i - \overline{x}\right)^2 \cdot \sum\left(y_i - \overline{y}\right)^2}} \tag{2.5}$$

   Where: $\eta\left(x_i, y_i\right)$ is the correlation function, $x_i = \ln\left[-\ln\left(1 - \frac{F(i,n)}{100}\right)\right]$, $y_i = \ln\left(t_i\right)$, $\overline{x} = \frac{\sum x_i}{r}$, $\overline{y} = \frac{\sum y_i}{r}$. t_i is the degradation time and r is the number of degraded samples.

   - For large degradation data ($r > 20$) the shape and scale parameters of the Weibull distribution are estimated using the least squares regression method. This method implies the determination of the slope and the C-intercept, prior to the estimation of the Weibull parameters. The shape parameter β is expressed as:

$$\beta = \frac{1}{m\left(x_i, y_i\right)} = \frac{\sum\left(x_i - \overline{x}\right)^2}{\sum\left(x_i - \overline{x}\right) \cdot \left(y_i - \overline{y}\right)} \tag{2.6}$$

   Where: $m\left(x_i, y_i\right) = \frac{\sum(x_i - \overline{x}) \cdot (y_i - \overline{y})}{\sum(x_i - \overline{x})^2}$, is the slope function. The scale parameter is obtained using the exponential of the C-intercept function. This yields the following expression:

$$\theta = \exp c = \exp\left[\overline{y} - m\left(x_i, y_i\right) \cdot \overline{x}\right] \tag{2.7}$$

FIGURE 2.1: Critical coefficient values[41].

Where: $C = \overline{y} - m\,(x_i, y_i) \cdot \overline{x}$, is the C-intercept function.

The proposed recommendations form the backbone of the Weibull statistical analysis. On the basis of the obtained parameters, the probability density function (PDF), the unreliability or (CDF) as well as the reliability and the hasard functions of the degradation times of the Weibull distribution can be determined. These probability functions provide reasonable means or tools of analysis and prediction of the failure or degradation rate and the survival or reliability, and more importantly of the lifetime estimates of the samples involved.

3. Meshkatoddini [45] used Monte Carlo algorithm in order to statistically study the conduction phenomenon in thin ZnO varistors. The following observations are made:

    - The number of conducting ZnO grains that provide the current path between the electrodes of thin varistors fits a log normal statistical distribution.

- The turn on point or the conduction threshold voltage and the non-linearity coefficient of the ZnO varistors can be controlled by a small fraction of non-conducting grains.

From these observations, it could be deduced that the increase in the number of ZnO conducting paths of varistor could be associated to the device conduction, which is associated to the probability of degradation. Therefore, the Log normal statistical distribution could also be applied to degradation studies.

2.4.2 Probabilistic Analysis

1. Amicucci, D'Elia and Gentile [46] included the physical behaviour of a metal oxide material in order to improve the mathematical model based on probabilistic arguments, and aimed at estimating the failure probability of MOVs as a result of lightning-related stresses. The study shows that:

   - The obtained model enables the expected life of MOV, expressed as the mean time to failure ($MTTF$), to be estimated in terms of the number of lightning flashes that influence the protected circuit.

2. Brown [47] conducted a comprehensive study on the degradation phenomena of MOV-based arresters. Amongst other observations highlighted in the study, the following are noted:

   - The lifetime of a MOV can be expressed in terms of the Arrhenius rate equation:

   $$t = t_o \cdot \exp\left[\frac{E_a - f(V)}{RT}\right] \tag{2.8}$$

   Where: t is the time to degradation, t_o and R are constants, E_a is the activation energy, $f(V)$ is the applied voltage and T is the absolute temperature.

   - The failure rate of MOVs under normal operation can be estimated by the Arrhenius model, if the most significant stress is thermal and the expected mean life (ML) is logarithmically related to the inverse of temperature.

2.5 Physics of Electrical Degradation in MOVs

The degradation symptoms of varistor arresters could be regarded as manifestations of change process in the microstructure of these protective devices. The relationship between the fundamental causes and symptoms of electrical degradation could be well understood in terms of the microstructure behaviour of varistor arresters. The following studies have attempted to provide better understanding of electrical degradation mechanism:

1. He et al [48] studied the mechanisms of ZnO varistor degradation under long-term ac voltage operation and temperature. Fifteen varistors of 18 mm diameter were therefore subjected to accelerated degradation test under the following major conditions: ac applied voltage ratios ($AVR = V_{max}/V_{1mA}$): 1.072; 1.042; 1.004; 0.984 and environmental temperatures of 20 ^{o}C and 45 ^{o}C, and lastly for a q- value of 0.75 at the following temperatures: 90 ^{o}C, 110 ^{o}C, 130 ^{o}C, 150 ^{o}C and 170 ^{o}C. A watt loss versus time characteristic of the varistor samples in use is measured and plotted to analyse the degradation process. The following observations were made:

    - For AVR >0.9 and environment temperature T >160 ^{o}C, a steep rise of the watt loss is observed until thermal breakdown takes place. This is generally attributed to low intergranular barrier (usually observed in poor quality varistor devices), which at higher operating voltage and temperature, will cause high resistive current and therefore high watt loss able to overcome the varistor thermal dispersion capability. This will subsequently lead to thermal breakdown of the device.
    - For AVR >0.9 and an environment temperature of $T \leq 100^{o}$C, a steep rise of the watt loss is observed, followed by a slow down period characterised by small increases in the watt loss, before a sharp rise in the watt loss magnitude, which eventually leads to thermal breakdown of the device. The steep rise in the watt loss can be attributed to the decrease of the schottky barrier height as a result of recombination of Zn interstitials near the schottcky barrier interface and the Zinc holes, under the influence of applied voltage and temperature. The resistive current will therefore increase leading to increase in the watt loss. The small increase in the watt loss could be explained by the presence of Zn interstitials in the schottky barrier which slows down the decrease process of the barrier height. The sharp increase in the watt loss result from further decrease of the barrier height to a stage that prompted resistive current to increase leading to thermal breakdown of the device.
    - For AVR >0.9 and temperature T >100 ^{o}C, a rise in the watt loss is firstly observed, followed by a decrease before reaching a stable value. The decrease in the watt loss could be attributed to the thermal treatment phenomenon which causes the neutral atoms to separate in the intergranular region, and thus leading to the increase of the barrier height.

These findings fundamentally suggest that the three basic outcomes of accelerated degradation test on varistor devices could be understood in terms of the schottky barrier height, the migration of zinc interstitials and the thermal treatment of the varistors.

2. Zheng et al [49] studied the space charge characteristics of aged or degraded ZnO varistors of 10 mm diameter and 1.4 mm thickness. These samples were degraded using 8/20 μs current impulse of the following peak amplitudes: 50 x 50 A; 100 x 50 A; 200 x 50 A; 100 x 100 A; and 200 x 200 A. The $V-I$ test was conducted on both degraded and non-degraded samples, followed by the TSC and pulse electro-acoustic (PEA) tests. The following findings were made:

    - The higher the number of pulses, the higher the increase in the varistor temperature which causes more space charges and traps to be developed in the varistor microstructure and consequently a decrease in the schottky barrier height. This results in a drift of the $V-I$ characteristic curve towards the high conduction region.
    - An increase in the peak amplitude of the impulse current wave has a tendency to generate more available space charges and traps, thus reducing the schottky barrier height to enable a drift of the $V-I$ characteristic curve towards the high conduction region.
    - The TSC results confirm the migration of interstitial zinc ions which prompts the decrease of the schottky barrier height, hence the drift of $V-I$ characteristic curves towards the high conduction region.

    These findings mainly attributed the drift $V-I$ characteristic curve of degraded ZnO varistors, which is a key symptom of degradation or ageing, to the creation of space charges and traps followed by the migration of interstitial Zinc ions, as a result of successive high amplitude pulses discharged through these devices. This migration results in the decrease of the schottky barrier height.

3. He et al [50] studied the ageing mechanism of 25 individual grain boundaries in ZnO varistor arresters using microcontact measurement. Prior to this technique, ZnO varistor samples are degraded using accelerated degradation test at the following voltage and temperature: $0.85V_{1mA}/135\ ^{o}$C. The ageing time intervals consisted of 0, 24 and 48 hours. The microcontact measurements were conducted using a probe station, an optical high magnification microscope, and coaxial probes with 0.5 μm replaceable tip equipped with two probe positioners. These probes are manually adjusted by the positioners to make electrical contact with the deposited microelectrodes. A digital source meter was connected with the probes' coaxial

cables to determine the V–I curves of individual grain boundaries. The ageing or degradation rates of individual grains were also evaluated using equation 2.1. The following observations were made:

- Based on the leakage current measured in the pre-breakdown region, the degradation characteristics of individual grain boundaries could be either a monotonic (the $V - I$ curve gradually and monotonously move towards the high conduction region with ageing time) process. In this case, the leakage current continuously increases while the non-linear coefficient decreases. The width of the non-linear region of the $V - I$ curve is significantly reduced with ageing time. The breakdown voltage of this grain boundary is in the proximity of 3.02 V.
- The degradation characteristics of individual grain boundaries could also be a non-monotonic process (the drift of the $V - I$ curve towards the high conduction region is not continuous given a recovery phenomenon in the pre-breakdown region). In this case, the leakage current decreases then increases before eventually decreasing. However, the non-linear coefficient decreases. The breakdown voltage of this grain boundary is in the proximity of 3.31 V.
- Different grain boundaries may follow different ageing or degradation process as the ageing test time increased.
- Given the non-uniform ageing characteristic of individual grain boundaries, the degradation rates of different grain boundaries are consequently non-uniform and range from 10^{-7} to 10^{-3} A.h$^{-1/2}$. This basically implies that the degradation mechanism of a bulk ZnO varistor sample is the synthetical effect of several millions of individual grain boundaries with different ageing rates.

These findings fundamentally suggest that the degradation mechanism could be explained in terms of the migration of zinc interstitials and oxygen desorption at the interface of the grain boundaries. On the other end, the migration of negatively charged defects in grain boundaries towards the interface and the absorption of oxygen could form the basic mechanism of electrical properties recovery.

2.6 Conclusion

Degradation or ageing of MOV-base surge arresters results either from high-magnitude impulse currents discharged through these devices, or from long-term continuous exposure to ac or dc voltages. The degradation phenomenon generally upsets the stability and performance qualities of MOV arresters, which could be clearly observed in terms of various defective symptoms that may affect the electrical characteristics (Shift of the $V - I$ curve, increase of the leakage current, decrease of the non-linearity coefficient...) of these transient overvoltage protection units.

The reported studies related to the development of new oxide additives, in a bid to improve the electrical characteristics of varistor arresters, have indicated the use of accelerated degradation or ageing tests as reliable alternative to simulate long-term failure of MOV arresters under continuous ac or dc applied voltage and environmental temperature in few hours.

The current state of knowledge in this field is centred on diagnostic or monitoring techniques of the resistive leakage current, for the purpose of correct interpretation or evaluation of real health condition of arresters in service.

The leakage current of MOV arresters such as described in the literature consists of the resistive and capacitive current components. The resistive component, which consists of the fundamental and odd harmonic currents, is reported to be the most reliable indicator of degradation given its proportionality to the power losses or heat generated inside arrester devices. However, the magnitude of the resistive current component is shown to be sensitive to the environmental temperature as well as to harmonic disturbances embedded on the fundamental applied voltage across varistor arresters. Harmonics on the system voltage are reported to cause the magnitude of the resistive current to increase further. This ultimately raises the question of suspected influence of harmonics on accelerated degradation, and not only on leakage current-based diagnostic techniques as currently reported.

The deterioration of electrical properties of varistor arresters during ageing consists of visible outcome of a complex microstructural mechanism, which may be approached in terms of statistical and probabilistic analysis.

The gap in the knowledge of electrical degradation of MOV-based arresters is found to be on the probability of harmonic-induced accelerated degradation of these surge arrester devices on the long-term basis, given the well reported influence of harmonic frequencies on the resistive leakage current, which is relied upon for degradation diagnosis purpose.

Chapter 3

Experimental Work

3.1 Introduction

A description of the ZnO varistor samples as well as an account of the experimental work conducted in this study is provided in this chapter. The measurement techniques of desired electrical characteristics or properties of the varistor devices such as: the $V-I$ characteristic test performed on the samples before and after accelerated degradation test, the 50 Hz ac accelerated degradation test, with and without external harmonic-distorting load, as well as the high-amplitude impulse test are also discussed. The purpose of the tests conducted, standard procedures and expected measurement outcomes such as recommended by various standards are also highlighted in this part of the study.

3.2 Description of the Varistor Samples

The arrester samples, used in this work, consisted of 360 commercially-sourced low-voltage ZnO varistor disks from three leading manufacturers. The ZnO disks are coated with epoxy resin and the terminals are formed of tinned copper leads. These varistor arresters are assigned the following codes: BE; YW and RL sample groups, for identification purposes. The diameters of the varistor samples, the rated reference or varistor voltage (both at ac and dc), the clamping voltage, the maximum nominal discharge current and the MCOV of the sample groups are provided in table 3.1. The following alphabetical letters: W and H are further assigned to the identification codes described above in order to indicate whether or not accelerated degradation is conducted with or without an external source of harmonics. The letter W is used to designate the samples subjected to accelerated degradation without external source of harmonics. However, in this condition the increased voltage applied across varistor samples during the test,

Table 3.1: Electrical Specifications of the sample groups

Samples	Diameter	V_{1mAac}	V_{1mAdc}	V_c	Peak Current (8/20 μs)	MCOV
BE	20	205	170	340	8	130
YW	20	200	170	340	6.5	130
RL	20	228	184	340	6.5	130
Unit	mm	V	V	V	kA	V

and the resulting distorted current flow cause harmonic distortion in the mains voltage. Therefore, BEW01 referred to sample number 1 of the BE group is subjected to accelerated degradation without external harmonic source. On the other end, the letter H is used to designate the samples subjected to degradation test with an external source of harmonics. BEH referred to samples from BE group degraded in a presence of an external harmonic source connected to the system.

3.3 $V - I$ Characteristic Test

The IEEE standard C62.62^{TM} [51] recommends the watt loss and leakage current tests be conducted as part of the characteristic or performance tests on arrester devices. Yet, the varistor's watt loss, the leakage current and the reference voltage consist of various aspects of the $V - I$ characteristic curve [29]. Therefore, the $V - I$ test consists of a reliable alternative technique to measure these important electrical characteristics of varistor arresters under normal operating condition. Furthermore, the $V - I$ curve could be used to obtain the non-linear coefficient of the varistor arresters, and could consequently be relied upon to provide good indication of the health condition of MOV arresters in the context of degradation [9, 26].

3.3.1 Procedure

For the purpose of this test, a variable ac source is used to supply a 4-pin ac/dc bridge rectifier chip (RS 204), through a transformer. The varistor arrester under test is connected across the dc terminals of the ac/dc bridge converter. The TBM 811 digital ammeter, able to provide current readings from micro-ampere scale, is connected in series with the device under test to monitor the current. The Escort EDM-82 digital voltmeter is connected across the MOV arrester to provide voltage readings. The current measured in the milli- ampere scale consisted of: 10^{-3}, 10^{-2}, 10^{-1}, 1, 10 and 100. The $V - I$ test set up is shown in figure 3.1. The $V - I$ measurement points obtained at room temperature are used to plot the $V - I$ characteristic curves (plotted with Microsoft Excel 2010) for the samples BEW, BEH, YWW, YWH, RLW and RLH, before and after ac accelerated degradation test. The $V - I$ measurements obtained for all the sample groups, before and after ac degradation test, are shown in Appendix A.

FIGURE 3.1: V-I test set up

3.3.2 Measured Parameters

The $V - I$ readings obtained are used to plot the characteristic curve of the samples, using the graphic plot tool of the Microsoft Excel package. The reference voltage V_{1mAdc} is read off the voltmeter when the ammeter reads a current of 1 mA. The coefficient of non-linearity is obtained using relationship 2.2. Degradation on varistor samples could therefore be observed on the basis of the $V-I$ shift towards the high current region, which should be confirmed in terms of a decrease in the dc reference voltage V_{1mAdc} and the coefficient of non-linearity [24, 26]. Although the change in the reference voltage should be higher than 5% [52], in order to confirm degradation, this study rather considered at least 5% change ($\Delta V_{1mAdc} \geq 5\%$) in the reference voltage. The mean values of the $V-I$ measurement points can be used to plot the mean $V - I$ curve of the samples before and after degradation. In this context, the percentage change in the mean value of the reference voltage measurement point, before and after degradation, could be determined as follows:

$$\triangle \overline{V}_{1mAdc} = \frac{(\overline{V_{b1mAdc}} - \overline{V_{a1mAdc}})}{\overline{V_{b1mAdc}}} \times 100 \tag{3.1}$$

Where: $\triangle\overline{V}_{1mAdc}$ is the percentage change in the mean reference voltage point, $\overline{V_{b1mAdc}}$ is the mean reference voltage before degradation, and $\overline{V_{a1mAdc}}$ is the mean reference voltage after degradation.

3.4 Accelerated Degradation Test

The IEEE C62.34 [53] and the IEEE C62.11^{TM} [54] both recommend the accelerated degradation or ageing test be conducted on MOV arresters, as means of simulating long-term performance characteristics of these SPDs. This test is based on the Arrhenius life test model, and is performed at elevated voltage and temperature over a period of time. The simultaneous action of both thermal and electrical stresses is very common in real life cases [40]. Therefore, the electro-thermal ageing test, such as referred to, is basically meant to simulate real life insulation degradation or ageing process [55], by extrapolation of the facts gathered to long-term degradation under normal service voltage and temperature conditions.

3.4.1 Procedure

This test is achieved by combining the following components: the heat chamber or oven, the 50 Hz ac supply voltage, the ac voltage controller (harmonic source), the harmonic filter unit (when harmonics are not required), the high-temperature conductors and the data acquisition units.

1. The Oven or Heat Chamber:

   Since temperature consists of an important aggravating factor of MOV-based surge arresters, the oven or heat chamber forms the most critical piece of equipment in the implementation of accelerated degradation test. This chamber provides a source of thermal stress, which in real life condition, could originate from the environment in which MOV arresters may be continuously subjected to. For short term degradation results, the magnitude of the thermal stress provided to the samples is accelerated using Arrhenius model. The oven used in this work consisted of the Nabertherm P330 which is described in [56]. This heat chamber is made up of 9 settable heating programs or courses (P1-P9), and 40 time-segments divided in groups of 10 blocks(A-J). Every block consists of 4 time-segments: 2 ramp and 2 holding times. Therefore, a heating program or course may consist of one or a combination of many time segment blocks. The temperature versus time diagram of the heating program adopted in this study is indicated in figure 3.2. This figure shows that the temperature used for this degradation test is $T_{2B} = 135^oC$, which is held at time t_{2B} (second time-segment of block B) set for 96 hours. The ramp and holding (transition) times are each set for 5 minutes. The waiting or OFF time refers to the time-period before the first ramp time. This basically resulted in t_{2B} being reached approximately 30 minutes (including temperature fluctuations time) after the oven start up time. To ensure that this test process ends after 96 hours, all temperature and time-segments beyond T_{2B} and t_{2B} are assigned a zero value during programming. This ensures that after the set test time is over, the oven will switch off and enters the cooling mode. The oven is independently supplied from a three-phase source.

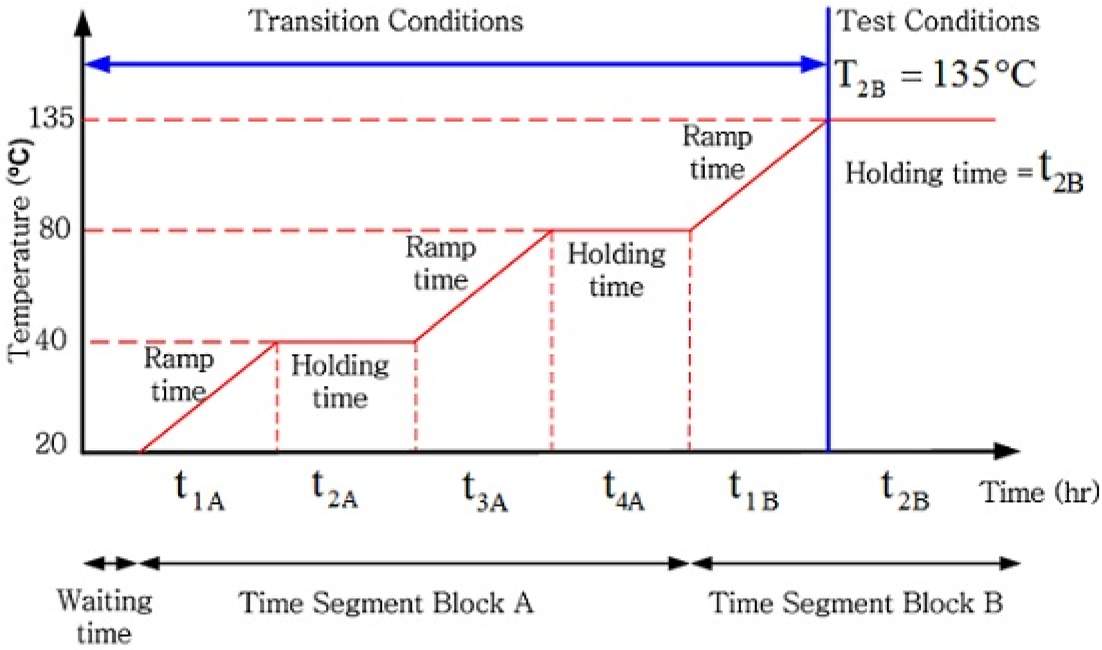

FIGURE 3.2: Heating Program: Time vs Temperature

2. The 50 Hz ac Supply Voltage:

The 50 Hz ac supply voltage represents the ac field stress to which MOV devices may be continuously subjected to in transmission or distribution circuits.

The combination of the heat chamber and the 50 Hz ac supply form the basis of continuous electro-thermal ageing or degradation phenomena. The continuous magnitude of the ac field stress provided is 85% of the sample breakdown voltage (See table 3.1). The 50 Hz ac supply voltage is sourced from a 220/500 V step up transformer which in turn is supplied from a variable ac voltage source. This arrangement is made to provide electrical isolation and to maintain the variable ac source at low voltage value. For the entire test period, the voltage stress ensured across the transformer output terminals is 85% of the ac reference voltage ($0.85V_{1mAac}$) for respective samples. This supply voltage system is time-controlled using an electronic timer-unit set to trigger 30 minutes after the oven is set on. All five conductors supplying ZnO samples are each terminated to the transformer output via 250 V, 125 mA protective fuses. Therefore, when the current through a ZnO device reaches a value beyond 125 mA, the fuse is blown out to safely isolate the varistor device from the supply.

3. The External Source of Harmonics:

The external source of harmonics represents the source of harmonic disturbances that may be affecting the 50 Hz applied voltage appearing across MOV devices. This source of harmonics consisted of a triac-based ac voltage controller unit connected across the secondary output terminals of the transformer. This unit is made to control a dominantly resistive load of 83.3 $k\Omega$. The firing angle of the controller consisted of a potentiometer-based control knob, which is adjusted in a manner that resulted in the applied voltage stress to the entire system be distorted dominantly with the 3^{rd} and the 5^{th} harmonic frequencies, as well as other odd harmonics such as the 7^{th} and 9^{th}.

4. The Data Acquisition System:

The data acquisition system consisted of 1×3-channel K5020 and two MT250 data logger units, capable of recording voltages across each of the five varistor samples in a sampling rate of 30 seconds. The data logging process is trigger as soon as the voltage source is launched. This enabled us to distinguish the samples that failed from those that manage to survive the process. The 2-channel TDS 1001B Tektronix digital scope is also used to monitor the applied voltage waveform, while the 4-channel Rigol DS 1204B digital scope is utilised to capture the leakage current signal in comma separate values (CSV) format. For this purpose, the current signal is recorded through a 5/1 A current transformer (CT) together with a current probe connected to the scope. The leakage current measurement is provided in Appendix B.

5. High Temperature Conductors:

   Each test run accommodated 5 varistor samples connected across terminal blocks, which are mounted in parallel on a concrete platform. To reinforce the insulation between the terminal blocks, the concrete platform is coated with a high-temperature (750^oF) RTV silicone adhesive sealant. The connection between the terminal blocks and the 50 Hz ac voltage source is made using 1.5 mm^2 high-temperature and single-core silicon conductors (Silflex), capable to withstand a temperature of 180^oC [57].

The connection arrangement of varistor samples across the terminal blocks inside the oven is illustrated in figure 3.3, whereas the block diagram illustrating the connection of the harmonic source in the test system is shown in figure 3.4.

FIGURE 3.3: Connection arrangement of Varistor Samples

In the event of harmonic source not being required, both the resistive load and the varistor arresters inside the oven are supplied from the transformer output terminals, through a single-phase harmonic filter (FN 2090) in an attempt to completely eliminate harmonic distortion in the applied voltage stress. However, the conduction through varistor devices at elevated voltage and temperature caused the applied voltage stress to experience similar types of harmonic frequencies, as indicated above, yet at much lower content or permissible levels [58]. The block diagram illustrating the connection of single-phase harmonic filter in the test system is shown in figure 3.5. The complete accelerated degradation test system used in this study is shown in figure 3.6.

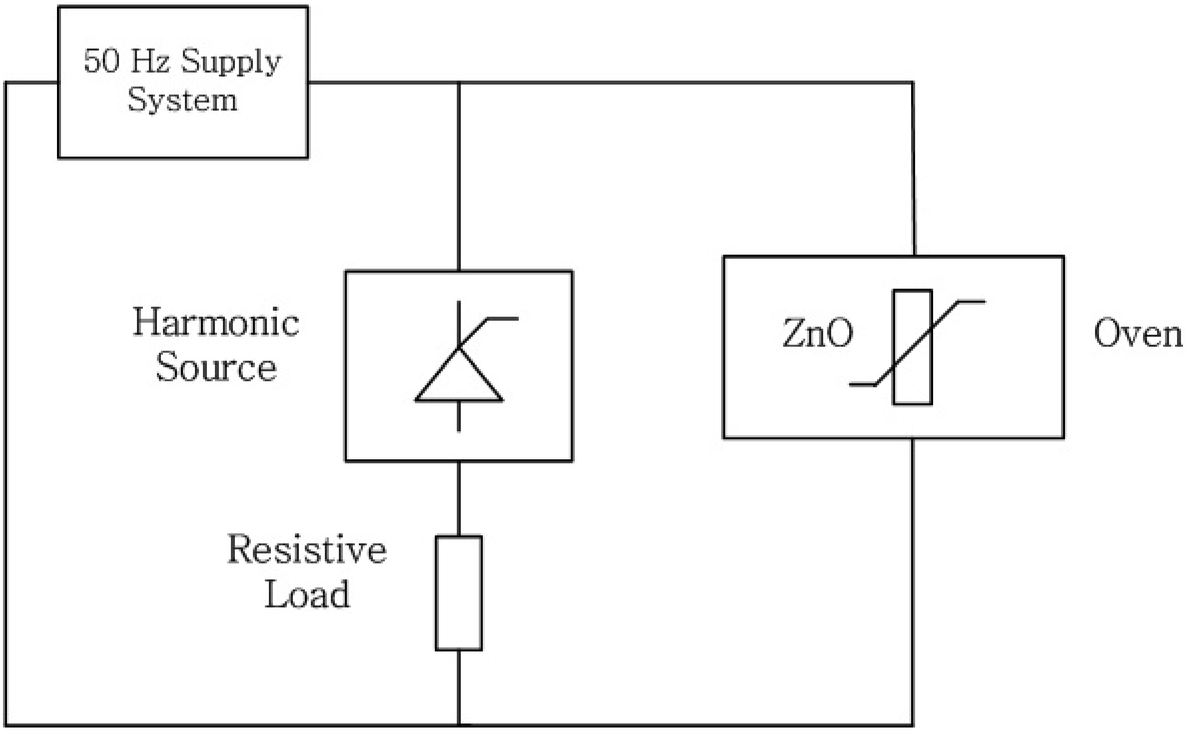

FIGURE 3.4: Harmonic source connection

3.4.2 Measured Parameters

The failure or degradation times obtained as a result of this test are extrapolated to time-values, corresponding to standard operation at 40^{o}C, using the Arrhenius life accelerating model described in [53, 54]. This is expressed in equation 3.2 below:

$$t_i\,(hour) = t_m \times 2.5^{(T_{2B}-40)/(10)} \tag{3.2}$$

Where: t_i is the extrapolated degradation time-value, t_m and T_{2B} are actual measured degradation time and applied temperature, respectively. The expression: $2.5^{(T_{2B}-40)/(10)}$ is termed the accelerating factor. The degradation status of the samples is verified on the basis of the following conditions:

1. Degraded Samples: $t_m \leq t_{2B}$ and $\triangle \mathrm{V}_{1mAdc} \geq 5\%$
2. Survived Samples: $t_m = t_{2B}$ and $\triangle V_{1mAdc} < 5\%$
3. Spoiled Samples: $t_m < t_{2B}$ and $\triangle V_{1mAdc} < 5\%$

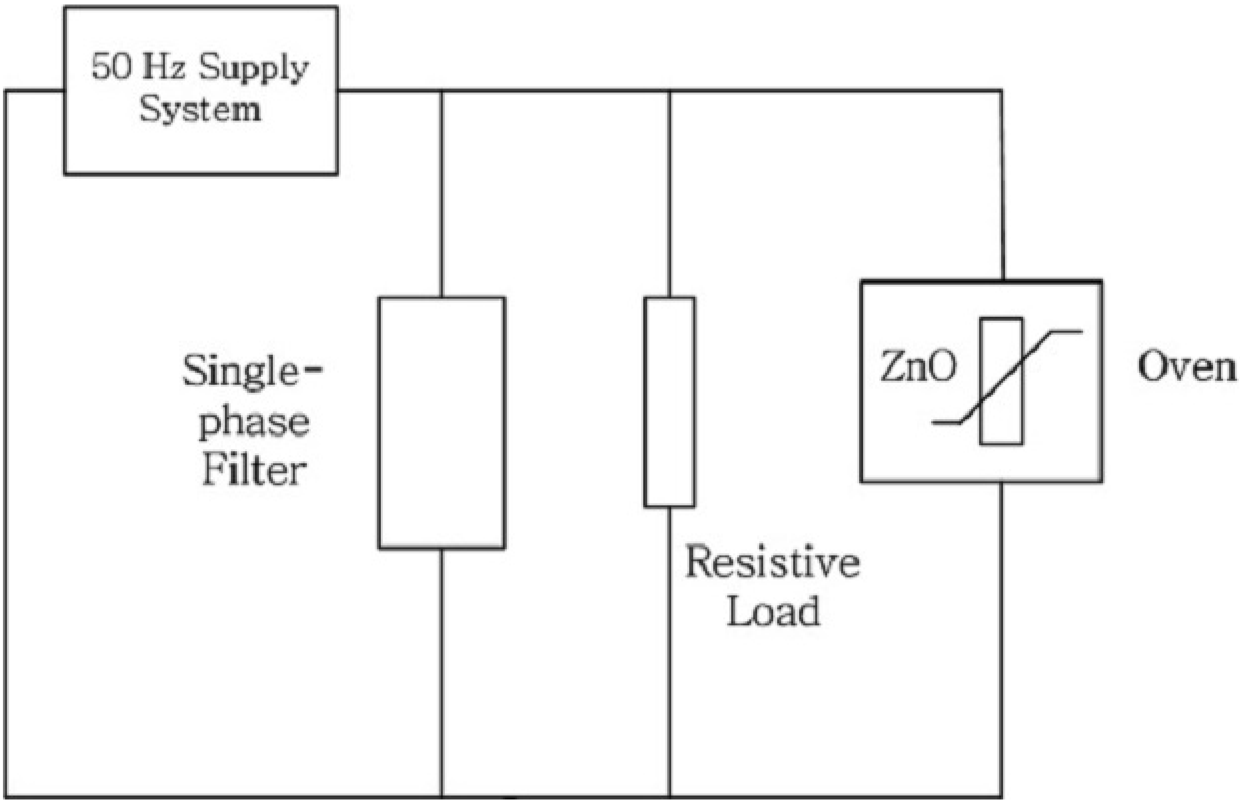

FIGURE 3.5: Harmonic filter connection

FIGURE 3.6: Accelerated degradation test set up

For degraded and spoiled samples, the time to degradation pattern, recorded in the data logger, is interrupted at given random time. This is shown in figure 3.7. However the degradation or failure condition can only be confirmed after the $V-I$ test is conducted, at room temperature. For survived samples, the time to degradation pattern recorded completes the full time cycle of the test process, and the $V-I$ test proves to be unsuccessful. This is shown in figure 3.8.

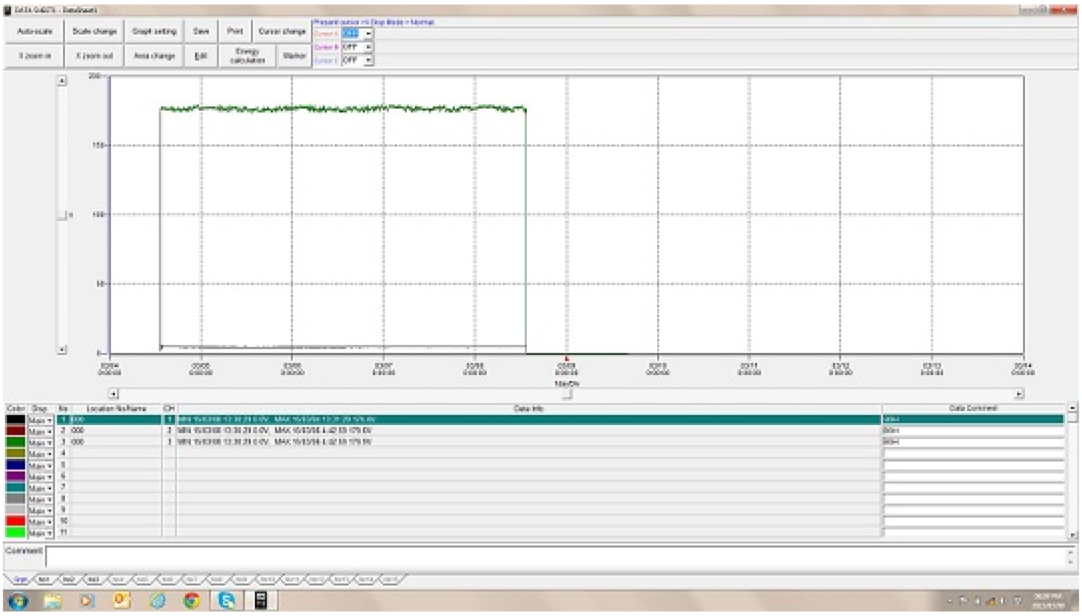

FIGURE 3.7: Degradation time pattern for failed or spoiled samples

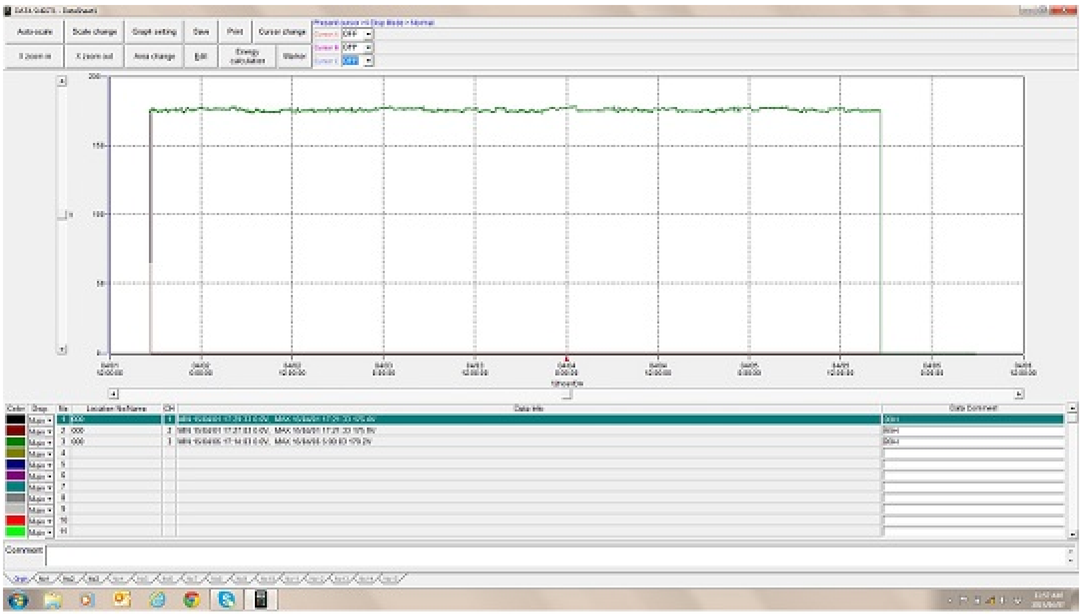

FIGURE 3.8: Degradation time pattern for survived samples

The time-values obtained in equation 3.2 are important factors to the determination of the scale and the shape parameters of the Weibull probability distribution, and subsequently the hasard or degradation rate, the survival or reliability and the probability density functions of the varistor samples under harmonic distortion conditions. The recorded breakdown times for the samples are provided in Appendix C.

3.5 Impulse Tests

The surge performance characteristics of varistor arresters can be studied on the basis of standard combination waveform [53, 54]. This waveform consists of: 1.2/50 μs open-circuit voltage and 8/20 μs short-circuit current. For the purpose of this test, the clamping voltage of varistor samples before and after ac degradation test is studied.

3.5.1 Procedure

This test is performed using a combination impulse generator which consisted of: a 250 V ac variable source supplying a diode rectifier unit, through a 220/22 000 V step-up transformer, 4 x 34.5 μF series-connected capacitor units, a dumping gap system, wave shape components, high voltage (HV) probes and the 2-channel TDS 1001B Tektronix digital scope.

The variable ac source and the step-up transformer serve to supply the diode rectifier input. The high-voltage dc that results from the rectifier is used to charge up the capacitors. The charging voltage across the capacitors is monitored using a 1000:1 HV probe, which in turn is connected to a digital voltmeter.

The dumping gap system consists of a switch operated solenoid which is intended to ensure complete discharge of capacitors to earth. The wave shape components consisted of resistors and inductors connected across the capacitor units.

The Pearson coil, which is a high-frequency current transformer, was used to step-down the current prior measurement using a current probe. An additional 1000:1 HV probe is connected across the output terminals of the generator together with the sample under test. Both the current and voltage are captured using a digital scope.

Each varistor sample is connected across the output terminal of the impulse generator, and is subjected to 8/20 μs impulse currents ranging from 10 kA to 15 kA. The clamping voltage is captured and subsequently measured on the scope's screen. The set up of the combination generator is shown in figure 3.9.

Figure 3.9: Impulse test set up

3.5.2 Measured Parameters

For the purpose of the impulse tests, the clamping voltage (V_c) parameter of the ZnO varistor arrester samples is measured. The clamping voltage helps to indicate whether or not the surge protection characteristic of varistor samples is affected as a result of degradation. The test measurements obtained are provided in Appendix D.

3.6 Conclusion

The ZnO varistor samples used in this study are described in terms of their size and electrical characteristics. The recommended experimental methodology applicable to this study: the 50 Hz accelerated degradation test with and without an external harmonic source, the dc $V-I$ characteristic test and the high-frequency impulse test are discussed. The various standards that provide the guidelines related to procedures and expected measurement outcomes are also referred to in this chapter.
The $V-I$ characteristic tests is conducted before and after degradation of the samples. This test enables the following critical characteristics to be probed: the reference voltage and the non-linearity coefficient. The 50 Hz ac accelerated degradation test is aimed

at simulating the long-term degradation phenomenon of varistor samples at different content of harmonic distortion. The relevance of this test, as far as this study is concerned, resides in the fact that the extrapolated time to degradation or life estimates of varistor samples and subsequently the degradation rate can be statistically determined. The impulse tests conducted serve to test the signs of degradation in terms of surge protection characteristics, by studying the clamping voltage between varistor samples degraded at different content of harmonic distortion.

Chapter 4

Analysis of Electrical Degradation under Harmonic Distortion

4.1 Introduction

In this chapter, the probability of aggravated electrical degradation of ZnO arresters, as a result of continuous operation under distorted ac voltage, is analysed using the three-parameter Weibull statistical tool, given the failure-free characteristic of the distribution across some time interval [59]. The scale and shape parameters of the degradation time distribution obtained, in each of the arrester population observed, are estimated prior to the determination of the hasard or degradation rate function, the survival or reliability function as well as the PDF. The average values of the coefficient of non-linearity and that of the clamping voltage for the varistor populations studied are also computed. The hypothesis testing is applied, using the likelihood ratio test, in order to test any possibility of equal estimated parameters between the distributions involved, which may lead to similar probability functions. The probability of aggravated degradation, as a result of increased harmonic currents during continuous exposure to distorted ac voltage stress, is assessed using the mean life comparison test. Therefore, this chapter consists of three case studies aimed at analysing the degradation time pattern of the BE, YW and RL varistor arrester populations when subjected to acceleration degradation test with and without external harmonics.

4.2 Weibull Plots and Probability Functions

Subsequent to the accelerated degradation test on ZnO arrester populations, the degradation indicators such as described in section 3.4.2 are verified. This process enables the non-degraded (survived and spoiled) samples to be removed. The extrapolated times as well as the percentage cumulative degradation of the arresters are determined using equations (3.2) and (2.3), respectively. The data obtained from these equations can be utilised to test the good fitness of the obtained distribution, using equation (2.4) as well as figure 2.1. Therefore the CDF of the distribution can be plotted, and the probability functions (Reliability and Degradation rate functions) can also be deduced, following the estimation of the parameters, as described in 2.4.1. The block diagram of this process is given in figure 4.1.

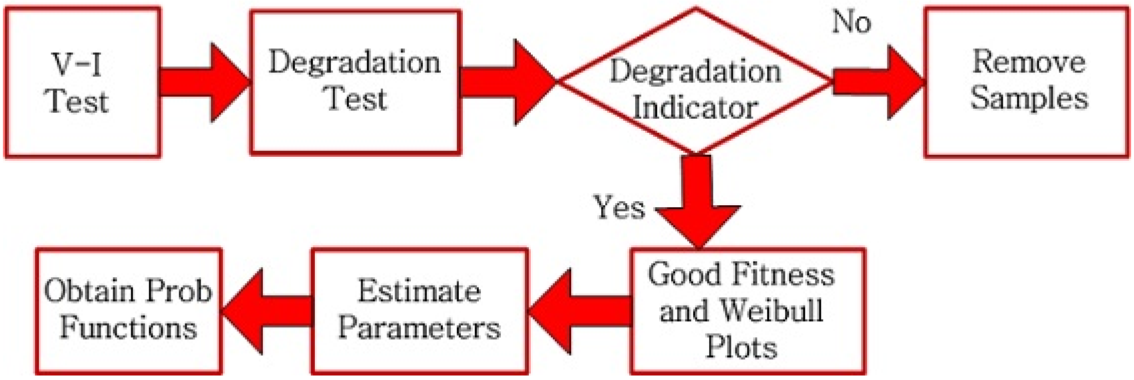

FIGURE 4.1: Block diagram of the Weibull Probability Analysis

4.2.1 Probability Functions and Electrical Degradation

Since electrical degradation of various populations of ZnO arresters is studied over a determined period of time, and the recorded time to degradation fits the Weibull probability distribution. The density function of the time to degradation distribution is modelled using the three-parameter Weibull. This is expressed as follows:

$$f(t, \beta, \theta, \gamma) = \frac{\beta}{\theta} \cdot \left(\frac{t-\gamma}{\theta}\right)^{\beta-1} \exp\left(-\frac{t-\gamma}{\theta}\right)^{\beta} ; t \geqslant \gamma \geqslant 0 \tag{4.1}$$

Where: $f(t, \beta, \theta, \gamma)$ is the PDF which represents the probability of electrical degradation occurring at random time t within the defined time-interval. β is the shape parameter of the distribution, θ is the scale parameter, and γ is the location parameter or the minimum time to degradation of the distribution.

The PDF consists of a product of two functions: the hasard and the reliability functions. The hasard function is used to indicate the frequency or rate at which electrical degradation in a studied population of ZnO arresters is taking place across a given time-interval. This function can therefore be termed as the degradation rate function. It is expressed as follows:

$$h(t) = \frac{\beta}{\theta} \cdot \left(\frac{t-\gamma}{\theta}\right)^{\beta-1} ; t > \gamma > 0, \beta > 0, \gamma > 0 \tag{4.2}$$

Where: $h(t)$ is the degradation rate function, expressed in failures per hour.

The reliability function is the complement of the CDF, and represents the probability of survival of ZnO arrester components under the conditions subjected to. This is expressed as:

$$R(t) = \exp\left(-\frac{t-\gamma}{\theta}\right)^{\beta} ; t > \gamma > 0, \beta > 0, \theta > 0 \tag{4.3}$$

Where: $R(t)$ is the reliability function.

Therefore, the CDF or probability of electrical degradation of a ZnO arrester population can be expressed as follows:

$$F(t) = 1 - \exp\left(-\frac{t-\gamma}{\theta}\right)^{\beta} ; t > \gamma > 0, \beta > 0, \theta > 0 \tag{4.4}$$

Where: $F(t)$ is the CDF or the probability of electrical degradation.

It is worth noting that higher probability of survival implies lower probability of degradation, and consequently lower degradation rate. This therefore suggests that the probability of electrical degradation of a ZnO population can be analysed on the basis of the probability functions.

4.2.2 Hypothesis Testing and Mean Life Comparison

The probability functions described in section 4.2.1 are dependent on the estimated parameters of the Weibull probability distribution. Therefore, equal estimated parameters could lead to the possibility of equal probability functions, and in turn to similar degradation behaviour. In this study, the hypothesis testing is applied to test any possibility of equal reliability and degradation rate functions of the resulting Weibull distributions (time to degradation with and without external harmonics). The following hypotheses are formulated:

1. The null hypothesis (H_0): $f_1(t) = f_2(t)$ which implies: $h_1(t) = h_2(t)$ and $R_1(t) = R_2(t)$, $t \in [t_1, t_j]$.

2. The alternative hypothesis (H_a): $f_1(t) \neq f_2(t)$ which implies: $h_1(t) \neq h_2(t)$ and $R_1(t) \neq R_2(t)$, $t \in [t_1, t_j]$.

The likelihood ratio could be used as the statistic test of the hypothesis testing. In order to favour the null hypothesis over the alternative one, the likelihood ratio should be higher than the chi-square distribution (χ^2) distribution, at 0.01 significance level with 1 degree of freedom (df) [60, 61]. Therefore, the statistic test is given as follows:

$$z = -2\ln \frac{\prod_{i=1}^{j} \left\{ \frac{\beta_1}{\theta_1} \cdot \left(\frac{t-\gamma}{\theta_1}\right)^{\beta_1 - 1} \exp\left[-\left(\frac{t-\gamma}{\theta_1}\right)^{\beta_1} \right] \right\}}{\prod_{i=1}^{j} \left\{ \frac{\beta_2}{\theta_2} \cdot \left(\frac{t-\gamma}{\theta_2}\right)^{\beta_2 - 1} \exp\left[-\left(\frac{t-\gamma}{\theta_2}\right)^{\beta_2} \right] \right\}} \geq \chi^2_{0.01} \tag{4.5}$$

Where: $\chi^2_{0.01}$ is the chi-square distribution at 0.01 significance level.

In this case, electrical degradation analysis based on reliability function seeks to predict and compare the mean life of two ZnO arrester populations. The mean life or the mean time to degradation of a population or a system consists of an integral evaluation of the reliability function [62, 63]. For acceleration degradation on a population or system, the mean life or mean time to degradation is expected to be reduced. Therefore, the mean life of arrester population subjected to accelerated degradation test, in the presence of an external source of harmonics, is compared to that of similar arrester population degraded without harmonics. The mean life is expressed as follows:

$$ML = \int_0^{\infty} R(t)\, dt = \int_0^{\infty} \left[\exp\left(-\frac{t-\gamma}{\theta} \right)^{\beta} \right] dt \tag{4.6}$$

Where: ML is the mean life of an arrester population.

For aggravated electrical degradation: $\mathrm{ML}_1 > \mathrm{ML}_2$, which implies that $\int_0^{\infty} R_1(t)\, dt > \int_0^{\infty} R_2(t)\, dt$. ML_1 and ML_2 are the mean lives of ZnO arrester population degraded without and with external harmonics, respectively. The time at which a certain proportion of ZnO arrester population will degrade can be estimated by re-arranging equation (4.4). This yields the following expression:

$$t_p = \theta \left[-\ln\left(1 - \frac{p}{100}\right) \right]^{1/\beta} + \gamma \tag{4.7}$$

Where: t_p is time at which $p\%$ of arresters will be degraded, and p is the proportion of arresters.

Therefore, the percentile or B-live test at 10%, 50% and 90% can be conducted to predict the time at which $p\%$ proportion of arrester components are likely to degrade.
The time to degradation could also be expressed in terms of the corresponding reliability value, in order to estimate the time reduction factor as well as the probability of time reduction, at any given point on the reliability curve. This could be better observed in terms of figure 4.2.

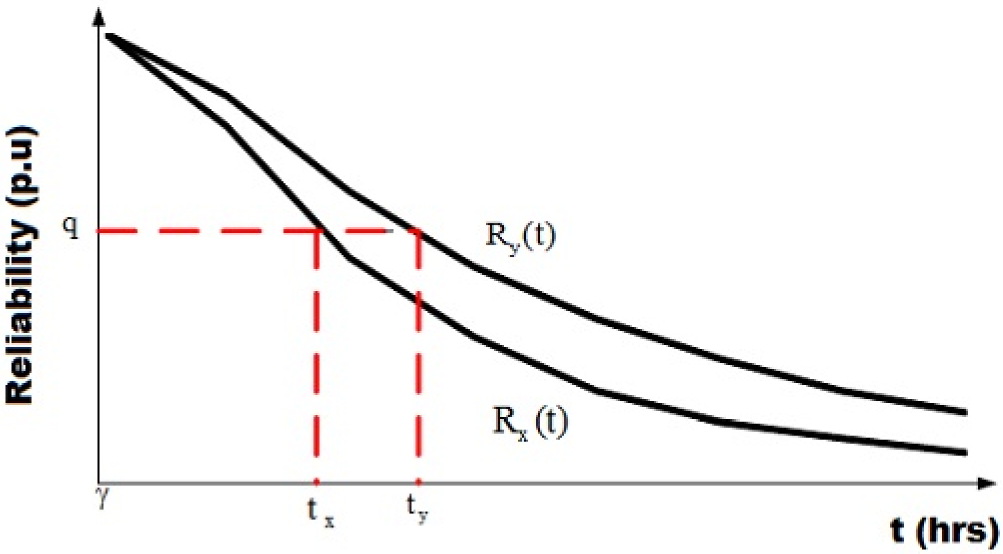

FIGURE 4.2: Time reduction at equal reliability Point

The time (t_x) and (t_y) can be obtained by re-arranging equation (4.4). This yields the following: $t_x = \theta_x \left(-\ln q\right)^{1/\beta_x} + \gamma$ and $t_y = \theta_y \left(-\ln q\right)^{1/\beta_y} + \gamma$. Therefore, at any reliability value $\left(q = 1 - \frac{p}{100}\right)$, the time reduction factor between similar arrester components subjected to different content of external harmonics is given as follows:

$$\delta_{xy} = \frac{t_x}{t_y} = \frac{\theta_x \left(-\ln q\right)^{1/\beta_x} + \gamma}{\theta_y \left(-\ln q\right)^{1/\beta_y} + \gamma} \tag{4.8}$$

Where: δ_{xy} is the time or life reduction factor between time to degradation t_x and t_y, θ_x and θ_y are respective scale parameters, β_x and β_y are shape parameters, γ is the minimum life parameter, $R_x\left(t\right)$ and $R_y\left(t\right)$ are reliability functions, and q is the reliability value.

The probability of time t_x being greater than or equal to t_y implies the probability of reduced time to degradation between two distributions, which must be higher than 0.5 or 50%. This is expressed by the following probability condition [64]:

$$Pr\left[t_x \geq t_y\right] = \int_0^\infty f_y(t)R_x(t)dt > 0.5 \tag{4.9}$$

Where: $Pr\left[t_x \geq t_y\right]$ is the probability of reduced time to degradation, $f_y\left(t\right)$ is the PDF and $R_x\left(t\right)$ is the reliability function.

In case the conditional probability expressed in (4.9) is less than 0.5, this will imply that the opposite statement expressed as: $Pr\left[t_y \geq t_x\right] = 1 - \int_0^\infty f_y(t)R_x(t)dt > 0.5$ is therefore true.

4.3 Case study 1: Analysis of BE Varistor Samples

In this section, the electrical behaviour of ZnO arrester samples, identified as BEW and BEH group arresters, is analysed and compared on the basis of the $V - I$ characteristic curve and coefficient of non-linearity, the clamping voltage and the probability functions of the time to degradation distribution obtained. The time-domain of the continuous applied ac voltage stress across BEW samples is shown in figure 4.3.

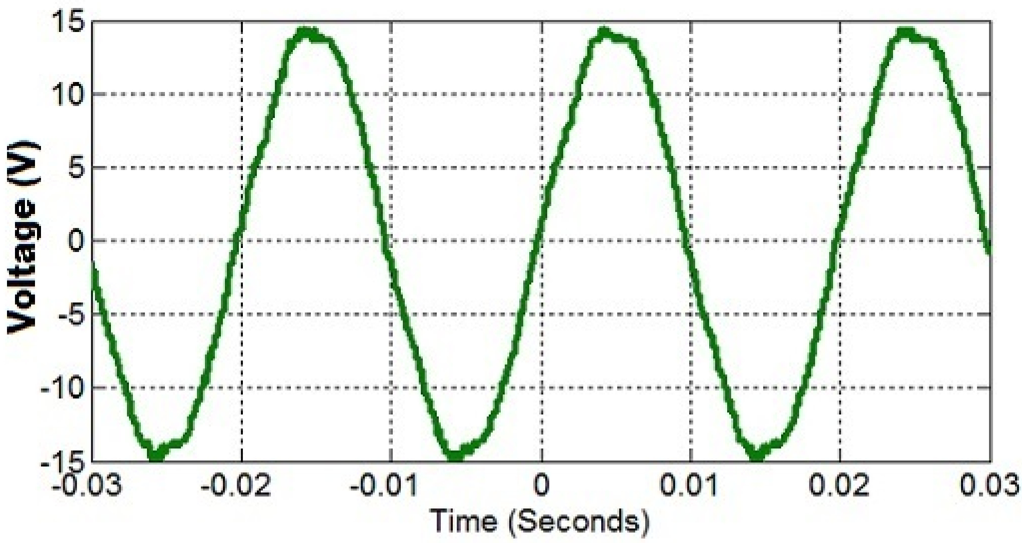

Figure 4.3: Applied Voltage Stress BEW

The frequency components associated to this voltage are indicated in figure 4.4. The level of harmonic components is found to be 1.89% for the 3^{rd}, 2.5% for the 5^{th} and 0.94% for the 7^{th} (See Appendix B).

The time-domain of the continuous applied ac voltage stress across BEH samples is shown in figure 4.5, and the harmonic components associated to the voltage across BEH samples are indicated in figure 4.6. The level of harmonic components is as follows: 6.24% for the 3^{rd}, 5.58% for the 5^{th} and 6.63% for the 7^{th} (See Appendix B).

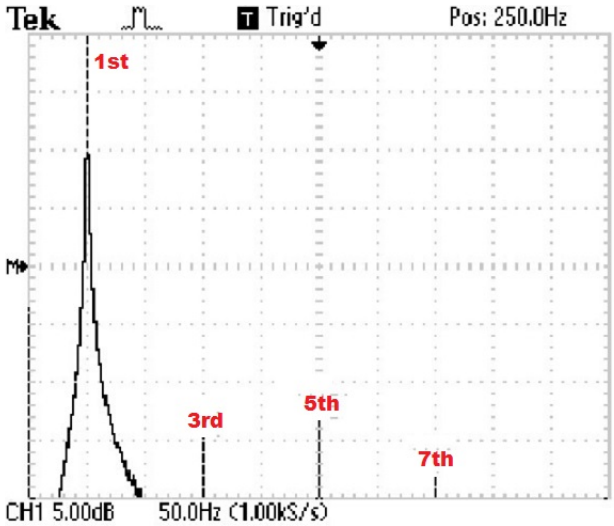

FIGURE 4.4: Frequency Components BEW

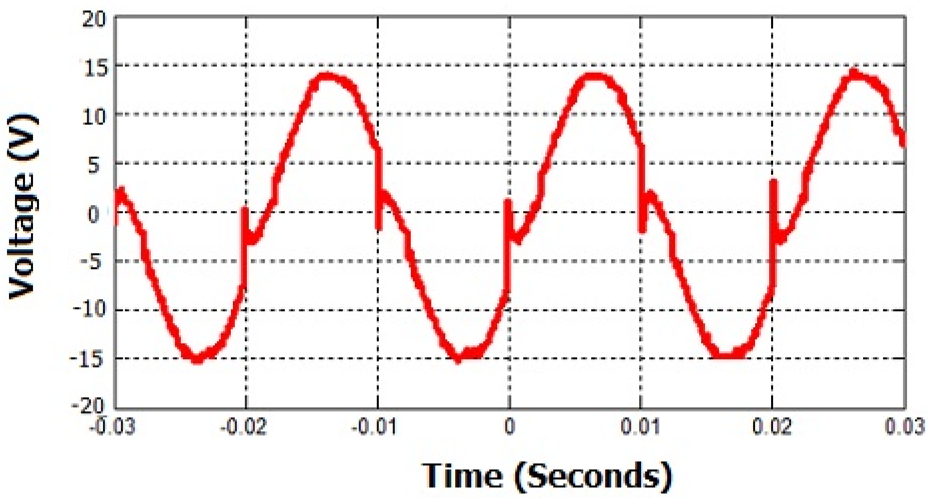

FIGURE 4.5: Applied Voltage Stress BEH

4.3.1 V-I curve and Coefficient of non-linearity

Based on the $V - I$ measurements of the BEW and BEH varistor samples provided in Appendix A, the following classification could be drawn out in terms of the conditions specified in section 3.4.2. This is indicated in Table 4.1 below:

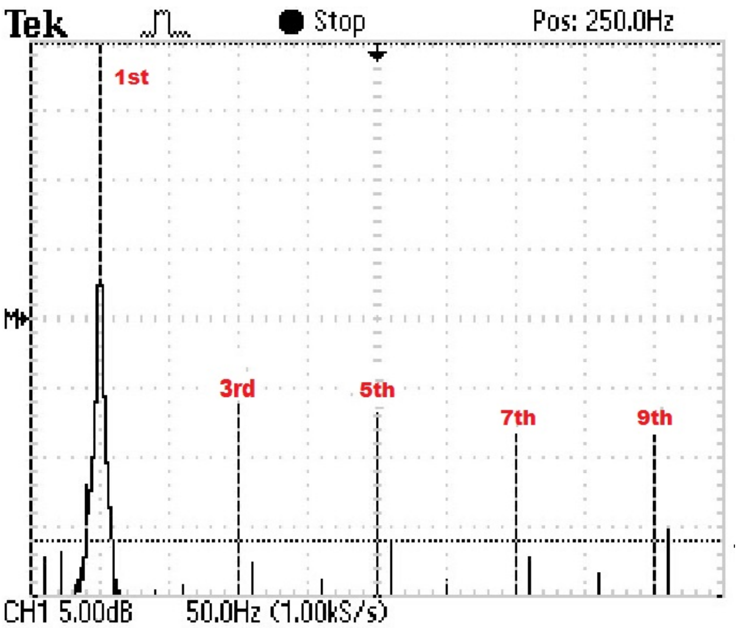

Figure 4.6: Frequency Components BEH

Table 4.1: Classification of Tested BE Samples

BE Sample Group	Degraded	Survived	Spoiled
BEW	27	30	3
BEH	37	18	5

The mean $V-I$ characteristic of the degraded BEW and BEH samples, before and after accelerated degradation test, can therefore be plotted and thus enabling the percentage change for the mean V_{1mAdc} of the BEW and BEH samples be determined using equation (3.1). The BEW and BEH mean $V-I$ curves are shown in figure 4.7.
This reveals a percentage change for the mean V_{1mAdc} of 10.80% for the BEW samples and 43.75% for the BEH samples. The coefficient of non-linearity could also be determined on the basis of the mean $V-I$ characteristic curves of the BEW and BEH samples, by using equation (2.2). This yields the following: before degradation the mean coefficient of non-linearity for BE samples is found to be 82, and after degradation this coefficient is worked out to be 53, which represents 35.37% reduction for BEW samples, and mean value of 15, which shows 81.71% reduction for BEH samples. These values are indicated in table 4.2. Therefore, the BEH arrester components are proven to have their stability characteristics significantly reduced as compared to the BEW components.

Table 4.2: Change in Reference Voltage and Coefficient of non-linearity (BE Samples)

BE Samples	$\overline{V}_{1mAdc}$ (V)	α	$\Delta\overline{V}_{1mAdc}$ (%)	$\Delta\alpha$ (%)
Non-degraded	176	82	-	-
BEW	157	53	10.80	35.37
BEH	99	15	43.75	81.71

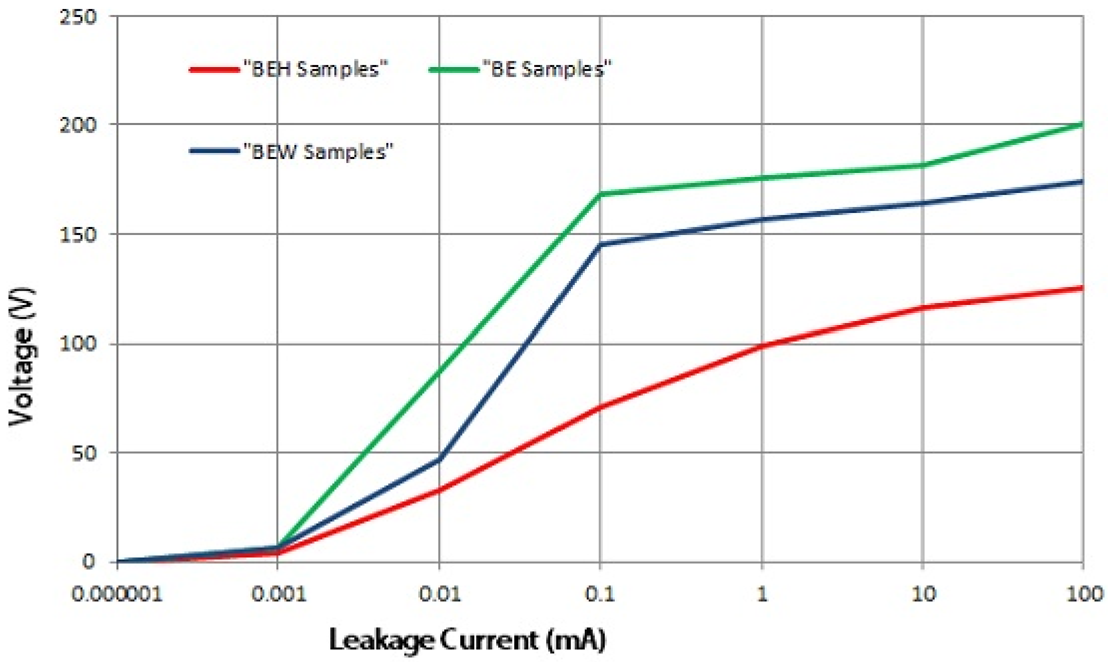

FIGURE 4.7: Mean V-I curve BE Samples

4.3.2 Clamping Voltage for BE Samples

The surge protection characteristics tested on BE varistor samples upon the discharge of peak surge currents, ranging between 10 kA and 15 kA, show the mean clamping voltage of 0.4 kV for non-degraded samples, and a mean clamping voltage value of 0.5 kV for both BEW and BEH ZnO arrester samples. This is indicated in table 4.3.

TABLE 4.3: Clamping Voltages

BE Samples	Clamping Voltage ($\overline{V}_c$) [kV]
Non-degraded	0.4
BEW	0.5
BEH	0.5

These values show that although the clamping voltage for degraded components is higher than non-degraded, there is however no difference in terms of the clamping voltage value of arresters subjected to higher or lower magnitude of harmonic content. The respective clamping or protection voltages are shown in figures 4.8, 4.9 and 4.10.

4.3.3 Probability Functions of BE Samples

The accelerated breakdown time-points (t_i) and the percentage cumulative degradation $F(i, n)$ obtained respectively from (3.2) and (2.3), are used to plot the CDF of the BEW

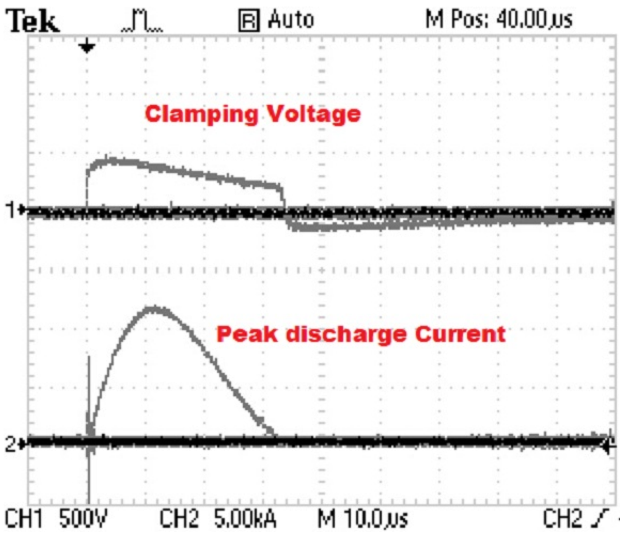

FIGURE 4.8: Clamping Voltage BE Samples

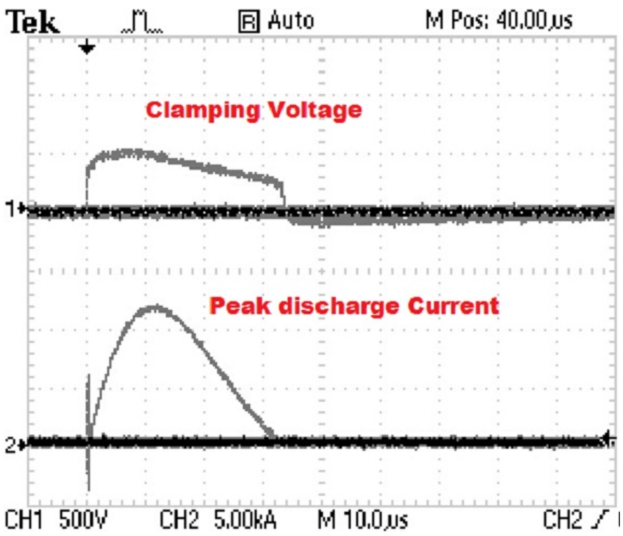

FIGURE 4.9: Clamping Voltage BEW Samples

and BEH time to degradation probability distribution. This is shown in figures 4.11 and 4.12, respectively. The time-points, the percentage cumulative degradation as well as the determination process of the distribution parameters are shown in Appendix C.
The correlation factors obtained for the BEW and BEH distributions, using equation (2.4), are found to be: $\eta_1 = 0.958317$ and $\eta_2 = 0.955857$. It could be seen that the obtained correlation coefficients are higher than the critical values shown in figure 2.1, which is an indication of good fit to the Weibull probability distributions. Applying the three-parameter Weibull probability distribution described above, the following parameters and functions are assigned to BEW samples: β_1, θ_1, γ_1, $h_1(t)$, $R_1(t)$ and $f_1(t)$. Similarly, β_2, θ_2, γ_2, $h_2(t)$, $R_2(t)$ and $f_2(t)$ are also assigned to the BEH samples. The shape and scale parameters obtained respectively from equations (2.5) and (2.6),

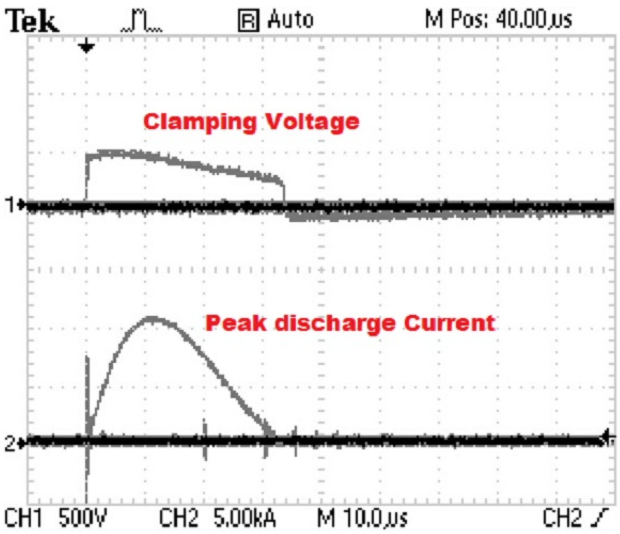

FIGURE 4.10: Clamping Voltage BEH Samples

for BEW and BEH distributions are indicated in table 4.4. From the CDF graphs described above, it could be shown that both distributions displayed the minimum time to degradation or location parameter of 100.6 hours.

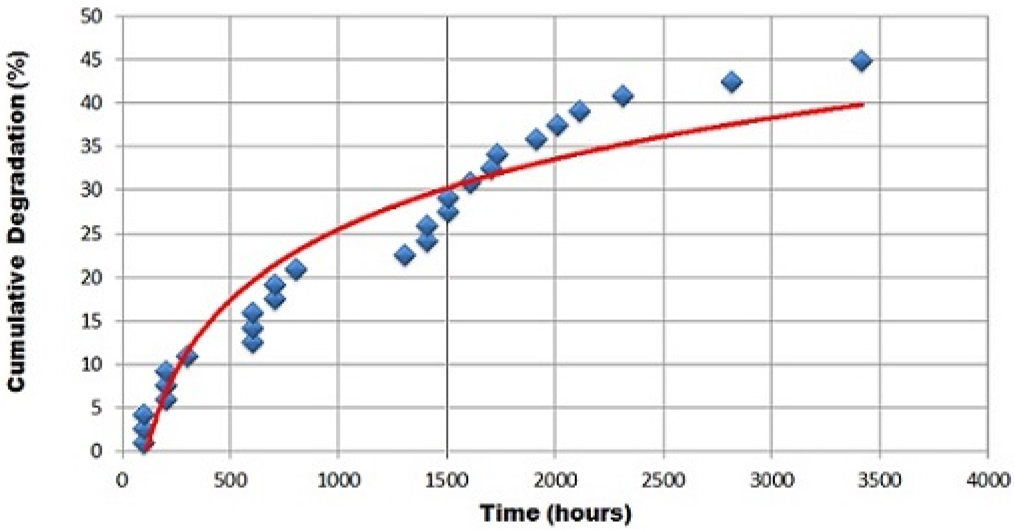

FIGURE 4.11: Cumulative Density Function BEW Samples

TABLE 4.4: Estimated Weibull Parameters of BEW and BEH distributions

Distributions	β	θ	γ
BEW	0.98	4167.6	100.6
BEH	1.093	2746.5	100.6

Applying the likelihood ratio test described in equation (4.5) yields a value of $z = 2.1460$ which is less than the corresponding chi-square distribution value (See Appendix D) at 0.01 significance level $\left(\chi^2_{0.01} = 6.635\right)$. This therefore favours the alternative hypothesis,

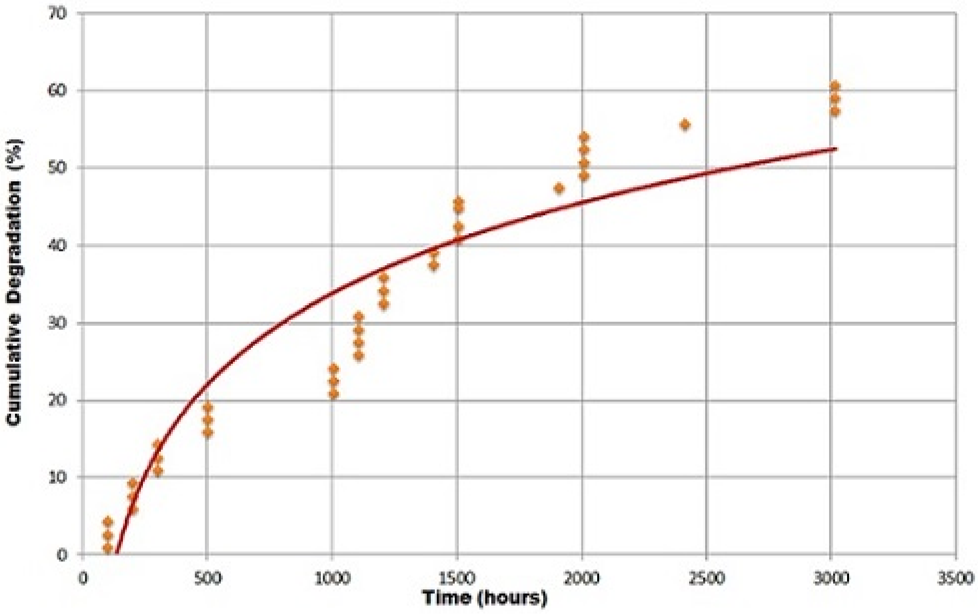

Figure 4.12: Cumulative Density Function BEH

and implies no possibility of similar degradation rate or reliability functions. The reliability and degradation rate graphs are shown in figures 4.13 and 4.14, respectively. These graphs indicate that BEH arrester samples show higher degradation rate and therefore prove to be less reliable than BEW arrester samples across the observed time-interval. The obtained PDF curves of the BEW and BEH arrester populations are also shown in figure 4.15. This indicates higher density of degradation when higher harmonics are present in the applied voltage.

The mean life of these arrester populations can be determined using equation (4.6). This equation indicates that the mean life of BEW arrester population is found to be 4252.65 hours. On the other end, the mean life of the BEH arrester population is worked out to be 2512.81 hours. This shows that arrester population degraded in the presence of an external source of harmonics experienced 40.91% reduction in terms of their mean life value, which is in agreement with the plotted curves of the reliability and degradation rate functions of these respective ZnO arrester populations.

The results obtained from the percentile or B-live and the acceleration factor test conducted on BE samples are indicated in table 4.5. These results show that for the same observed proportion of arresters, the time to degradation for BEH arrester devices is shorter than that of BEW arrester samples. The time reduction factor at 10%, 50% and 90% reliability can also be determined using equation (4.8). This shows that the time ratio or life reduction factor, as obtained at indicated reliability points, is not uniform and shows a decreasing trend. This therefore implies a non-uniform increasing trend of the degradation rate.

TABLE 4.5: Degradation times of $p\%$ Arrester Components

$p\%$	t_p BEW [hour]	t_p BEH [hour]	δ_{xy} (x = BEH, y = BEW)
10	519.99	451.04	0.87
50	2967.8	2064.6	0.70
90	9861.6	5991.4	0.61

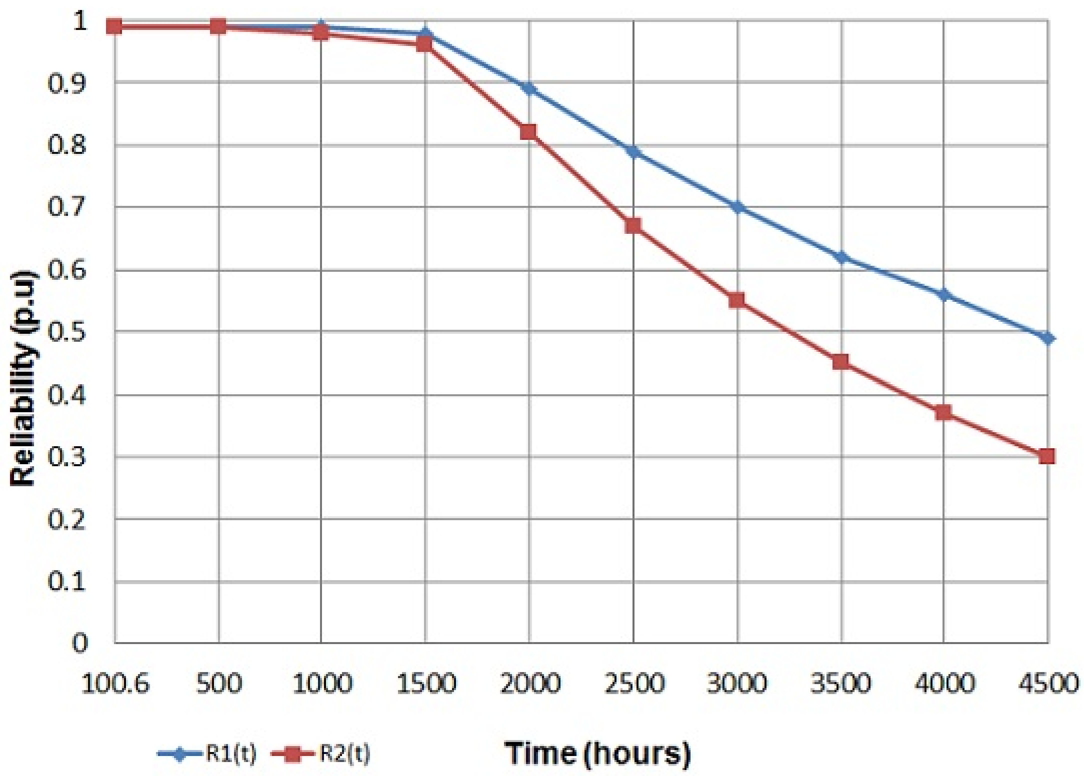

FIGURE 4.13: Reliability curves BEW and BEH Samples

The probability $Pr\,[t_2 \geq t_1]$ is determined using equation (4.9). This yields 0.4107 or 41.07% probability of BEW arrester devices experiencing shorter degradation time than BEH. Therefore, the probability of reduced degradation time for BEH arrester should be: $Pr\,[t_1 \geq t_2]$ = 1 - $Pr\,[t_2 \geq t_1]$ = 0.5893 or 58.93%.

4.4 Case Study 2: Analysis of YW Varistor Samples

The electrical characteristics of the ZnO arrester population identified as YWW and YWH are analysed and compared, on the basis of the $V - I$ characteristic curve and coefficient of non-linearity, the clamping voltage and the probability functions of the time to degradation distribution obtained. The time-domain of the continuous applied ac voltage stress across YWW samples is shown in figure 4.16. The frequency components associated to this voltage are indicated in figure 4.17. The level of harmonic components

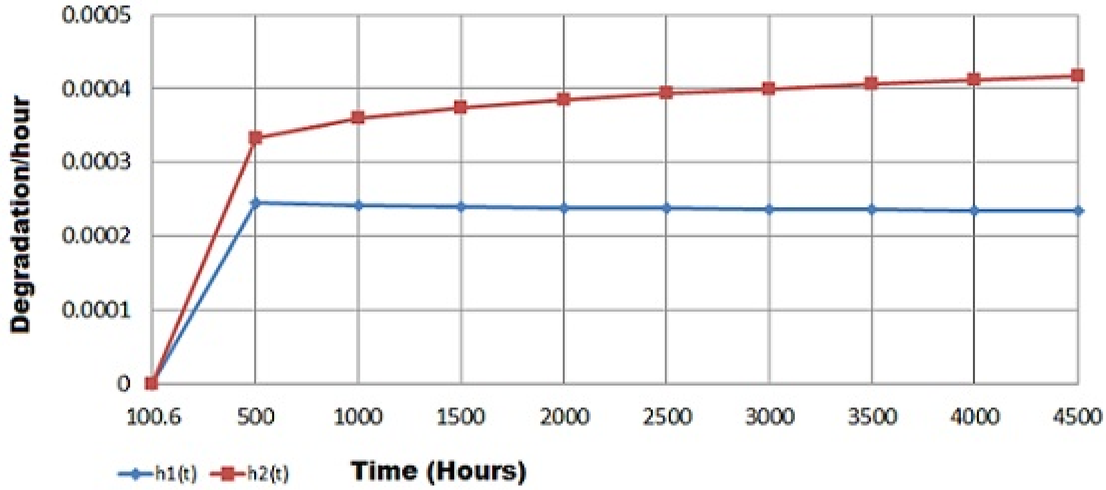

FIGURE 4.14: Degradation rate curves BEW and BEH Samples

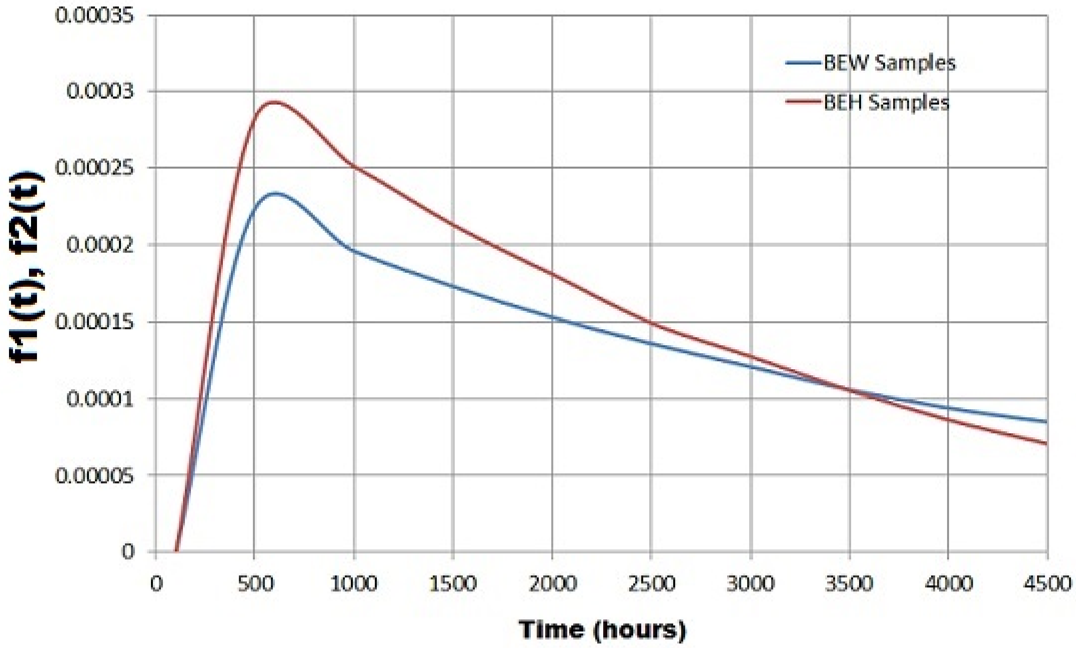

FIGURE 4.15: Probability Density Functions BEW and BEH Samples

is found to be 1.28% for the 3^{rd}, 1.89% for the 5^{th} and 0.72% for the 7^{th} (See Appendix B). The time-domain of the continuous applied ac voltage stress across YWH samples is shown in figure 4.18, and the frequency components associated to the voltage across YWH samples are indicated in figure 4.19. The level of harmonic components are as follows: 9.8% for the 3^{rd}, 6.9% for the 5^{th} and 5.8% for the 7^{th} (See Appendix B).

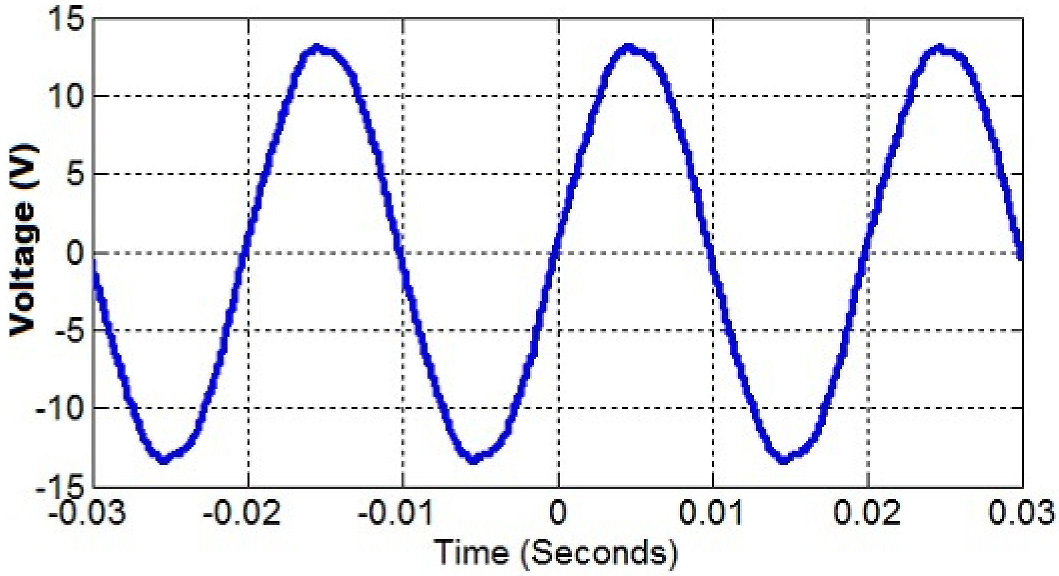

FIGURE 4.16: Applied Voltage Stress YWW

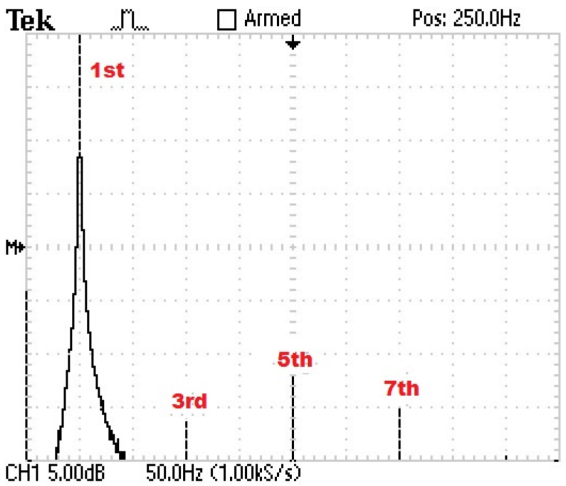

FIGURE 4.17: Frequency Components YWW

4.4.1 V-I curve and Coefficient of non-linearity

The $V-I$ measurements of both the YWW and YWH samples (See Appendix B) enable the classification of the tested ZnO arresters be conducted on the basis of the conditions described in 3.4.2. This is indicated in table 4.6.

TABLE 4.6: Classification of Tested YW Samples

YW Sample Group	Degraded	Survived	Spoiled
YWW	36	11	13
YWH	47	6	7

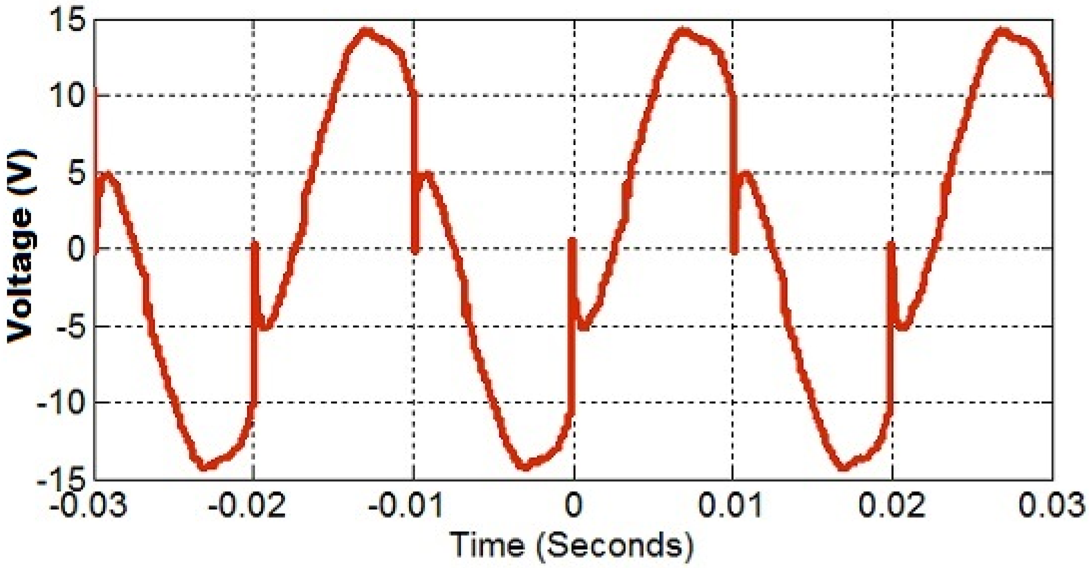

FIGURE 4.18: Applied Voltage Stress YWH

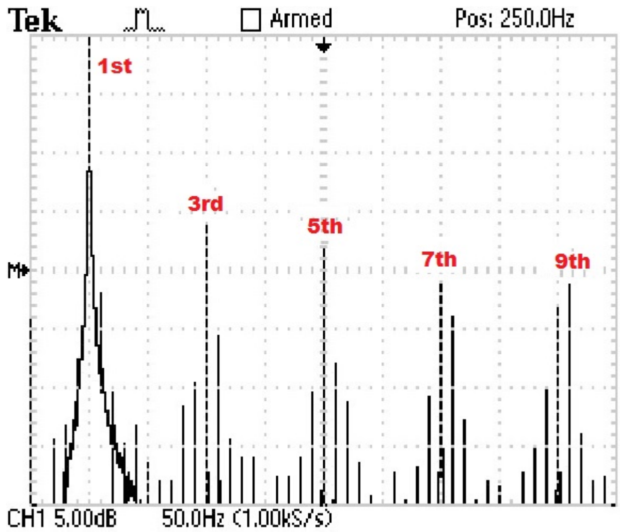

FIGURE 4.19: Frequency Components YWH

The $V-I$ characteristic of the degraded YWW and YWH samples, is plotted, and the variation of the V_{1mAdc} can thus be observed to be 40.49 % for the YWW and 65.64 % for the YWH samples. The mean $V-I$ curve of these samples is provided in figure 4.20. The coefficient of non-linearity deduced from the plotted $V-I$ characteristic yields the following: before degradation the mean coefficient of non-linearity for YW samples is found to be 48, and after degradation this coefficient is worked out to be 14, which represents 70.83% reduction for YWW samples, and mean value of 12, which shows 75.00% reduction for YWH samples. These values are indicated in table 4.7. It can be observed that the stability of YWH arrester samples is further compromised.

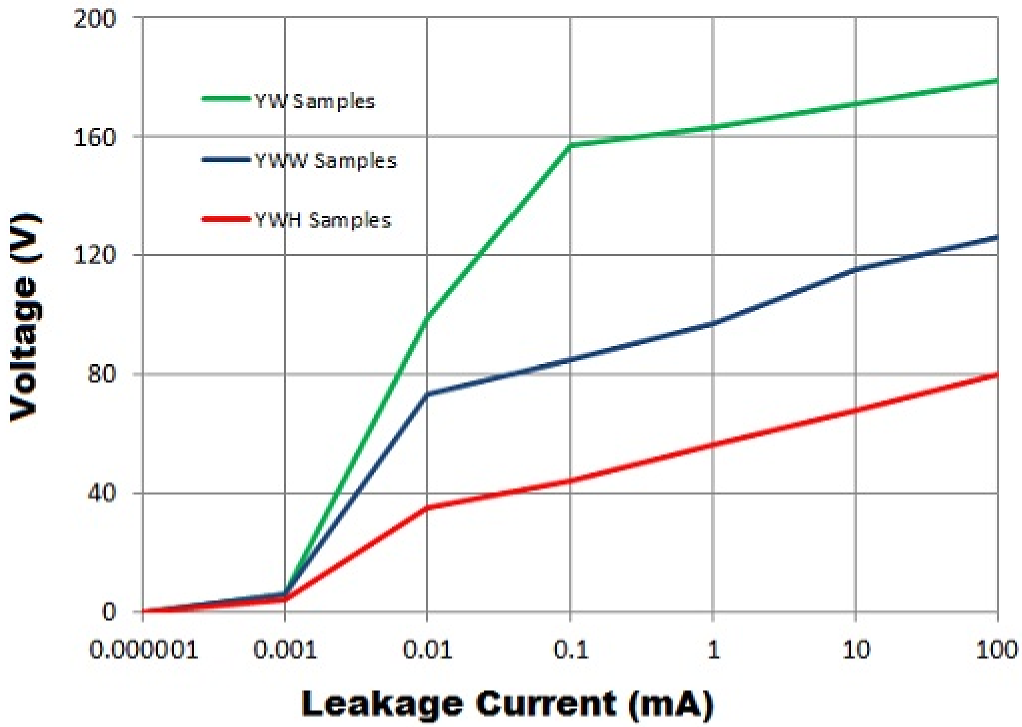

FIGURE 4.20: V-I curve YW Samples

TABLE 4.7: Change in Reference Voltage and Coefficient of non-linearity (YW Samples)

YW Samples	$\bar{V}_{1mAdc}$ [V]	α	$\Delta\bar{V}_{1mAdc}$ (%)	$\Delta\alpha$ (%)
Non-degraded	163	48	-	-
YWW	97	14	40.49	70.83
YWH	56	12	65.64	75.00

4.4.2 Clamping Voltage for YW Samples

Both YWW and YWH arrester samples subjected to peak surge currents, ranging between 10 kA and 15 kA, display an increase of the protection or clamping voltage as compared to samples not subjected to the degradation process. These values show that although the clamping voltage for degraded components is higher than non-degraded, there is however no difference in terms of the clamping voltage value of arresters subjected to higher or lower magnitude of harmonic content. This is indicated in table 4.8.

Table 4.8: Clamping Voltages YW Samples

YW Samples	Clamping Voltage ($\overline{V}_c$) [kV]
Non-degraded	0.35 - 0.4
YWW	0.4 - 0.5
YWH	0.4 - 0.5

The respective clamping or protection voltages are shown in figures 4.21, 4.22 and 4.23.

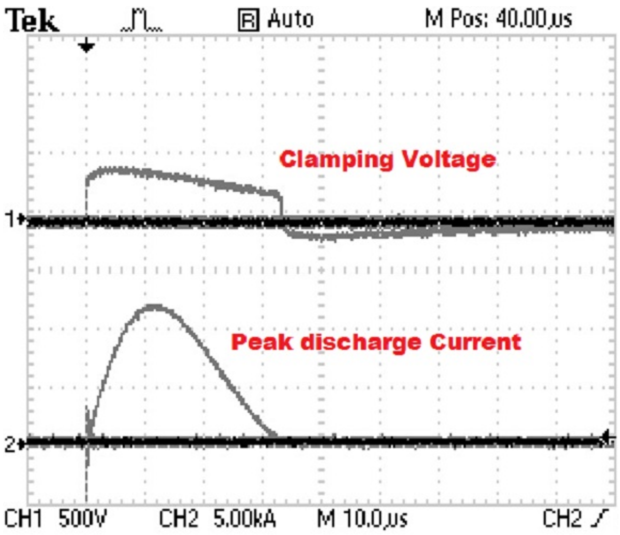

Figure 4.21: Clamping Voltage YW Samples

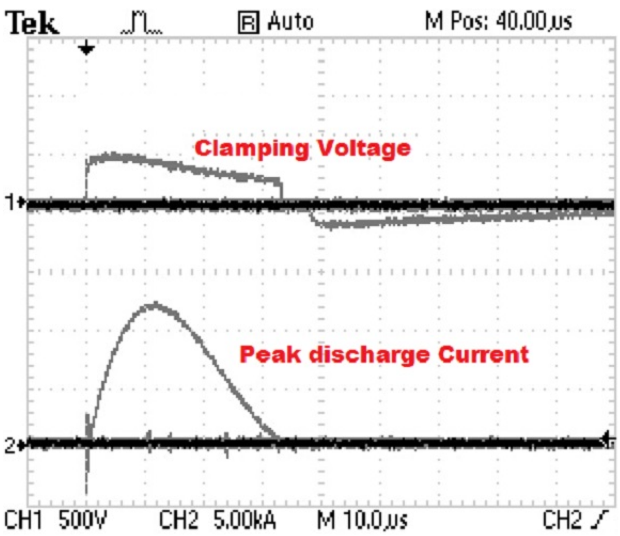

Figure 4.22: Clamping Voltage YWW Samples

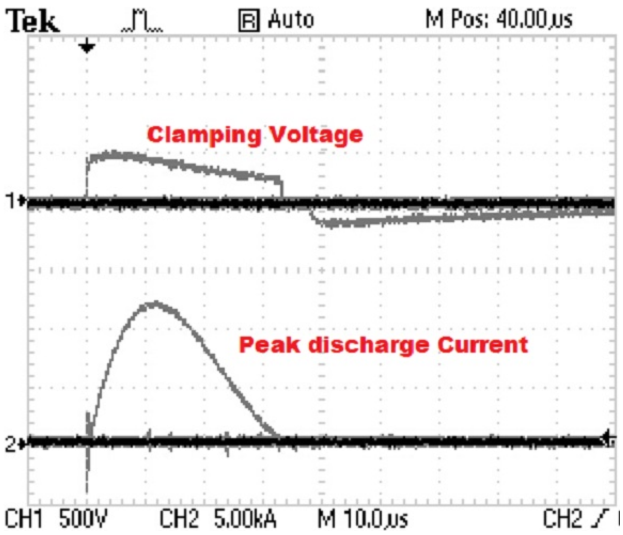

FIGURE 4.23: Clamping Voltage YWH Samples

4.4.3 Probability Functions of YW Samples

Using the breakdown time-points (t_i) and the percentage cumulative degradation $F(i, n)$ relative to the YWW and YWH samples (See Appendix C), the respective CDF can therefore be plotted. This is indicated in figures 4.24 and 4.25.

The CDF obtained show good fit to the Weibull probability distribution, with correlation factors of 0.935602 and 0.951579 for the YWW and YWH arrester population, respectively. The estimated parameters of these distributions are indicated in table 4.9. The likelihood ratio test is found to be 0.63976 which therefore rules out any possibility of similar degradation or reliability functions for both distributions (See Appendix D). Based on the reliability and degradation rate functions obtained, it can be seen that the YWH arrester population showed higher degradation rate as compared to the YWW varistors. This therefore proves low reliability. The reliability and degradation graphs of the YWW and YWH arrester populations are shown in figures 4.26 and 4.27, respectively. The mean life of YWW and YWH ZnO arrester population is obtained using relationship (4.6). This shows that the mean life time of YWW arrester population is 863.288 hours, whereas that of the YWH varistors is determined to be 538.464 hours. This indicates that YWH arresters experienced 37.63% reduction in terms of their mean life value, which is confirmed in the reliability curves.

The reliability and degradation rate graphs demonstrate that the YWH arrester population have higher degradation rate and therefore lower reliability compared to the YWW population. This can also be confirmed in terms of the PDF curves which show higher density of degradation for YWH arrester devices. This is shown in figure 4.28. The percentile test results indicated in table 4.10, demonstrates that for any similar $p\%$ of arresters, the time to degradation for YWH is shorter than that of YWW arrester population.

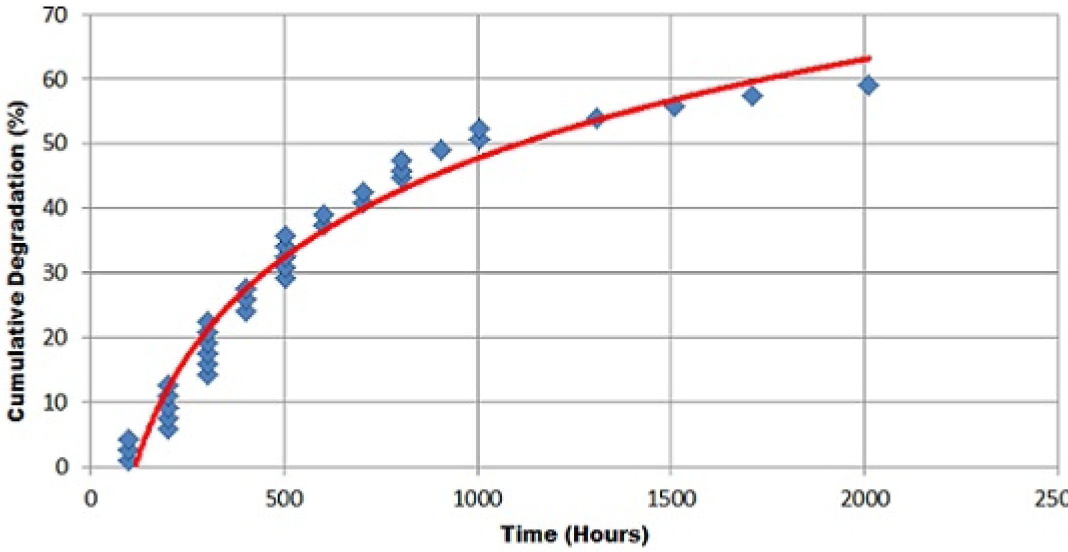

FIGURE 4.24: Cumulative Density Function YWW Samples

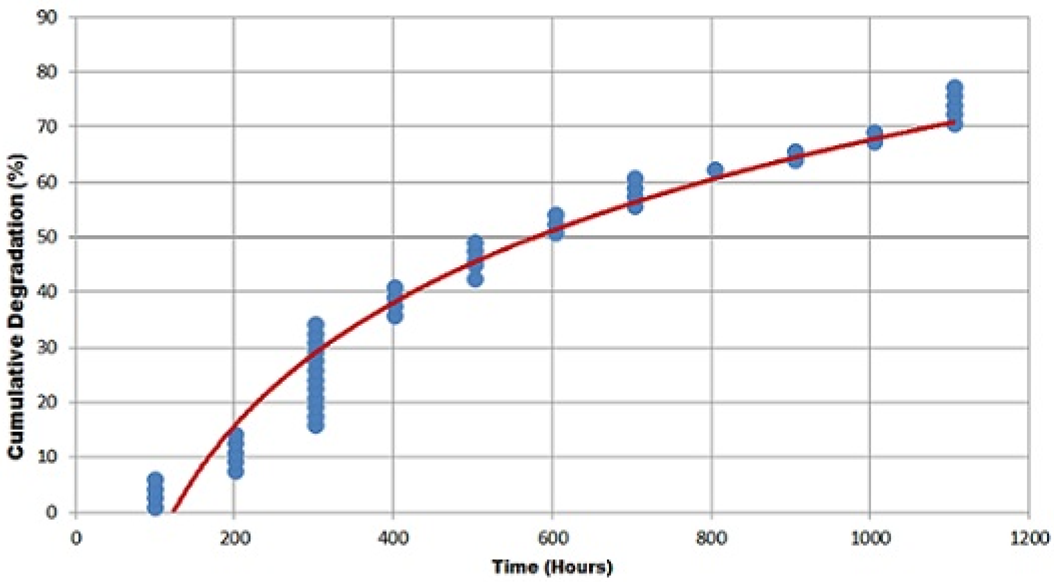

FIGURE 4.25: Cumulative Density Function YWH Samples

The time reduction factor at 10%, 50% and 90% reliability are determined using (4.8). This shows that the life reduction factor for YWH arrester samples, at the observed reliability points, is decreasingly trending at not uniform. The probability $Pr\left[t_2 \geq t_1\right]$ is determined using equation (4.9). This yields 0.2384 or 23.84% probability of YWW arrester devices experiencing shorter degradation time than YWH. Therefore, the probability of reduced degradation time for YWH arrester should be: $Pr\left[t_1 \geq t_2\right] = 1 - Pr\left[t_2 \geq t_1\right] = 0.7616$ or 76.16%.

Table 4.9: Estimated Weibull Parameters of YWW and YWH distributions

Distributions	β	θ	η
YWW	1.46	1103.3	100.6
YWH	1.71	726.68	100.6

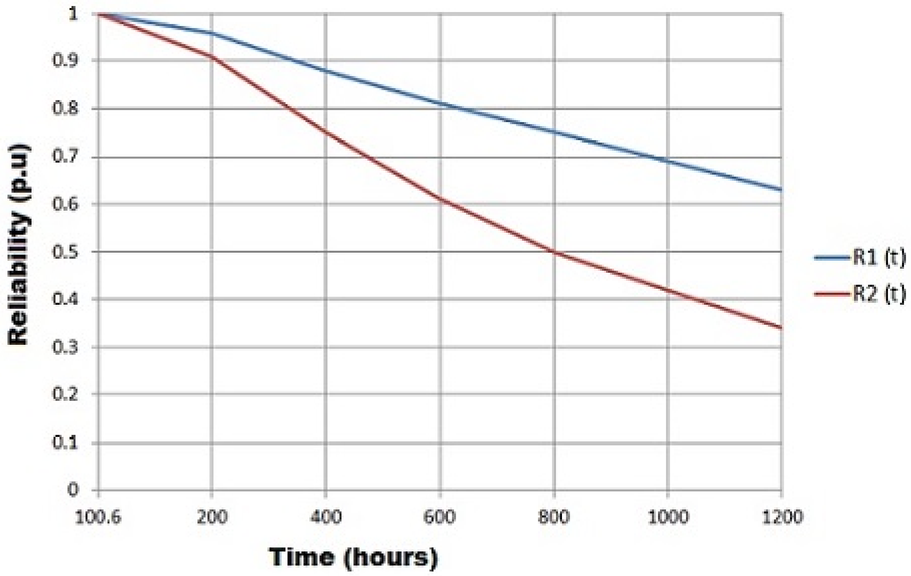

Figure 4.26: Reliability Curves YWW and YWH Samples

Table 4.10: Degradation times of p% Arrester Components

p%	t_p YWW [hour]	t_p YWH [hour]	δ_{xy} (x = YWH, y = YWW)
10	336.81	295.5	0.88
50	958.96	687.09	0.72
90	2054	1284.1	0.63

4.5 Case study 3: Analysis of RL Varistor Samples

The electrical characteristics of the ZnO arrester population identified as RLW and RLH are analysed and compared, on the basis of the $V-I$ characteristic curve and coefficient of non-linearity, the clamping voltage and the probability functions. The time-domain of the continuous applied ac voltage stress across RLW samples is shown in figure 4.29, and the frequency components associated to this voltage are indicated in figure 4.30. The level of harmonic components is found to be 1.49% for the 3^{rd}, 2.65% for the 5^{th} and 0.12% for the 7^{th} (See Appendix B).
The time-domain of the continuous applied ac voltage stress across RLH samples is shown in figure 4.31, and The frequency components associated to the voltage across RLH samples are indicated in figure 4.32. The level of harmonic components are as follows: 4.5% for the 3^{rd}, 5.5% for the 5^{th} and 4.7% for the 7^{th} (See Appendix B).

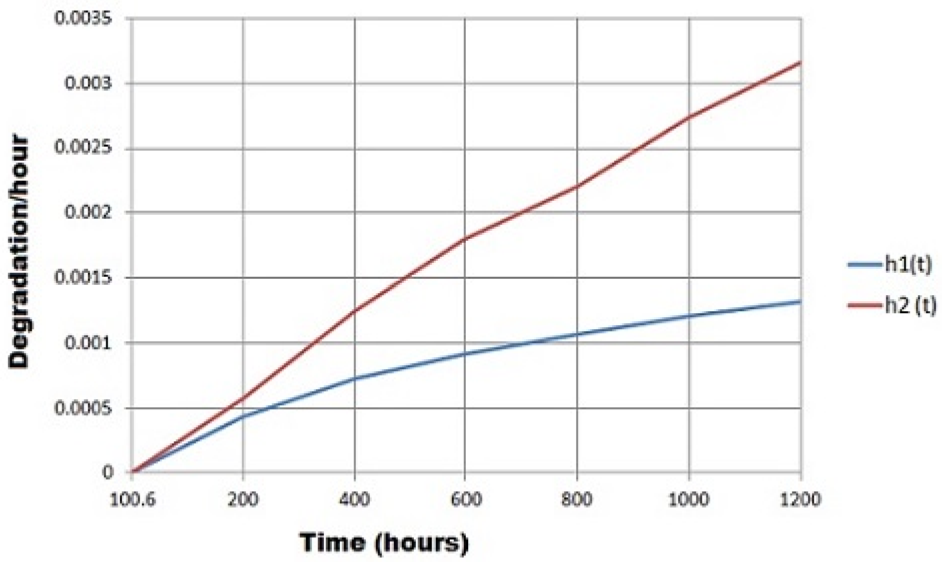

FIGURE 4.27: Degradation rate curves YWW and YWH Samples

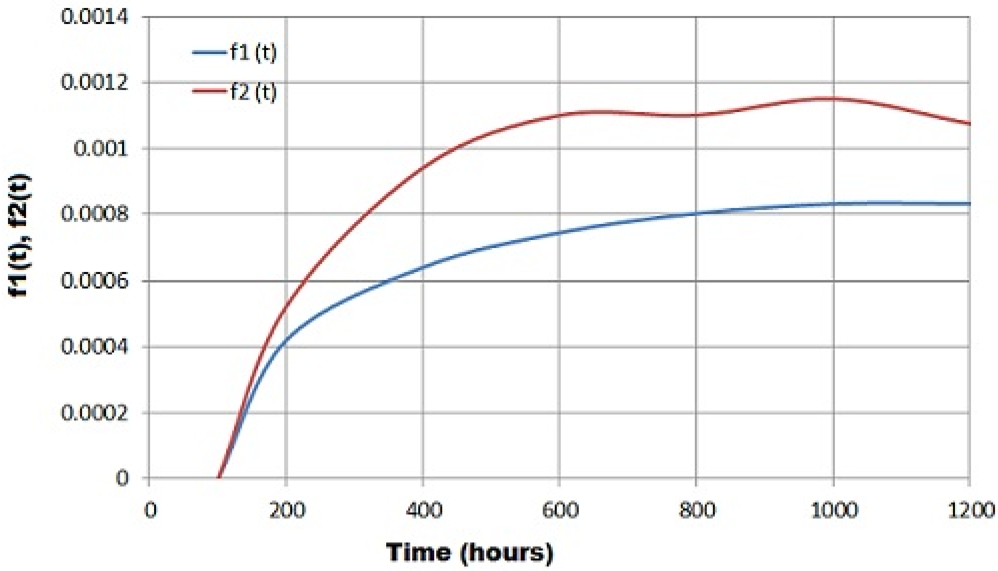

FIGURE 4.28: Probability Density Function YWW and YWH Samples

4.5.1 V-I curve and Coefficient of non-linearity

The $V - I$ measurements of the RLW and RLH samples (See Appendix B) render the classification of the tested devices possible. This classification is conducted on the basis of the conditions described in 3.4.2, provides a classification of the samples after accelerated degradation test. This is indicated in table 4.11. The $V - I$ characteristic of the degraded RLW and RLH samples, is plotted, and the variation of the V_{1mAdc} can thus be observed to be 49.14 % for the RLW and 66.29 % for the RLH samples. The $V - I$ curve of these samples is provided in figure 4.33.

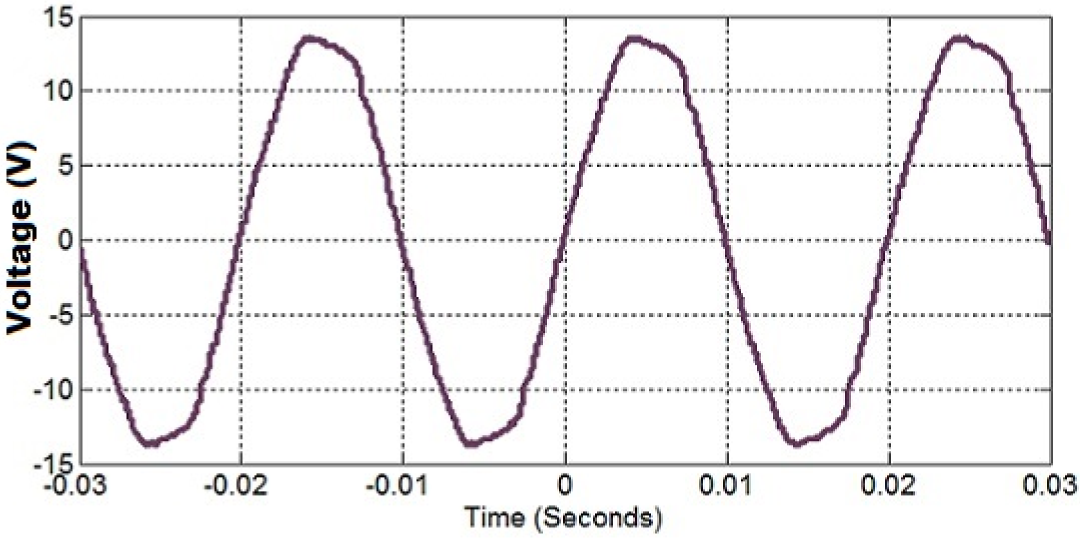

Figure 4.29: Applied Voltage Stress RLW

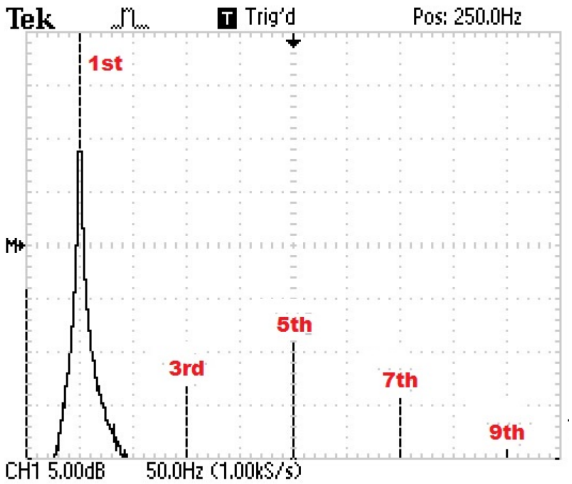

Figure 4.30: Frequency Components RLW

The coefficient of non-linearity obtained from the plotted $V - I$ characteristic reveals the following: before degradation the average coefficient of non-linearity for RL samples is found to be 52, and after degradation this coefficient is worked out to be 17, which represents 67.31% reduction for RLW samples, and mean value of 12, which shows 76.92% reduction for RLH samples. These values are shown in table 4.12.

Table 4.11: Classification of Tested RL Samples

RL Sample Group	Degraded	Survived	Spoiled
RLW	41	12	7
RLH	56	1	3

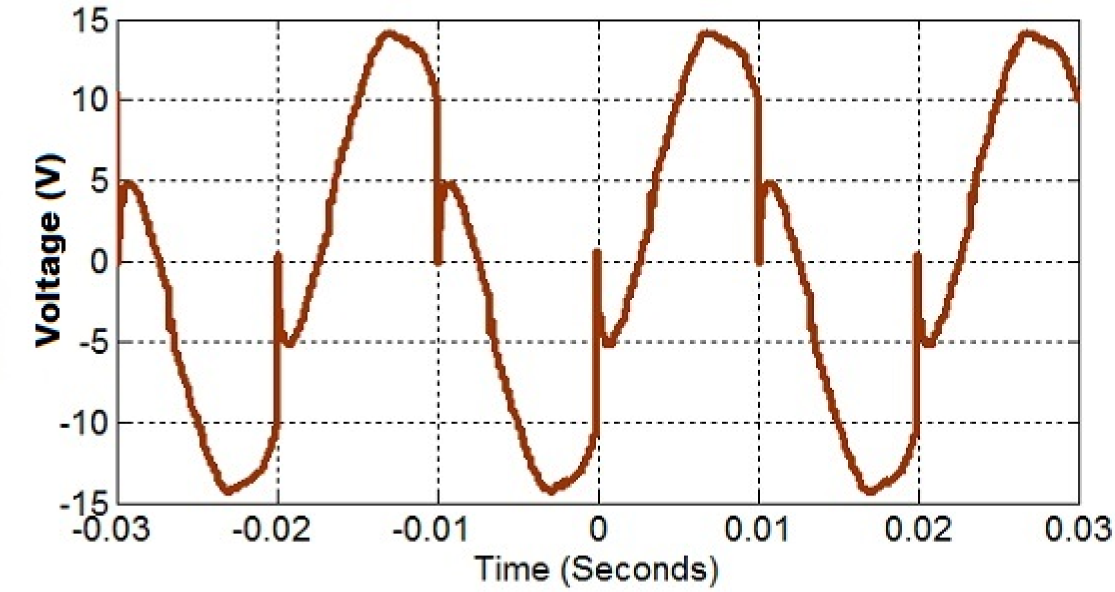

FIGURE 4.31: Applied Voltage Stress RLH

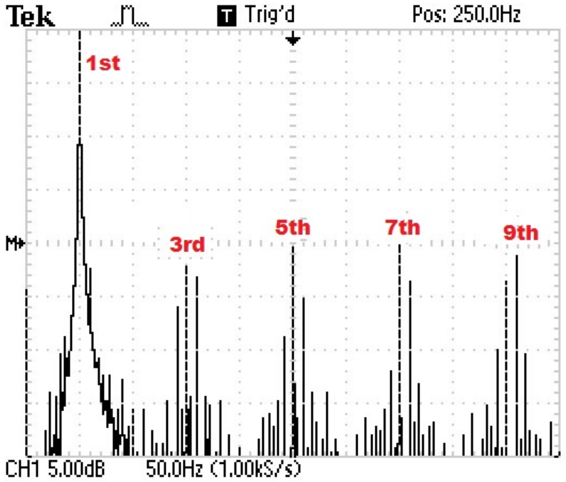

FIGURE 4.32: Frequency Components RLH

4.5.2 Clamping Voltage for RL Samples

The RLW and RLH arrester samples subjected to peak surge currents, ranging between 10 kA and 15 kA, show increase of the clamping voltage as compared to the samples not subjected to the degradation process. These values show that although the clamping voltage for degraded components is higher than non-degraded, there is however no difference in terms of the clamping voltage value of arresters subjected to higher or lower magnitude of harmonic content. This is indicated in table 4.13, and the respective clamping or protection voltages are shown in figures 4.34, 4.35 and 4.36.

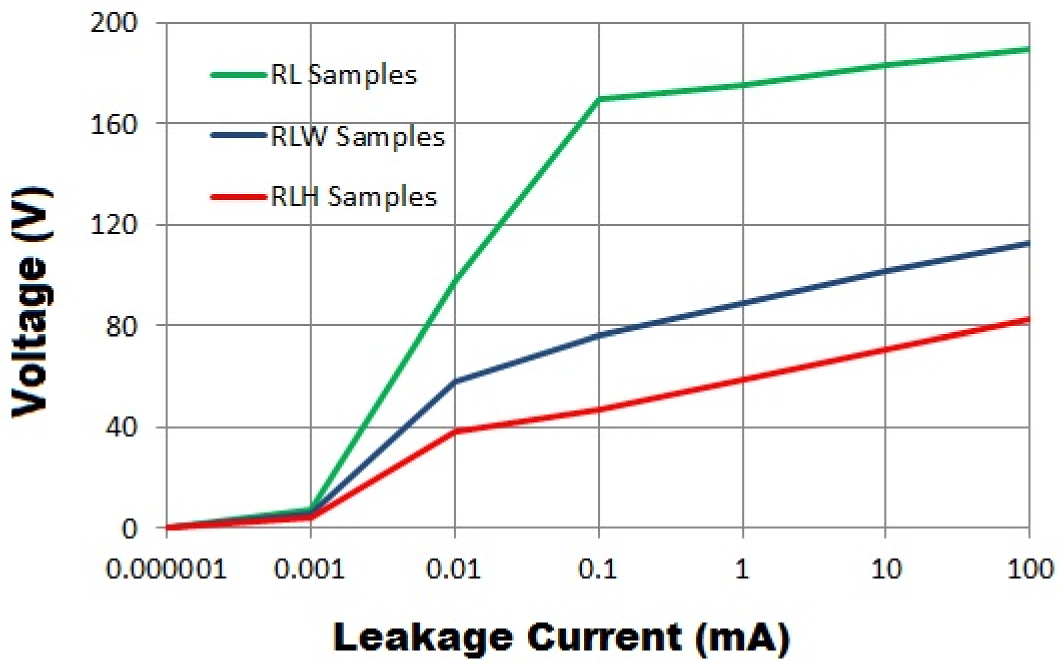

FIGURE 4.33: V-I curve RL Samples

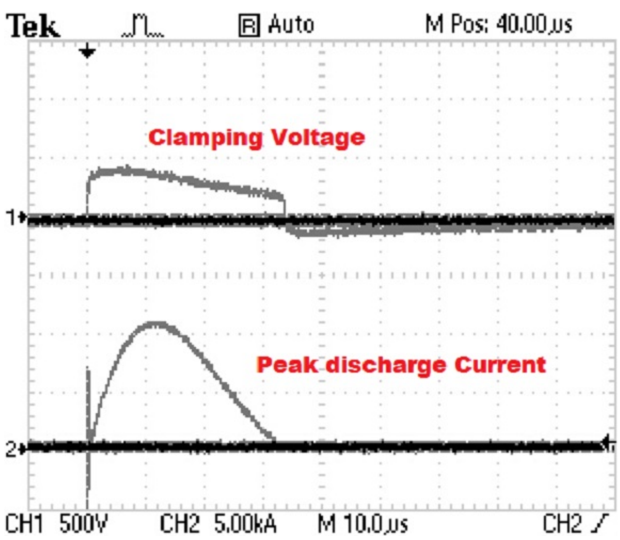

FIGURE 4.34: Clamping Voltage RL Samples

TABLE 4.12: Change in Reference Voltage and Coefficient of non-linearity (RL Samples)

RL Samples	$\overline{V}_{1mAdc}$ [V]	α	$\Delta\overline{V}_{1mAdc}$ (%)	$\Delta\alpha$ (%)
Non-degraded	175	52	-	-
RLW	89	17	49.14	67.31
RLH	59	12	66.29	76.92

TABLE 4.13: Clamping Voltages for RL Samples

YW Samples	Clamping Voltages ($\overline{V}_c$) [kV]
Non-degraded	0.35 - 0.4
RLW	0.4 - 0.5
RLH	0.4 - 0.5

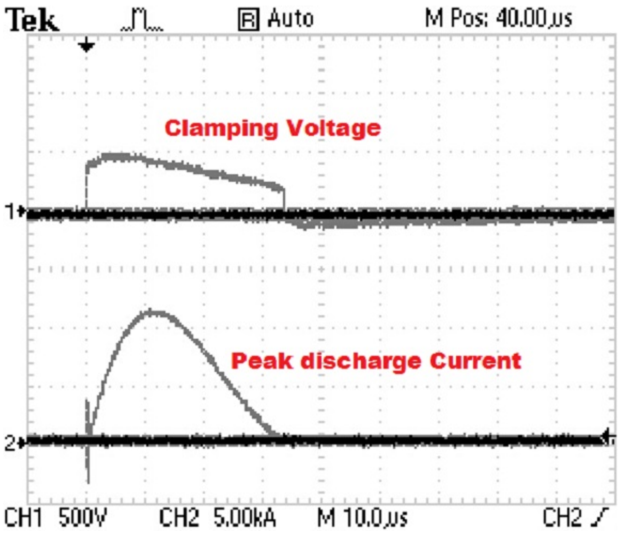

FIGURE 4.35: Clamping Voltage RLW Samples

4.5.3 Probability Functions of RL Samples

The breakdown time-points (t_i) and the percentage cumulative degradation $F(i, n)$ relative to the RLW and RLH arrester populations (See Appendix C), are used to plot the respective CDF of the probability distributions obtained. This is indicated in figures 4.37 and 4.38.
The CDF obtained show good fit to the Weibull probability distribution; this is supported by the correlation factors obtained: 0.969156 and 0.974395 for the RLW and RLH arrester population, respectively. The estimated parameters of these distributions are therefore given in table 4.14.

The likelihood ratio test is found to be -1.2855 which rules out any possibility of similar degradation rate and reliability functions for both distributions (See Appendix D). Based on the degradation rate and reliability function, it could be observed that the RLH

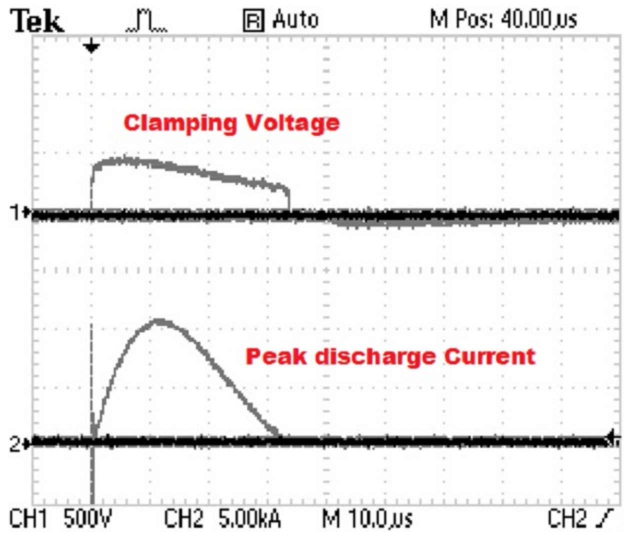

FIGURE 4.36: Clamping Voltage RLH Samples

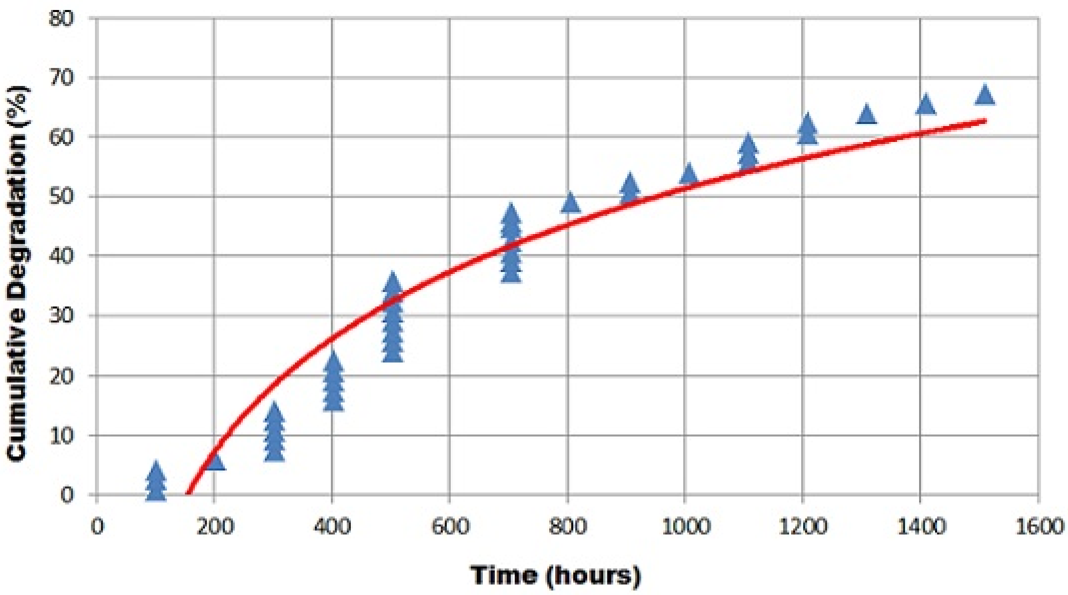

FIGURE 4.37: Cumulative Density Function RLW Samples

TABLE 4.14: Estimated Weibull Parameters of RLW and RLH distributions

Distributions	β	θ	η
RLW	1.63	1079.4	100.6
RLH	1.8	765.22	100.6

arrester population are likely to experience shorter time to degradation as compared to the RLW arrester samples. The reliability and degradation graphs of the RLW and RLH arrester populations are shown in figures 4.39 and 4.40, respectively. The mean life of RLW and RLH ZnO arrester population is obtained using relationship (4.6). This shows that the mean life time of RLW arrester population is 770.852 hours, whereas that of

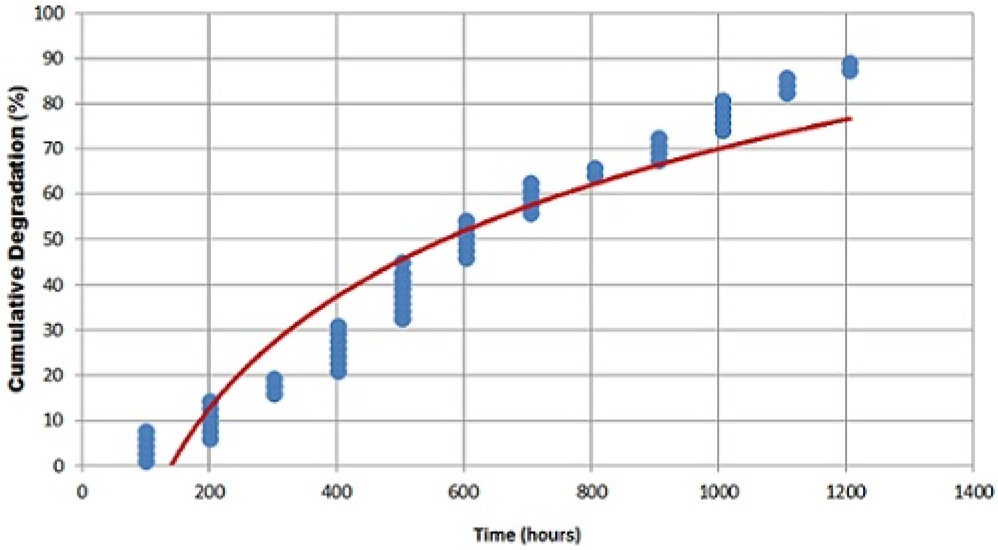

FIGURE 4.38: Cumulative Density Function RLH Samples

the RLH varistors is determined to be 538.622 hours. Therefore, a 30.13% reduction in terms of the mean life is recorded.

The reliability and degradation rate graphs demonstrate that the RLH arrester population display higher degradation rate and therefore lower reliability compared to the RLW population. This can also be confirmed in terms of the PDF curves shown in figure 4.41, which indicates higher density of degraded RLH arrester samples. The percentile and time reduction test results indicated in table 4.15, which demonstrate that for any similar $p\%$ of arresters, the time to degradation for RLH is shorter than that of RLW arrester population.

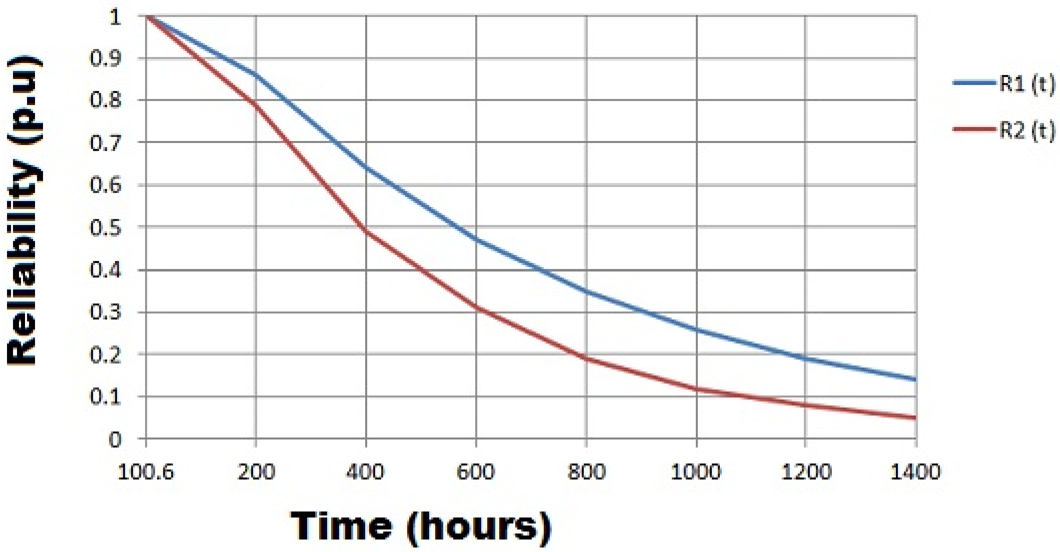

FIGURE 4.39: Reliability curves RLW and RLH Samples

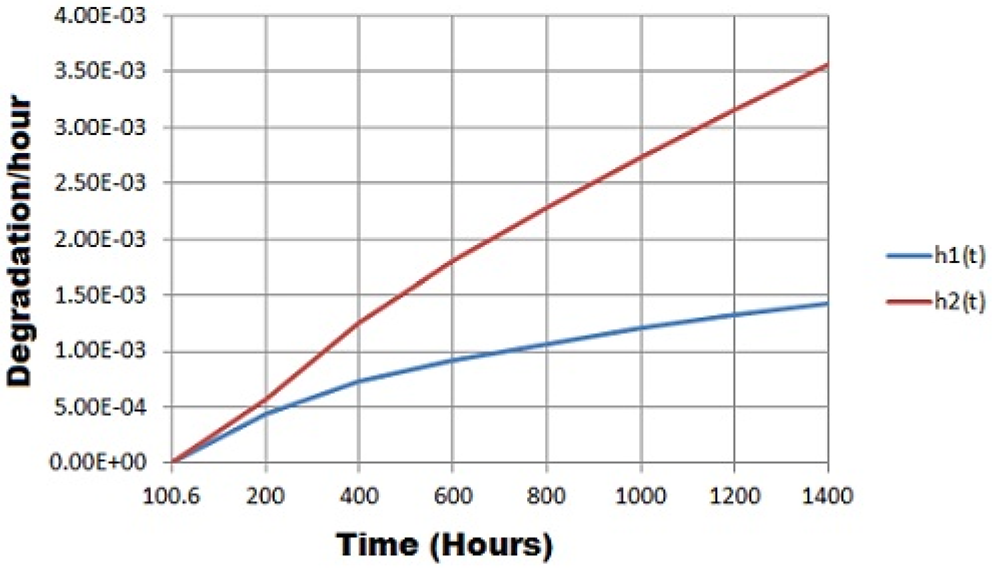

Figure 4.40: Degradation rate curves RLW and RLH Samples

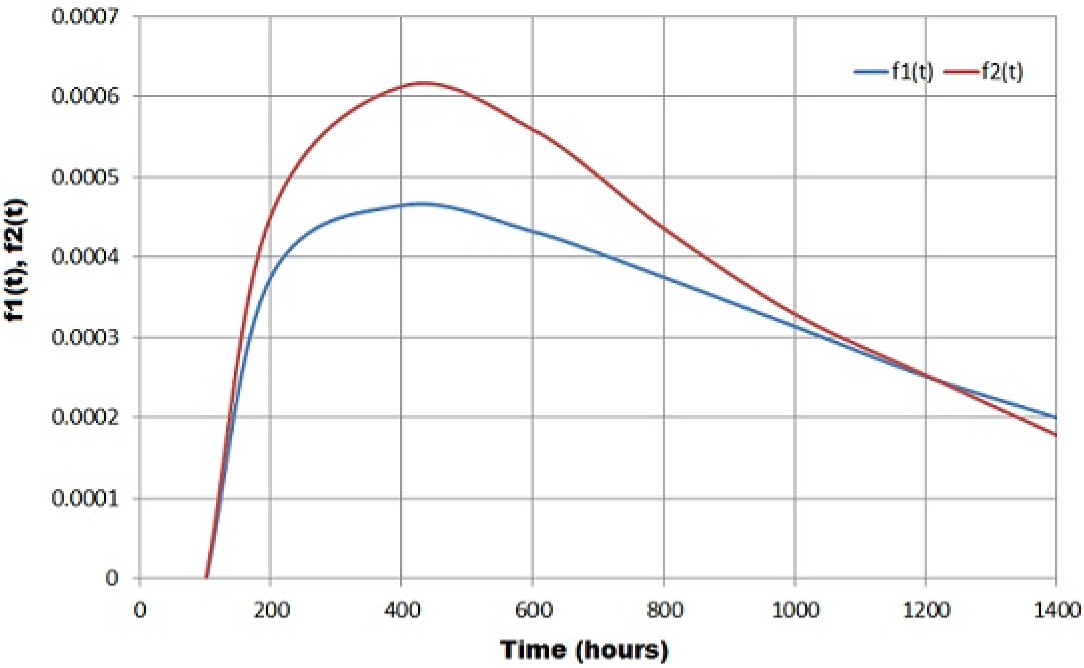

Figure 4.41: Probability Density Function RLW and RLH Samples

TABLE 4.15: Degradation times of p% Arrester Components

p%	t_p RLW [hour]	t_p RLH [hour]	δ_{xy} (x = RLH, y = RLW)
10	371.99	319.79	0.86
50	962.64	724.85	0.75
90	1901.1	1316.8	0.69

The time reduction factor observed at 10%, 50% and 90% reliability points are determined using (4.8). This shows that the time or life reduction shows non-uniform decreasing trend. The probability $Pr\,[t_2 \geq t_1]$ is determined using equation (4.9). This yields 0.2900 or 29.00% probability of RLW arrester devices experiencing shorter degradation time than RLH. Therefore, the probability of reduced degradation time for RLH arrester should be: $Pr\,[t_1 \geq t_2]$ = 1 - $Pr\,[t_2 \geq t_1]$ = 0.70991 or 70.99%.

4.6 Conclusion

In this section, the three-parameter Weibull probability distribution is applied to analyse the probability of aggravated electrical degradation of ZnO arrester populations, subjected to thermal and distorted ac voltage stress. The distortion is originated from an external source of harmonics. The electrical stability of ZnO devices is also tested on the basis of the $V-I$ characteristic curve and the coefficient of non-linearity. The protection function of arrester devices is equally analysed using the clamping voltage measurement. In all the three case studies presented in this chapter, arrester devices degraded in the presence of external harmonics showed the following: significant reduction in the mean life (40.91% for BE, 37.63% for YW and 30.13% for RL samples); non-uniform decreasing reliability trend and therefore increasing degradation at non-uniform rate; and a higher probability of reduced time to degradation (58.93% for BEH, 76.16% for the YWH and 70.99% for the RLH). The CDF observed across the three case studies, shows higher value of the estimated shape parameter and lower value of the estimated scale parameter, for the time to degradation probability distribution of arresters degraded in the presence of external harmonics. The possibility of estimated parameters of one distribution being equal to the other is ruled on the strength of the likelihood ratio test results obtained in each of the cases observed. This therefore implies that higher harmonic components embedded in the applied voltage stress results in higher degradation or failure rate and therefore lower reliability, which consequently promote higher density of degraded arrester devices, significant reduction of the mean life as a result of a higher time acceleration factor as well as a higher probability of reduced time to degradation. On the other end, the electrical stability of ZnO devices, subjected to accelerated degradation with external harmonics in the applied voltage stress, supported the observations made in terms of the probability functions. It could be noticed in the case studies undertaken that the mean values of the reference voltage and the coefficient of non-linearity are significantly reduced for the arrester samples subjected to external harmonics. The BEH arresters declined by 43.75% and 81.71% in terms of the reference voltage and the coefficient of non-linearity, respectively. The YWH observed a decrease of 65.64% in the reference voltage and of 75% in the coefficient of non-linearity. The RLH in turn showed a decline of 66.29% and 76.92% in terms the reference voltage and the coefficient of non-linearity. Although an increase in the clamping voltage is observed in some of the cases observed, it could be observed that the effect of external harmonics on the protection quality is not significantly pronounced given the similar margin of the clamping voltage value measured before and after degradation with external harmonics.

Chapter 5

The Effect of Voltage Harmonics on the Resistive Current

5.1 Introduction

In the previous chapter, the influence of harmonics on the probability of accelerated or aggravated electrical degradation is mainly approached on the basis of the mean time to degradation, the comparison of the $V-I$ characteristic of MOV samples, as well as in terms of the surge clamping performance. In this section, an attempt to analyse the observed lifetime reduction and accelerated loss of stability of MOV samples in terms of the resistive component of the total leakage current is undertaken. Therefore, the impact of externally applied distorted voltage on the behaviour of the resistive current and consequently on the mechanism of electrical degradation is also described. The CSV measurements of the leakage current spectrum, obtained in both conditions of the accelerated degradation test, are used in conjunction with the Fourier's expansion-based technique to decompose the total leakage current. The ion migration and diffusion theories are examined in the light of distorted applied field stress.

5.2 Decomposition of the Leakage Current

The knowledge of the resistive component of the total leakage current of ZnO arrester is essential to the condition or health assessment of these devices [30]–[35]. Given the distorted and periodic nature of the total leakage current and the applied voltage waveforms measured across ZnO arresters, the generalised Fourier's expression of a distorted signal can be applied to model these measured electrical quantities (leakage current and applied voltage) of varistor arresters. From this model, the instantaneous power equation, which consists of the active and reactive component, can be further developed. Since the power losses experienced by surge arresters subjected to distorted voltage are determined by the summation of power losses resulting from each component in the applied voltage [36, 65, 66, 67]. The resistive current component is therefore derived from the active or resistive power equation resulting from all frequency components in the applied voltage. The generalised Fourier's expression of a distorted signal is written as follows[68, 69]:

$$i\left(t\right)=\frac{a_o}{2}+\sum_{h=0}^{2}\left[a_{(2h+1)}\cos\omega_{(2h+1)}t+b_{(2h+1)}\sin\omega_{(2h+1)}t\right] \tag{5.1}$$

Where: $i\left(t\right)$ is the leakage current function; h is an integer, $a_o=\frac{2}{T}\int\limits_0^T i\left(t\right)dt$, $a_{(2h+1)}=\frac{2}{T}\int\limits_0^T i\left(t\right)\cdot(cos(2h+1)t)\,dt$ and $b_{(2h+1)}=\frac{2}{T}\int\limits_0^T i\left(t\right)\cdot(sin(2h+1)t)\,dt$, are Fourier coefficients of respective harmonic frequencies, and T, is the period of the function.

In order to evaluate the Fourier coefficients, the following 20 equally divided time-points across the full cycle of the waveform $(18^o, 36^o, 54^o, 72^o...360^o)$ are located in the CSV data obtained. The corresponding current values are also sourced from the same CSV data (See Appendix B). These data enable the determination of the Fourier coefficients of the leakage current or the applied voltage. The generalised Fourier's equation described in (5.1) can thus be re-written using the general expression of a non-sinusoidal equation of an electrical quantity [70]. This yields the following current expression:

$$i\left(t\right)=\frac{I_o}{2}+\sum_{h=0}^{m}\sqrt{2}I_{(2h+1)}sin\left[\omega_{(2h+1)}t+\phi_{(2h+1)}\right] \tag{5.2}$$

Where: $I_{(2h+1)}=\sqrt{a^2_{(2h+1)}+b^2_{(2h+1)}}$ is the RMS value of $i\left(t\right)$, $\omega_{(2h+1)}=\frac{2(2h+1)\Pi}{T}$ is the angular frequency, and $\phi_{(2h+1)}=\arctan\frac{a_{(2h+1)}}{b_{(2h+1)}}$ is the respective phase angle of the harmonic frequency component, with h and m are integers.

Applying the above steps to the measured voltage across ZnO varistor arresters, will also enable the non-sinusoidal voltage equation to be expressed as follows:

$$v\left(t\right)=\frac{V_o}{2}+\sum_{h=0}^{m}\sqrt{2}V_{(2h+1)}sin\left[\omega_{(2h+1)}t+\psi_{(2h+1)}\right] \tag{5.3}$$

Where: $V_{(2h+1)}$ is the RMS value of $v(t)$, and $\psi_{(2h+1)}$, is the phase angle of respective frequency voltage component.

Since the resistive component of the leakage current is associated to the active power or watt losses (W_R) in conductive ZnO varistor arresters [48, 67, 71]. This power component can be derived from the instantaneous power $w(t)$ equation given by the product of equations (5.1) and (5.2). This yields the following equation (neglecting dc components):

$$w(t) = \sum_{h=0}^{m} \sqrt{2} I_{(2h+1)} sin\left[\omega_{(2h+1)}t + \phi_{(2h+1)}\right] \cdot \sqrt{2} V_{(2h+1)} sin\left[\omega_{(2h+1)}t + \psi_{(2h+1)}\right] \quad (5.4)$$

From equation (5.4), the active or resistive power equation is determined as follows:

$$W_R = \sum_{h=0}^{m} V_{(2h+1)} \cdot I_{(2h+1)} cos\left[\psi_{(2h+1)} - \phi_{(2h+1)}\right] \quad (5.5)$$

Where: W_R is the active or resistive power component, and $I_{(2h+1)} cos\left[\psi_{(2h+1)} - \phi_{(2h+1)}\right]$ represents the resistive current at $(2h+1)^{th}$ harmonic component.

The magnitude of the total resistive components constituting the leakage current could be effectively determined using the expression:

$$I_R = \sqrt{\sum_{h=0}^{m} \left[I_{(2h+1)} cos\left(\psi_{(2h+1)} - \phi_{(2h+1)}\right)\right]^2} = \sqrt{I_1^2 + I_3^2 + I_5^2 + ...I_m^2} \quad (5.6)$$

Where: I_R is the total resistive component of the total leakage current, I_1, I_3, I_5 and I_m are fundamental, third harmonic, fifth and m^{th} harmonic resistive currents, respectively.

Based on the resistive current component thus obtained the variations of each harmonic resistive component as a result of respective voltage harmonic frequency can be determined. The contributions of individual harmonic currents towards the total resistive current through ZnO devices can also be quantified.

5.3 Resistive Current Analysis

Applying the above described technique, the leakage current and the CSV current and voltage data of five randomly selected ZnO arrester devices, obtained in both accelerated degradation test conditions of the study, are used to assess the behaviour of the resistive current components (fundamental, third and fifth) before and after harmonic injection from the external source of harmonics.

5.3.1 BE Samples

The CSV data of the leakage current waveforms of five randomly selected BEW and BEH arrester samples are exported to the Matlab software package 7.0 in order to plot the leakage current signal. This is shown in figures 5.1 and 5.2, respectively.

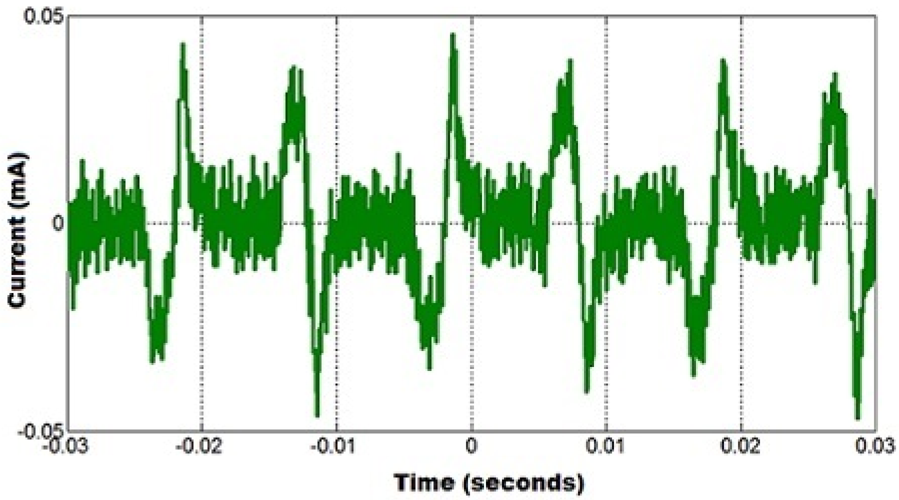

FIGURE 5.1: Leakage Current BEW

The magnitude of the resistive fundamental and harmonic current components, determined using the above procedure, for randomly selected BEW (before external harmonic injection) and BEH (after harmonic injection) arrester samples are shown in figure 5.3. This indicates that the external source of harmonic causes the resistive current component to increase further. The total resistive current before and after external injection of harmonics is obtained using equation (5.6). This yields 0.014 mA and 0.191 mA, respectively. Therefore, it could be observed that the most dominant current components in the resistive leakage current, in both degraded arrester populations, are the fundamental and the THRC. These components respectively represent 92.86% and 38.46% of the resistive current before harmonics injection, and 71.73% and 54.45% of the resistive current after harmonics injection. The fifth harmonic component amounts to 21.43% and 42.93% of the resistive current in each respective case. The increase in the resistive current, observed in arrester population degraded in the presence of external harmonics, can be attributed to the contribution of harmonic voltage components to the resultant biasing voltage. This explains the pronounced shift in the $V-I$ curve, the high degradation rate function and other parameters as opposed to the BEW arrester population.

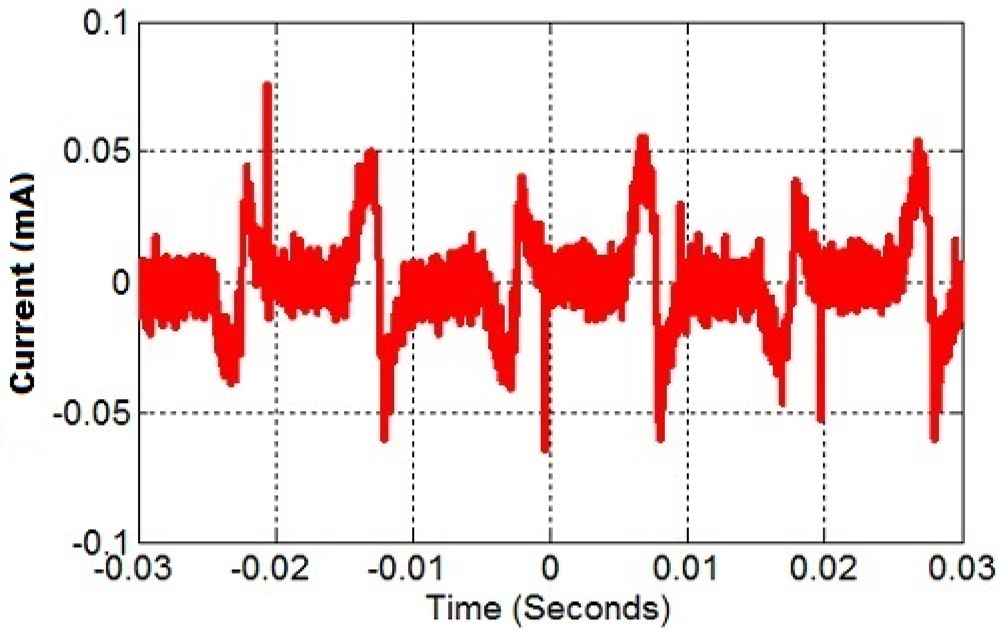

Figure 5.2: Leakage Current BEH

The degradation signs observed in BEH arrester population are therefore attributed to the rise in the resistive current, which in turn results from harmonic components in the applied voltage. Furthermore, it could be noticed that an increase from 1.89% to 6.24% in the third harmonic voltage content and from 2.5% to 5.58% in the fifth harmonic voltage content, the rise in the resulting current components are from 0.005 mA to 0.104 mA and 0.003 mA to 0.082 mA of the fundamental component, respectively. This illustrates the contribution of each voltage harmonic component to the increase of the total resistive current, hence to the electrical degradation process.

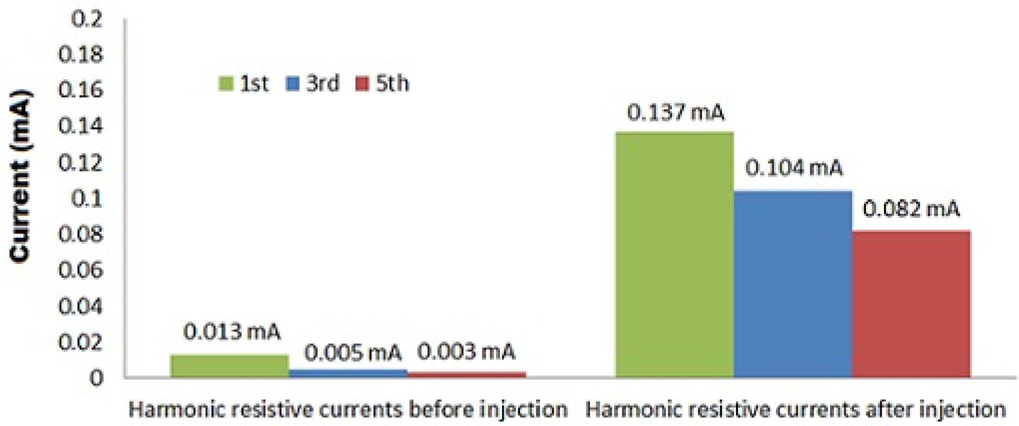

Figure 5.3: Resistive Current Components BE Samples

5.3.2 YW Samples

The CSV data of the leakage current waveforms of the YWW and YWH arrester samples are exported to the Matlab software package version 7.0 in order to plot the leakage current signal. The leakage current waveforms obtained for the YWW and YWH arrester populations are depicted in figures 5.4 and 5.5, respectively.

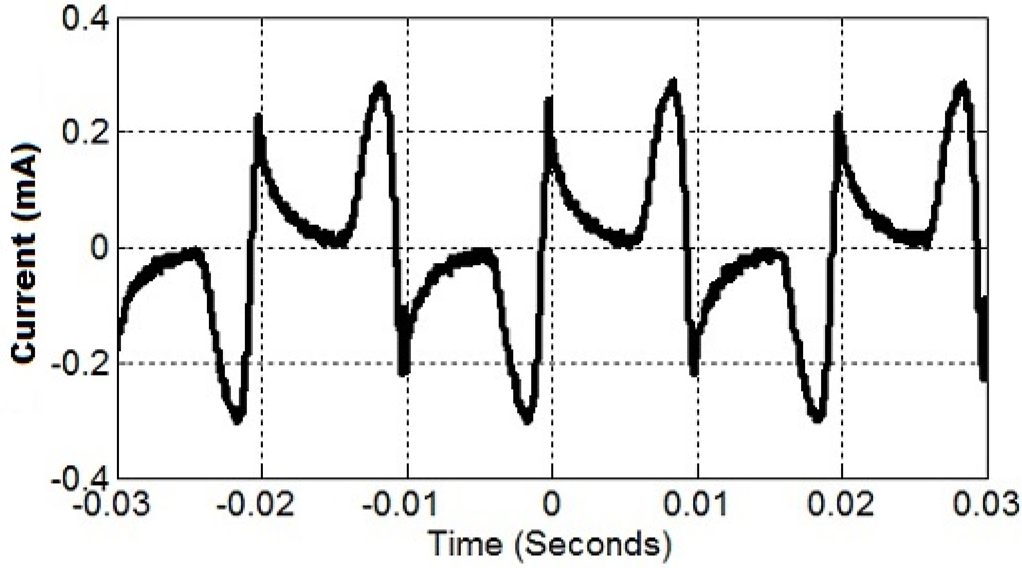

FIGURE 5.4: Leakage Current YWW

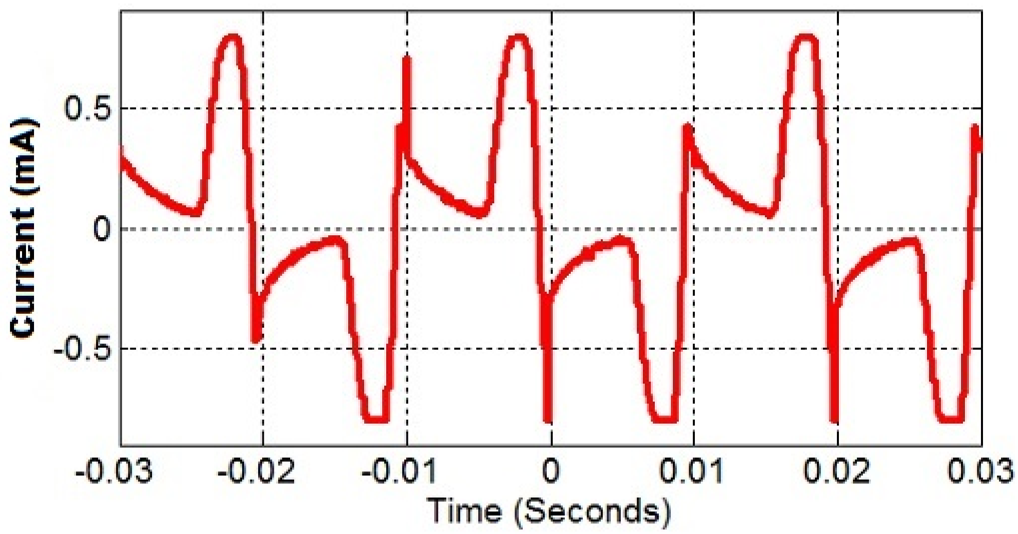

FIGURE 5.5: Leakage Current YWH

The magnitude of the fundamental and harmonic resistive current components obtained from randomly selected YWW and YWH arrester devices are also determined. This is indicated in figure 5.6. As observed in the case of BE samples, further increase of the resistive current is noted as a result of the connection of an external source of harmonics.

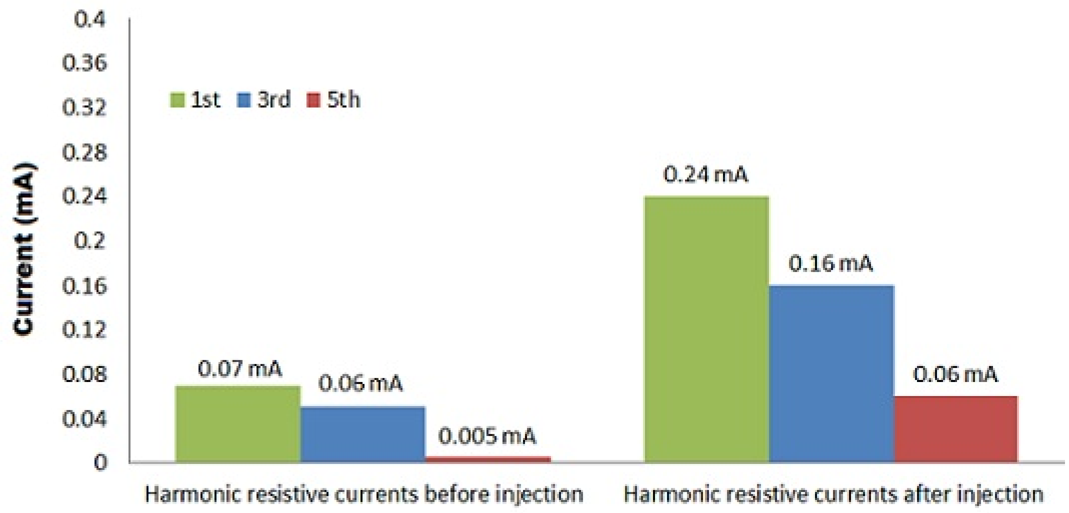

Figure 5.6: Resistive Current Components YW Samples

The total resistive current before and after external injection of harmonics is obtained using equation (5.6). This reveals 0.092 mA and 0.295 mA, respectively. Therefore, it could be observed that the fundamental and the THRC are the most dominant harmonic current components in the resistive leakage current, in both arrester populations degraded with and without external harmonic source, since they consist respectively of 76.09% and 65.22% of the resistive current before injection of harmonics, and 81.36% and 54.24% of the resistive current after harmonics injection. The fifth harmonic current represents 54.35% and 20.34% of the resistive current, respectively. The increase in the resistive current, observed in arrester population degraded in the presence of an external source of harmonics, is attributed to the harmonic voltage components in the applied voltage. These voltage components individually contribute to the rise of the overall biasing voltage across ZnO arrester devices. This therefore indicates the shorter time to degradation and other signs of ageing experienced by YWH arrester population. These degradation signs are caused by the increase of the resistive current which is subsequently triggered by the presence of harmonic components in the applied voltage. Furthermore, it could be noticed for an increase from 1.28% to 9.8% in the third harmonic voltage content and from 1.89% to 6.9% in the fifth harmonic voltage content, the change in the resulting current components are from 0.06 mA to 0.16 mA and 0.005 mA to 0.06 mA, respectively. This demonstrates the contribution of each voltage harmonic content to the growth in the total resistive current, hence to the increased probability of accelerated degradation.

5.3.3 RL Samples

Similarly to the steps followed above, the CSV data of the leakage current waveforms of the RLW and RLH arrester components are exported to the Matlab software package version 7.0 in order to plot the leakage current signal. The leakage current waveforms obtained for the RLW and RLH arrester populations are depicted in figures 5.7 and 5.8, respectively.

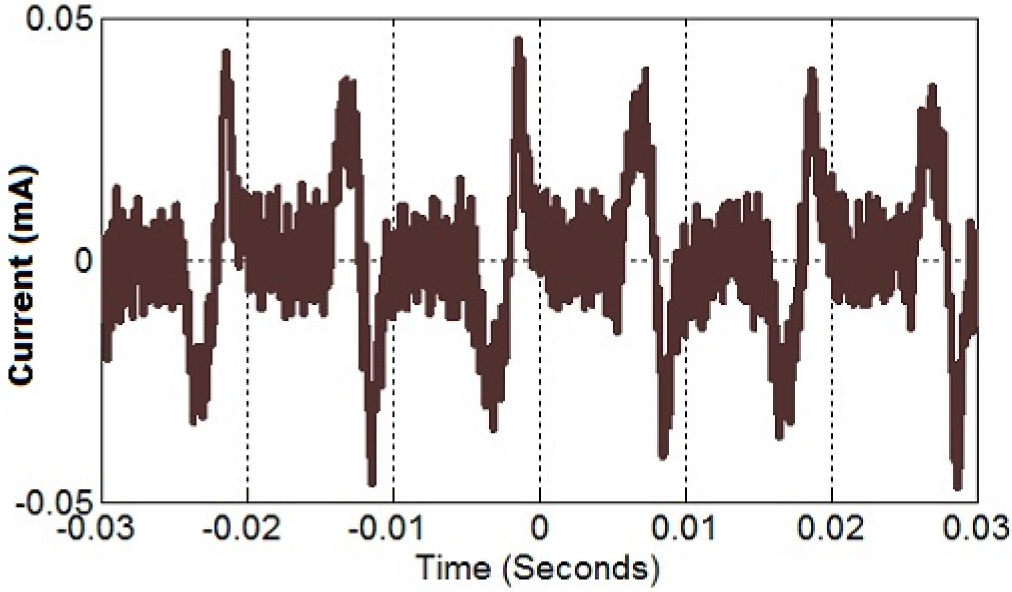

FIGURE 5.7: Leakage Current RLW

The fundamental and harmonic resistive currents obtained from randomly selected RLW and RLH arrester components are indicated in figure 5.9. This once again indicates that the external source of harmonic triggers further increase in the resistive current.
The total resistive current before and after external injection of harmonics such as expressed in equation (5.6) yields the following: 0.040 mA and 0.502 mA, respectively. Therefore, the fundamental and the THRC consist respectively of 88.22% and 7.5% of the resistive current, before external harmonics are injected, 71.71% and 55.78% of the resistive current. The fifth harmonic current represents 4.3% and 41.83% of the resistive current, respectively. The rise in the resistive current, observed in arrester population degraded in the presence of external harmonics, is attributed to the contribution of harmonic voltage components to the overall biasing voltage across these devices. The analysis of the RLH arrester devices showed severe degradation in terms of the $V-I$

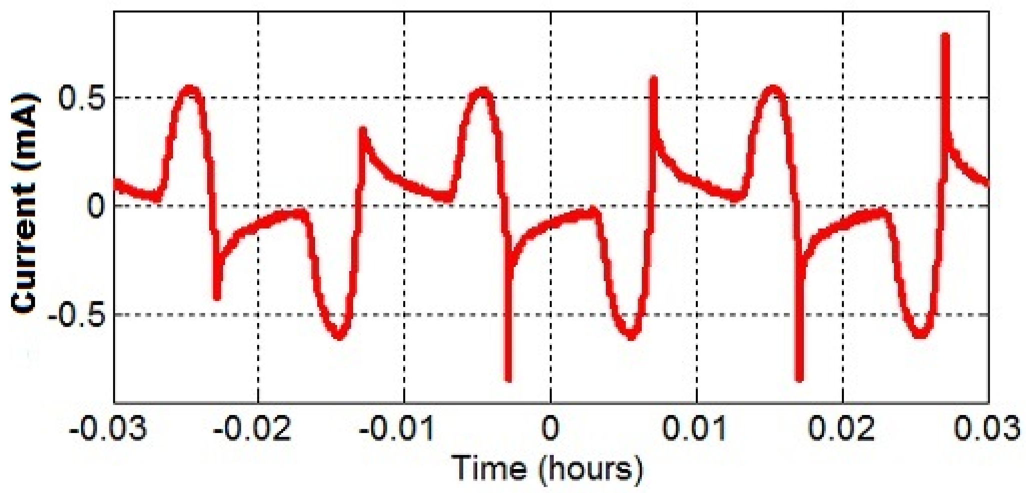

FIGURE 5.8: Leakage Current RLH

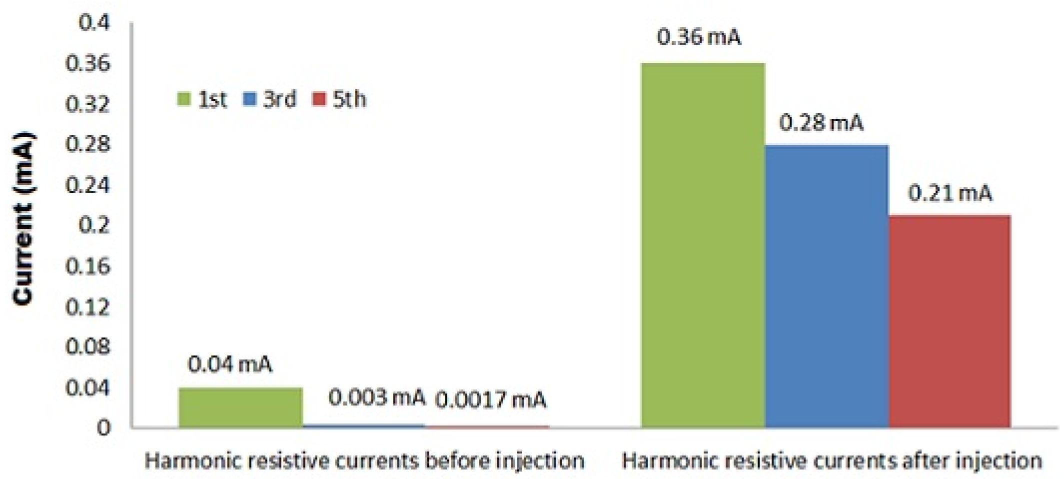

FIGURE 5.9: Resistive Current Components RL Samples

curve, degradation rate function and other parameters as opposed to the RLW components. This is related to higher resistive current, which is triggered by harmonic voltage components in the applied voltage. Furthermore, it could be noticed for an increase from 1.49% to 4.5% in the third harmonic voltage content and from 2.65% to 5.5% in the fifth harmonic voltage content, the change in the resulting current components are from 0.003 mA to 0.28 mA and 0.0017 mA to 0.21 mA, respectively. This indicates the impact of each voltage harmonic content to the magnitude rise of the total resistive current, hence to the prospect of accelerated degradation.

It is therefore important to understand the fundamental mechanism of this induced and potentially destructive current conduction through MOV arresters.

5.4 Mechanism of Accelerated Electrical Degradation

The electrical conduction through MOV arresters is fundamentally attributed to the ion migration (Zinc interstitials or oxygen vacancies) to the intergranular or the interface region of the varistor microstructure [48, 49, 72]. This charge migration phenomenon is made possible by the following important factors: the environmental temperature and the externally applied voltage stress to the arrester device. Therefore, both the applied electric field and temperature could be associated to the depletion of the trapped charges in the intergranular region, which is commonly referred to as the reduction of the schottky barrier height. Furthermore, the $C-V$ analysis technique such as demonstrated in [9, 20, 27], express the inter-dependency between the applied voltage stress and the capacitance of the intergranular region.

Therefore the higher increase in the resistive current component observed, in the varistor samples subjected to distorted applied voltage stress, could therefore be attributed to the effect of voltage harmonics on the migration of charges in the arrester microstructure. This basically implies that the rate of charge migration, which in turn causes the collapse of the barrier height or the decay in the capacitance of the grain boundary region, must have substantially increased as a result of harmonics embedded on the voltage stress. The external biasing effect of distorted voltage stress is described in figure 5.10.

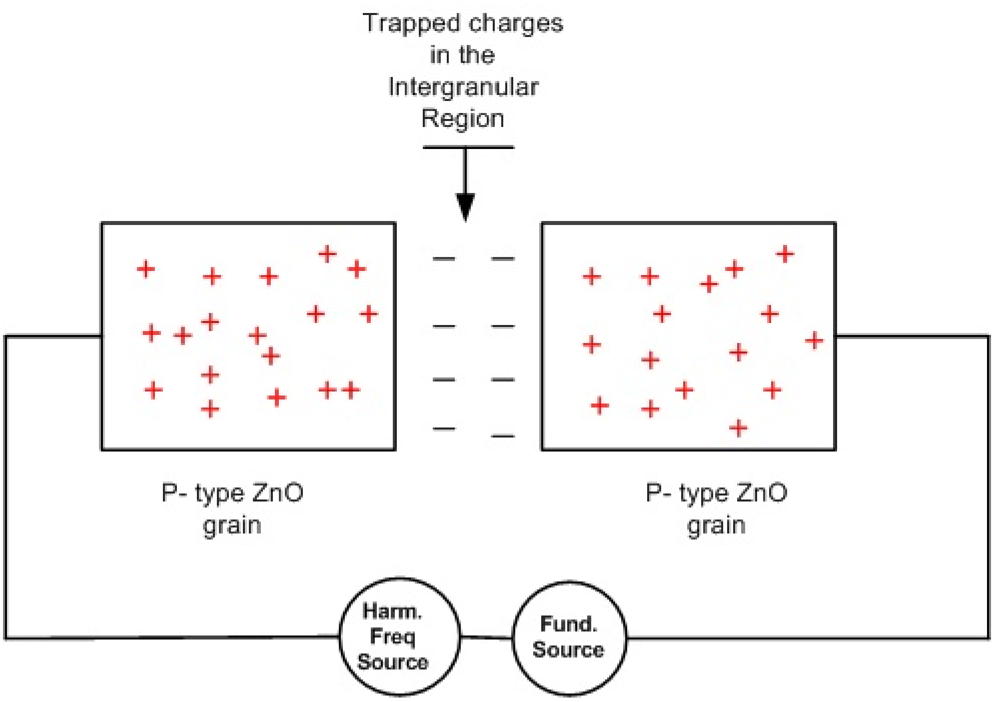

FIGURE 5.10: Distribution of charge carriers in ZnO microstructure

5.5 Conclusion

The total leakage current of ZnO arrester devices, used in the degradation tests conducted in this study, is decomposed in a bid to obtain the resistive component. The fundamental and harmonic components of the resistive current are further analysed and compared in terms of the content variations and contributions to the resistive current. The microstructural implications of accelerated electrical degradation were also discussed. In terms of the resistive current components, it could be observed that the fundamental and the THRC are the most dominant components in the resistive leakage current. All harmonic current components have the tendency to increase in response to the rise in the voltage harmonic content. The rise in the magnitude of the resistive current of the arrester samples degraded with external harmonics is an indication of the contribution of harmonic frequencies to ion migration and therefore the collapse of the schottky barrier height. Therefore, the harmonic frequencies in the applied voltage systematically contribute to the overall biasing voltage applied to the arresters. Based on these observations, voltage harmonic components in the applied voltage across BEH, YWH and RLH arresters are significant contributing factors to the accelerated degradation observed in these arrester populations. Therefore, the presence of higher content of third and fifth harmonic voltage contribute to the increase of the total leakage current, and hence to the high probability of aggravated electrical degradation of BEH, YWH and RLH ZnO arrester populations.

Chapter 6

Conclusions and Future Directions

6.1 Introduction

The inevitable exposure of ZnO arrester devices to harmonic distorted system voltage in modern electric systems, raises the fundamental question of possible aggravated or accelerated electrical degradation of these overvoltage protective units. Artificial accelerated degradation test, which consists of a highly recommended technique of simulating long-term degradation process under service conditions, is conducted on three sets of commercially-sourced ZnO arrester devices. The continuously applied voltage stress is distorted and the environmental temperature is maintained constant. The three-parameter Weibull statistical approach is thus applied in order to analyse the mean time to degradation or mean life, the probability of reduced time to degradation and the degradation rate functions of ZnO arrester samples. The $V-I$ characteristic as well as the clamping voltage of the arrester samples are equally measured to verify electrical degradation condition. The resistive component of the total leakage current is also evaluated in a bid to determine the impact of harmonic voltage frequencies, embedded in the applied voltage stress, on accelerated electrical degradation phenomenon of ZnO arresters.

6.2 Results Obtained

Subsequent to the test and process followed in this study in order to obtain the degradation time distribution, which showed good fit to the Weibull distribution, the results obtained in this study are presented and analysed in terms of the following probability functions and electrical parameters: the time to degradation or life expectancy of ZnO arresters, the hasard or degradation rate function, the $V - I$ characteristic, the clamping voltage and the resistive component of the leakage current.

6.2.1 Higher Probability of Degradation and Reduced Mean Life

The time to degradation of ZnO arresters under the test conditions of this study technically implies a measure of the probability of survival (life expectancy), or of reliable performance of these surge protective units under distorted supply voltage conditions. Therefore, the mean time to degradation or the mean life, the B-lives as well as the probability of reduced time to degradation between the arrester populations involved in this study are measured and compared. It is found across all the samples tested, that the mean life of ZnO arresters subjected to external harmonics is significantly reduced compared to that of arrester components tested without external harmonics. Similarly, the probability of reduced time to degradation for ZnO devices tested with external harmonics is considerably higher. This is also confirmed in terms of the time reduction factor obtained at 10%, 50% and 90% reliability. The B-live test results also indicates that for any p^{th} percentile of arrester components tested with higher content of harmonics, the time to degradation is shorter than that of arrester subjected to external harmonics. Therefore, the mean life or the life expectancy of ZnO arresters is significantly reduced when subjected to continuous supply voltage with harmonic distortion.

6.2.2 Higher Rate of Degradation

The hasard or the degradation rate function is used to provide the basis of analysis of the frequency or pace at which ZnO arresters, subjected to distorted voltage conditions, are likely to experience degradation. The results obtained indicate that the arrester populations, subjected to degradation with external harmonics, are found to be exhibiting a higher pace or frequency of degradation. However, this frequency of degradation is found to be increasing at non-uniform rate. Therefore, the higher the harmonic distortion content in the applied voltage, the higher the frequency or pace of degradation of ZnO arresters.

6.2.3 Accelerated Loss of Stability

The $V - I$ characteristic curves is used as an alternative technique to measure degradation and ultimately the stability of ZnO arresters under distorted conditions. The results obtained in terms of the $V - I$ curve, the reference voltage and the coefficient of non-linearity indicate further drift of the $V - I$ characteristic towards the high conduction region and consequently a significant decrease in the reference voltage and the coefficient of non-linearity for arrester populations, degraded in the presence of external harmonics. This therefore implies that higher harmonics in the applied voltage contribute to loss of stability and therefore to accelerated degradation or of Zinc oxide arresters.

6.2.4 Increased Clamping Voltage

The clamping voltage is measured in a bid to evaluate the impact of higher content of harmonic distortion on high-frequency performance of ZnO arresters. This revealed that ZnO arrester populations, subjected to degradation with external harmonics, experience an increase in the protection or clamping voltage. However, this increase in the clamping voltage value may not be necessarily higher than that of arrester populations subjected to applied voltage stress without external harmonics.

6.2.5 Voltage Harmonics and Accelerated Electrical Degradation

The analysis of the resistive component of the leakage current, under both accelerated degradation conditions observed in this study, shows that voltage harmonic components embedded on the applied voltage stress contribute to the overall biasing voltage of arrester components. This fundamentally suggests that voltage harmonics in the applied stress play a significant contributing role in the drift or migration of charged particles into the intergranular region. This results in the depletion of the trapped charges and therefore to the reduction of the barrier height. In other words, the overall capacitance effect of the device is overcome leading to various conductive paths being made available in the microstructure. This prompts an increase of harmonic current components and therefore the resistive current, which subsequently leads to rise in the watt losses and eventually to the demise of the arrester devices. Therefore, the higher the harmonic frequencies in the applied voltage, the higher the resistive current and the higher the probability of reduced life expectancy or accelerated degradation of MOV-based surge arresters.

6.3 Interpretation of the Results

The accelerated degradation test, such as implemented in this study, represents the influence of voltage harmonics on the long-term deterioration process of ZnO arresters operating under standard temperature and voltage conditions. The high probability of reduced life expectancy or time to degradation that resulted from this study implies that the reliability of ZnO arrester devices decreases with an increase in harmonic content in the applied voltage stress. The decrease in reliability comes as a result of increased resistive current which in turn will cause a rise in the watt losses, and subsequently a device breakdown of these overvoltage protective units.

The non-uniform and increasing rate of degradation of ZnO arresters may be attributed to the non-monotonic disintegration mechanism of grain boundaries that governs the degradation or failure process of individual arrester units. The trend at which this phenomenon takes place may not necessarily be the same for identical arrester components, and may change in the course of time to either become constant or even decrease. This also justifies the fact that some arrester devices have survived the test.

The accelerated loss of stability is an indication of the fact that harmonic components in the applied voltage contribute, on the long run together with temperature, to further decrease of the Schottcky barrier.

Although the increase in the clamping voltage is associated to the degradation indicators of ZnO arresters, however such an increase of the clamping voltage is not necessarily accelerated by harmonic content in the applied voltage. This suggests that the degradation time of ZnO arresters may not reflect a complete disintegration process of the grain boundaries of the MOV.

The continuous presence of harmonic frequency components in the applied voltage consists of additional electric field to the several millions of grain boundaries or microvaristor that constitute the ZnO arrester blocks. This additional field increases the overall biasing effect which in conjunction with the environmental temperature, do accelerate the migration process of charged particles.

6.4 Future Directions

This study introduces the probabilistic approach of accelerated electrical degradation of ZnO arresters operating in distorted electric circuits. Further studies should build on the foundation of this study in order to research on: accumulated energy absorbed by ZnO arresters subjected to the simultaneous effect of steady state harmonic and transient overvoltage; the analysis of the effect of harmonics on the breakdown voltage of ZnO arresters; the development of analytical models, capable of providing or describing the relationship between harmonic content in the applied voltage and the lifetime of MOV-based surge arresters, as well as on the reduction of the Schottky barrier height.

Appendix A

$V - I$ Measurements

The $V - I$ characteristic of arrester samples are given in the tables below:

Mean $V - I$ curve calculation:

BE Samples (Non-degraded)

$V_{0.001mA} = \frac{\sum V_{0.001mA}}{60} = 6$ V ; $V_{0.01mA} = \frac{\sum V_{0.01mA}}{60} = 97$ V; $V_{0.1mA} = \frac{\sum V_{0.1mA}}{60} = 170$ V; $V_{1mA} = \frac{\sum V_{1mA}}{60} = 175$ V; $V_{10mA} = \frac{\sum V_{10mA}}{60} = 185$ V; $V_{100mA} = \frac{\sum V_{100mA}}{60} = 200$ V.

BEW Samples (degraded without external harmonics)

$V_{0.001mA} = \frac{\sum V_{0.001mA}}{27} = 6$ V ; $V_{0.01mA} = \frac{\sum V_{0.01mA}}{27} = 49$ V; $V_{0.1mA} = \frac{\sum V_{0.1mA}}{27} = 147$ V; $V_{1mA} = \frac{\sum V_{1mA}}{27} = 160$ V; $V_{10mA} = \frac{\sum V_{10mA}}{27} = 175$ V; $V_{100mA} = \frac{\sum V_{100mA}}{27} = 185$ V.

BEH Samples (degraded with external harmonics)

$V_{0.001mA} = \frac{\sum V_{0.001mA}}{37} = 4$ V ; $V_{0.01mA} = \frac{\sum V_{0.01mA}}{37} = 39$ V; $V_{0.1mA} = \frac{\sum V_{0.1mA}}{37} = 80$ V; $V_{1mA} = \frac{\sum V_{1mA}}{37} = 100$ V; $V_{10mA} = \frac{\sum V_{10mA}}{37} = 135$ V; $V_{100mA} = \frac{\sum V_{100mA}}{37} = 145$ V.

YW Samples (Non-degraded)

$V_{0.001mA} = \frac{\sum V_{0.001mA}}{60} = 6$ V ; $V_{0.01mA} = \frac{\sum V_{0.01mA}}{60} = 99$ V; $V_{0.1mA} = \frac{\sum V_{0.1mA}}{60} = 157$ V; $V_{1mA} = \frac{\sum V_{1mA}}{60} = 163$ V; $V_{10mA} = \frac{\sum V_{10mA}}{60} = 171$ V; $V_{100mA} = \frac{\sum V_{100mA}}{60} = 179$ V.

YWW Samples (degraded without external harmonics)

$V_{0.001mA} = \frac{\sum V_{0.001mA}}{36} = 6$ V ; $V_{0.01mA} = \frac{\sum V_{0.01mA}}{36} = 73$ V; $V_{0.1mA} = \frac{\sum V_{0.1mA}}{36} = 85$ V; $V_{1mA} = \frac{\sum V_{1mA}}{36} = 97$ V; $V_{10mA} = \frac{\sum V_{10mA}}{36} = 115$ V; $V_{100mA} = \frac{\sum V_{100mA}}{36} = 126$ V.

YWH Samples (degraded with external harmonics)

$V_{0.001mA} = \frac{\sum V_{0.001mA}}{47} = 4$ V ; $V_{0.01mA} = \frac{\sum V_{0.01mA}}{47} = 35$ V; $V_{0.1mA} = \frac{\sum V_{0.1mA}}{47} = 44$ V; $V_{1mA} = \frac{\sum V_{1mA}}{47} = 56$ V; $V_{10mA} = \frac{\sum V_{10mA}}{47} = 68$ V; $V_{100mA} = \frac{\sum V_{100mA}}{47} = 80$ V.

RL Samples (Non-degraded)

$V_{0.001mA} = \frac{\sum V_{0.001mA}}{60} = 7$ V ; $V_{0.01mA} = \frac{\sum V_{0.01mA}}{60} = 98$ V; $V_{0.1mA} = \frac{\sum V_{0.1mA}}{60} = 170$ V; $V_{1mA} = \frac{\sum V_{1mA}}{60} = 175$ V; $V_{10mA} = \frac{\sum V_{10mA}}{60} = 183$ V; $V_{100mA} = \frac{\sum V_{100mA}}{60} = 190$ V.

RLW Samples (degraded without external harmonics)

$V_{0.001mA} = \frac{\sum V_{0.001mA}}{41} = 6$ V ; $V_{0.01mA} = \frac{\sum V_{0.01mA}}{41} = 58$ V; $V_{0.1mA} = \frac{\sum V_{0.1mA}}{41} = 76$ V; $V_{1mA} = \frac{\sum V_{1mA}}{41} = 89$ V; $V_{10mA} = \frac{\sum V_{10mA}}{41} = 102$ V; $V_{100mA} = \frac{\sum V_{100mA}}{41} = 113$ V.

RLH Samples (degraded with external harmonics)

$V_{0.001mA} = \frac{\sum V_{0.001mA}}{56} = 4$ V ; $V_{0.01mA} = \frac{\sum V_{0.01mA}}{56} = 38$ V; $V_{0.1mA} = \frac{\sum V_{0.1mA}}{56} = 47$ V; $V_{1mA} = \frac{\sum V_{1mA}}{56} = 59$ V; $V_{10mA} = \frac{\sum V_{10mA}}{56} = 71$ V; $V_{100mA} = \frac{\sum V_{100mA}}{56} = 83$ V.

TABLE A.1: $V - I$ measurement without external harmonics - BEW

Samples	0.001	0.01	0.1	1	10	100	current (mA)
1	6	53	147	162	177	185	V
2	6	49	152	160	175	188	V
3	6	47	143	157	179	184	V
4	6	52	151	156	174	185	V
5	6	54	143	154	175	189	V
6	6	47	150	160	175	189	V
7	6	53	148	161	172	187	V
8	6	52	147	159	177	189	V
9	6	49	153	164	176	186	V
10	7	54	148	157	170	185	V
11	6	53	146	160	175	185	V
12	6	49	149	160	175	186	V
13	6	49	148	160	179	188	V
14	6	55	151	161	177	187	V
15	6	49	143	165	176	186	V
16	6	47	149	166	175	189	V
17	5	51	146	164	178	188	V
18	6	50	145	158	175	185	V
19	6	48	150	156	168	178	V
20	5	47	146	162	169	180	V
21	6	56	148	161	176	186	V
22	6	51	147	160	175	185	V
23	6	49	145	159	175	185	V
24	5	50	145	157	169	180	V
25	6	47	146	160	174	184	V
26	6	50	149	157	175	186	V
27	6	50	143	161	177	187	V

Table A.2: $V - I$ measurement without external harmonics - BEH

Samples	0.001	0.01	0.1	1	10	100	current (mA)
1	4	40	83	104	136	145	V
2	4	41	82	102	130	148	V
3	4	40	83	104	135	144	V
4	4	39	81	100	130	145	V
5	5	38	80	100	131	149	V
6	3	40	80	100	132	149	V
7	4	40	84	104	135	147	V
8	4	38	77	97	137	149	V
9	5	40	83	101	136	146	V
10	5	39	78	99	130	145	V
11	4	39	76	97	135	144	V
12	4	41	79	100	135	146	V
13	4	39	81	102	139	148	V
14	4	40	80	101	137	147	V
15	4	42	83	103	136	146	V
16	4	40	79	100	135	149	V
17	4	39	76	97	128	138	V
18	4	43	84	103	135	145	V
19	4	41	80	99	128	138	V
20	4	40	76	100	139	146	V
21	4	42	81	101	136	146	V
22	4	39	77	97	135	145	V
23	4	38	85	102	135	145	V
24	4	37	82	100	129	140	V
25	4	40	80	101	134	144	V
26	4	35	79	100	135	146	V
27	4	39	80	100	137	147	V
28	4	41	81	101	135	145	V
29	4	35	82	102	128	148	V
30	4	35	84	101	139	140	V
31	4	39	80	100	136	146	V
32	4	40	80	100	135	145	V
33	4	41	81	102	135	145	V
34	4	38	83	101	139	140	V
35	4	37	79	101	139	144	V
36	5	39	82	100	135	146	V
37	4	41	75	94	137	147	V

TABLE A.3: $V - I$ measurement without external harmonics - YWW

Samples	0.001	0.01	0.1	1	10	100	current (mA)
1	6	70	86	98	118	125	V
2	6	71	86	96	116	128	V
3	6	70	83	98	115	126	V
4	6	73	85	97	114	125	V
5	6	72	85	99	115	126	V
6	6	73	88	97	117	126	V
7	5	70	84	99	115	127	V
8	6	74	87	97	117	129	V
9	6	73	83	96	116	126	V
10	6	74	80	98	113	125	V
11	6	73	86	97	115	124	V
12	6	71	86	97	115	127	V
13	6	75	85	96	114	127	V
14	6	73	83	94	114	127	V
15	6	72	82	98	116	126	V
16	6	70	83	95	115	129	V
17	6	75	86	97	116	128	V
18	6	73	84	97	115	126	V
19	6	71	85	97	117	126	V
20	6	75	88	97	117	126	V
21	6	73	87	97	116	127	V
22	6	77	87	97	115	127	V
23	6	74	85	95	115	125	V
24	6	75	82	93	114	126	V
25	5	70	87	97	114	126	V
26	6	75	81	95	115	126	V
27	6	69	80	99	117	127	V
28	6	71	81	97	115	125	V
29	6	75	85	95	118	128	V
30	6	73	85	95	113	126	V
31	6	75	85	95	116	126	V
32	6	70	85	96	115	125	V
33	6	71	81	95	115	125	V
34	6	73	88	98	114	126	V
35	6	75	85	97	115	126	V
36	6	75	85	97	115	126	V

Table A.4: $V - I$ measurement with external harmonics - YWH

Samples	0.001	0.01	0.1	1	10	100	current (mA)
1	4	33	46	56	68	78	V
2	5	35	46	56	68	78	V
3	5	34	43	58	67	76	V
4	4	34	45	57	69	75	V
5	4	35	45	59	65	76	V
6	4	36	48	57	67	76	V
7	4	33	44	59	65	77	V
8	5	35	47	57	67	79	V
9	4	35	43	56	66	76	V
10	4	34	40	58	63	83	V
11	4	33	46	57	65	80	V
12	4	35	46	57	65	80	V
13	4	35	45	56	64	81	V
14	4	33	43	54	64	83	V
15	5	34	44	58	66	80	V
16	4	33	44	55	65	81	V
17	4	35	46	57	66	78	V
18	4	33	44	57	72	76	V
19	4	32	45	57	67	76	V
20	5	35	43	57	67	80	V
21	4	33	42	57	68	83	V
22	4	37	47	57	68	77	V
23	4	34	45	55	69	85	V
24	5	35	44	53	70	80	V
25	5	33	47	56	73	80	V
26	4	35	44	55	65	80	V
27	4	39	44	54	67	77	V
28	5	32	42	57	65	85	V
29	4	35	45	55	68	78	V
30	4	33	45	55	71	81	V
31	4	35	44	55	73	83	V
32	4	33	46	56	70	80	V
33	4	32	43	55	72	81	V
34	4	33	48	58	73	86	V
35	4	35	40	57	70	80	V
36	4	35	45	57	70	76	V
37	4	35	44	55	65	76	V
38	4	39	46	59	67	80	V
39	4	39	46	57	69	82	V
40	4	35	45	55	70	81	V
41	4	35	45	55	63	76	V
42	4	35	45	55	66	86	V
43	4	32	45	56	68	85	V
44	4	38	40	55	65	80	V
45	4	33	40	58	64	76	V
46	4	35	45	57	70	81	V
47	4	35	40	57	72	80	V

Table A.5: $V - I$ measurement without external harmonics - RLW

Samples	0.001	0.01	0.1	1	10	100	current (mA)
1	5	59	76	86	103	113	V
2	6	60	76	86	96	114	V
3	6	60	73	88	97	117	V
4	6	57	75	87	99	109	V
5	6	58	75	89	102	112	V
6	5	56	78	87	97	115	V
7	5	58	74	89	105	115	V
8	4	58	77	87	97	114	V
9	6	57	73	86	103	113	V
10	6	61	70	88	103	113	V
11	6	62	76	87	105	115	V
12	6	58	76	87	105	115	V
13	6	58	78	90	104	114	V
14	6	59	78	87	99	109	V
15	6	58	76	88	104	114	V
16	6	57	76	91	100	110	V
17	6	57	76	90	103	113	V
18	5	59	77	87	102	112	V
19	6	60	75	89	103	111	V
20	6	58	73	89	97	113	V
21	6	58	72	90	100	110	V
22	6	57	77	93	103	112	V
23	6	60	75	89	103	114	V
24	6	56	76	89	101	110	V
25	6	59	77	89	102	112	V
26	6	58	76	87	102	111	V
27	6	59	76	90	105	116	V
28	6	62	76	87	100	114	V
29	6	58	75	92	102	112	V
30	6	63	75	87	102	112	V
31	6	56	76	89	103	113	V
32	6	58	76	89	100	113	V
33	6	58	75	89	102	112	V
34	6	60	78	90	103	113	V
35	6	61	76	87	102	112	V
36	6	57	75	87	102	111	V
37	6	58	76	92	101	111	V
38	6	55	76	89	102	113	V
39	6	57	76	89	104	113	V
40	6	57	75	89	101	112	V
41	6	56	75	89	102	112	V

Table A.6: $V - I$ measurement without external harmonics - RLH

Samples	0.001	0.01	0.1	1	10	100	current (mA)
1	4	39	46	58	73	83	V
2	4	40	46	60	76	84	V
3	4	40	43	58	77	87	V
4	4	37	45	60	79	89	V
5	5	38	45	59	72	82	V
6	4	36	48	57	77	85	V
7	5	38	44	59	75	85	V
8	5	38	47	59	77	84	V
9	4	37	43	56	73	83	V
10	4	41	48	58	73	83	V
11	4	42	46	57	75	85	V
12	4	38	46	57	75	85	V
13	4	38	48	60	74	84	V
14	5	39	48	57	79	89	V
15	5	38	46	58	74	84	V
16	4	37	46	61	70	80	V
17	3	37	46	60	73	83	V
18	4	39	47	60	72	82	V
19	4	40	45	59	73	81	V
20	4	38	47	59	77	83	V
21	3	38	48	60	70	80	V
22	5	37	47	63	73	82	V
23	4	40	45	59	73	84	V
24	4	36	46	59	71	80	V
25	4	39	47	59	72	82	V
26	4	38	46	57	72	81	V
27	4	39	46	60	68	86	V
28	4	42	46	57	70	84	V
29	4	38	47	62	72	82	V
30	4	43	47	57	66	82	V
31	4	36	47	59	67	83	V
32	3	38	46	59	70	83	V
33	4	38	45	59	72	82	V
34	4	40	48	60	73	83	V
35	5	41	46	57	72	82	V
36	4	37	45	57	72	81	V
37	4	38	46	62	71	81	V
38	4	35	46	59	72	83	V
39	5	37	46	59	65	83	V
40	4	37	45	59	66	82	V
41	4	36	47	59	67	82	V
42	4	40	47	56	70	84	V

TABLE A.7: $V - I$ measurement without external harmonics - RLH (Continued)

43	4	40	45	58	71	87	V
44	4	37	50	57	70	89	V
45	4	38	45	59	72	82	V
46	4	36	48	57	70	85	V
47	4	38	49	59	65	85	V
48	4	38	47	57	65	84	V
49	4	37	50	56	65	83	V
50	4	41	49	58	69	83	V
51	4	42	46	57	75	85	V
52	4	38	46	57	67	85	V
53	4	38	48	60	76	80	V
54	4	39	48	57	68	89	V
55	4	38	49	58	70	79	V
56	4	38	49	58	69	80	V

Table A.8: $V - I$ measurement Before degradation (BE samples)

Samples	0.001	0.01	0.1	1	10	100	current (mA)
1	6	87	170	177	187	201	V
2	6	93	175	182	191	208	V
3	6	97	176	182	192	208	V
4	6	90	173	181	191	207	V
5	6	95	173	182	190	207	V
6	6	100	169	179	188	202	V
7	6	88	174	182	191	207	V
8	6	90	178	185	195	210	V
9	6	101	168	175	184	200	V
10	7	92	171	177	187	201	V
11	6	91	168	176	185	199	V
12	6	82	167	176	184	198	V
14	6	80	165	174	183	197	V
15	6	91	166	173	182	196	V
16	6	83	168	174	183	199	V
17	7	87	173	181	191	206	V
18	7	92	175	182	191	206	V
19	6	88	166	176	184	199	V
20	6	91	175	182	192	205	V
21	6	83	165	173	182	196	V
22	6	91	177	183	192	209	V
23	6	80	174	183	190	205	V
24	6	94	167	173	183	198	V
25	6	98	179	185	195	211	V
26	6	97	171	179	188	203	V
27	6	85	168	176	186	200	V
28	6	100	176	183	192	209	V
29	6	101	169	176	186	200	V
30	7	101	176	183	192	207	V
⋮	⋮	⋮	⋮	⋮	⋮	⋮	V
60	7	101	176	183	192	207	V

Appendix B

Measurement of the Applied Voltage and the Leakage Current

The measurement of the applied voltage are:

TABLE B.1: Measurement of the applied voltage

x	y	cosx	ycosx	sinx	ysinx	cos3x	ycos3x	sin3x	ysin3x
18	4.40	0.9511	4.1847	0.3090	1.3597	0.5878	2.5863	0.8090	3.5597
36	7.60	0.8090	6.1486	0.5878	4.4672	-0.3090	-2.3486	0.9511	7.2281
54	11.2	0.5878	6.5833	0.8090	9.0610	-0.9511	-10.6519	0.3090	3.4610
72	13.6	0.3090	4.2027	0.9511	12.9344	-0.8090	-11.0027	-0.5878	-7.9939
90	14	0	0	1	14	0	0	-1	-14
108	13.6	-0.3090	-4.2027	0.9511	12.9344	0.8090	11.0027	-0.5878	-7.9939
126	12	-0.5878	-7.0535	0.8090	9.7082	0.9511	11.4127	0.3090	3.7082
144	8.8	-0.8090	-7.1194	0.5878	5.1726	0.3090	2.7194	0.9511	8.3693
162	4.4	-0.9511	-4.1847	0.3090	1.3597	-0.5878	-2.5863	0.8090	3.5597
180	-0.8	-1	0.8	0	0	-1	0.8	0	0
198	-4.8	-0.9511	4.5651	-0.3090	1.4833	-0.5878	2.8214	-0.8090	3.8833
216	-8	-0.8090	6.4722	-0.5878	4.7023	0.3090	-2.4722	-0.9511	7.6085
234	-11.6	-0.5878	6.8184	-0.8090	9.3846	0.9511	-11.0323	-0.3090	3.5846
252	-14.4	-0.3090	4.4499	-0.9511	13.6953	0.8090	-11.6499	0.5878	-8.4642
270	-14.8	0	0	-1	14.8	0	0	1	-14.8
288	-14	0.3090	-4.3263	-0.9511	13.3148	-0.8090	11.3263	0.5878	-8.2291
306	-12.4	24.17	-1.2849	7.25	1.359688	0.58779	2.586276	0.80902	3.559688
324	-9.2	0.8090	-7.4430	-0.5878	5.4077	-0.3090	2.8430	-0.9511	8.7498
342	-4.80	0.9511	-4.5651	-0.3090	1.4833	0.5878	-2.8214	-0.8090	3.8833
360	0.00	1	0	0	0	1	0	0	0

Since the value of 0.02 in the CSV data corresponds 360^o (See time-domain fig. 5.1 and others), the following relationship applies to determine the angle values in CSV data:

TABLE B.2: Measurement of the applied voltage

x	y	cos5x	ycos5x	sin5x	ysin5x	cos7x	ycos7x	sin7x	ysin7x
18	4.40	0	0	1	4.4	-0.5878	-2.5863	0.8090	3.5597
36	7.60	-1	-7.6	0	0	-0.3090	-2.3486	-0.9511	-7.2281
54	11.2	0	0	-1	-11.2	0.9511	10.6519	0.3090	3.4610
72	13.6	1	13.6	0	0	-0.8090	-11.0027	0.5878	7.9939
90	14	0	0	1	14	0	0	-1	-14
108	13.6	-1	-13.6	0	0	0.8090	11.0027	0.5878	7.9939
126	12	0	0	-1	-12	-0.9511	-11.4127	0.3090	3.7082
144	8.8	1	8.8	0	0	0.3090	2.7194	-0.9511	-8.3693
162	4.4	0	0	1	4.4	0.5878	2.5863	0.8090	3.5597
180	-0.8	-1	0.8	0	0	-1	0.8	0	0
198	-4.8	0	0	-1	4.8	0.5878	-2.8214	-0.8090	3.8833
216	-8	1	-8	0	0	0.3090	-2.4722	0.9511	-7.6085
234	-11.6	0	0	1	-11.6	-0.9511	11.0323	-0.3090	3.5846
252	-14.4	-1	14.4	0	0	0.8090	-11.6499	-0.5878	8.4642
270	-14.8	0	0	-1	14.8	0	0	1	-14.8
288	-14	1	-14	0	0	-0.8090	11.3263	-0.5878	8.2291
306	-12.4	0	0	1	-12.4	0.9511	-11.7931	-0.3090	3.8319
324	-9.2	-1	9.2	0	0	-0.3090	2.8430	0.9511	-8.7498
342	-4.80	0	0	-1	4.8	-0.5878	2.8214	-0.8090	3.8833
360	0.00	1	0	0	0	1	0	0	0

$18^o = \frac{18\times0.02}{360} = 1.00 \text{ x } 10^{-3}$; $36^o = \frac{36\times0.02}{360} = 2.00 \text{ x } 10^{-3}$; $54^o = \frac{54\times0.02}{360} = 3.00 \text{ x } 10^{-3}$; $342^o = \frac{342\times0.02}{360} = 1.900 \text{ x } 10^{-2}$; $360^o = \frac{360\times0.02}{360} = 2.00 \text{ x } 10^{-2}$

$$a_n = \frac{\sum ycosnx}{0.01} \quad \text{(B.1)}$$

$$b_n = \frac{\sum ysinnx}{0.01} \quad \text{(B.2)}$$

$$c_n = \sqrt{a_n^2 + b_n^2} \quad \text{(B.3)}$$

$$\psi_n = \arctan \frac{a_n}{b_n} \quad \text{(B.4)}$$

Table B.3: Harmonic Components of the applied voltage: BEW samples

order	a_n	b_n	c_n	ψ_n	%
1	-195.85	14530	14531	-0.77	-
3	273.97	-5.38	274.02	-88.88	1.89
5	360	1.78E-13	360	90	2.5
7	-30.366	139.72	136.38	-12.262	0.94

Table B.4: Harmonic Components of the applied voltage: BEH samples

order	a_n	b_n	c_n	ψ_n	%
1	-6594.5	12664	14278	-27.507	-
3	889.67	58.019	891.56	86.269	6.24
5	720	340	796.24	64.722	5.58
7	935.28	146.46	946.68	81.10	6.63

Table B.5: Harmonic Components of the applied voltage: YWW samples

order	a_n	b_n	c_n	ψ_n	%
1	115.91	13304	13305	0.5	-
3	160	-60	170.88	26.15	1.28
5	110.95	226.01	251.77	-69.44	1.89
7	-35.671	89.34	96.198	-21.77	0.72

Table B.6: Harmonic Components of the applied voltage: YWH samples

order	a_n	b_n	c_n	ψ_n	%
1	132550	9688.6	13290	85.819	-
3	1230.9	429.18	1303.6	70.79	9.8
5	760	520	920.87	55.62	6.9
7	-671.51	386.19	774.64	-60.096	5.8

Table B.7: Harmonic Components the applied voltage: RLW samples

order	a_n	b_n	c_n	ψ_n	%
1	187010	14046	187540	85.705	-
3	2800	-0.002	2800	21.921	1.49
5	1857.5	4615.9	497.56	-90	2.65
7	-198.11	112.55	227.85	-60.398	0.12

Table B.8: Harmonic Components of the applied voltage: RLH samples

order	a_n	b_n	c_n	ψ_n	%
1	1440.6	14212	14285	5.788	-
3	-588.89	-244.55	637.65	67.448	4.5
5	-520	-580	778.97	41.878	5.5
7	-474.43	-474.43	670.95	45	4.7

Table B.9: Measurement of the Leakage Current

x	y	cosx	ycosx	sinx	ysinx	cos3x	ycos3x	sin3x	ysin3x
18	0.096	4.20	0.4032	0.3090	0.0297	0.5878	0.0564	0.809	0.078
36	0.06	7.6	0.456	0.5878	0.03553	-0.3090	-0.0185	0.951	0.057
54	0.048	10.6	0.5088	0.8090	0.0388	-0.9511	-0.04565	0.309	0.015
72	0.028	12.8	0.3584	0.9511	0.0266	-0.8090	-0.0227	-0.588	-0.017
90	0.008	12.8	0.1024	1	0.008	0	0	-1	-0.008
108	0.012	12.4	0.1488	0.9511	0.0114	0.8090	0.0097	-0.588	-0.007
126	0.156	10.8	1.6848	0.8090	0.126	0.9511	0.148	0.3090	0.048
144	0.264	7.8	2.059	0.5878	0.1552	0.3090	0.0816	0.9511	0.251
162	0.188	4.00	0.752	0.3090	0.0581	-0.5878	-0.1105	0.8090	0.152
180	-0.184	-1	0.184	0	0	-1	0.184	0	0
198	-0.096	-4.4	0.4224	-0.3090	0.0297	-0.5878	0.0564	-0.809	0.078
216	-0.044	-8	0.352	-0.5878	0.0259	0.3090	-0.0136	-0.951	0.042
234	-0.044	-10.8	0.475	-0.8090	0.0356	0.9511	-0.0418	-0.309	0.0136
252	-0.032	-13	0.416	-0.9511	0.0304	0.8090	-0.0259	0.5878	-0.019
270	-0.016	-12.8	0.2048	-0.9511	0.0152	-0.8090	0.0129	0.588	-0.009
288	-14	0.3090	-4.3263	-0.9511	13.3148	-0.8090	11.3263	0.588	-8.23
306	-0.164	-11	1.804	-0.8090	0.1327	-0.9511	0.156	-0.454	0.075
324	-0.028	-8.00	2.24	-0.5878	0.1646	-0.3090	0.0865	-0.9511	0.266
342	-0.204	-4	0.816	-0.3090	0.0630	0.5878	-0.1199	-0.8090	0.165
360	0.196	0.4	0.0784	0	0	1	0.196	0	0

Table B.10: Measurement of the Leakage Current

x	y	cos5x	ycos5x	sin5x	ysin5x	cos7x	ycos7x	sin7x	ysin7x
18	0.096	0	0	1	-0.192	-0.58779	0.112856	0.80902	-0.15533
36	7.60	-1	0.136	0	0	-0.3090	0.04203	-0.9511	0.1293
54	11.2	0	0	-1	0.088	0.9511	-0.0837	0.3090	-0.027194
72	13.6	1	-0.064	0	0	-0.8090	0.0517773	0.5878	-0.037619
90	14	0	0	1	-0.04	0	0	-1	0.04
108	13.6	-1	-0.012	0	0	0.8090	0.009708	0.5878	0.0070535
126	12	0	0	-1	-0.156	-0.9511	-0.1483654	0.3090	0.048207
144	8.8	1	0.264	0	0	0.3090	0.08158	-0.9511	-0.25108
162	4.4	0	0	1	0.188	0.5878	0.110505	0.8090	0.152096
180	-0.8	-1	0.184	0	0	-1	0.184	0	0
198	-4.8	0	0	-1	0.096	0.5878	-0.05643	-0.8090	0.07767
216	-8	1	-0.044	0	0	0.3090	-0.0136	0.9511	-0.04185
234	-11.6	0	0	1	-0.044	-0.9511	0.041847	-0.3090	0.013597
252	-14.4	-1	0.032	0	0	0.8090	-0.02589	-0.5878	0.018809
270	-14.8	0	0	-1	0.024	0	0	1	-0.024
288	-14	1	-0.016	0	0	-0.8090	0.012944	-0.5878	0.009405
306	-12.4	0	0	1	-0.164	0.9511	-0.15597	-0.3090	0.050679
324	-9.2	-1	0.28	0	0	-0.3090	0.086526	0.9511	-0.2663
342	-4.80	0	0	-1	0.204	-0.5878	0.119909	-0.8090	0.16504
360	0.00	1	0.196	0	0	1	0.196	0	0

Table B.11: Resistive Current Components: BEW samples

Components	Sample 1	Sample 2	Sample 3	Sample 4	Sample 5	Ave.Value	Unit
Fund.	0.011	0.014	0.013	0.012	0.013	0.013	mA
Third	0.006	0.005	0.007	0.004	0.005	0.0054	mA
Fifth	0.004	0.004	0.0025	0.0026	0.003	0.00322	mA

Table B.12: Resistive Current Components: BEH samples

Components	Sample 1	Sample 2	Sample 3	Sample 4	Sample 5	Ave.Value	Unit
Fund.	0.137	0.14	0.134	0.137	0.138	0.137	mA
Third	0.109	0.105	0.101	0.099	0.104	0.104	mA
Fifth	0.079	0.085	0.082	0.08	0.082	0.082	mA

Table B.13: Resistive Current Components: YWW samples

Components	Sample 1	Sample 2	Sample 3	Sample 4	Sample 5	Ave.Value	Unit
Fund.	0.09	0.065	0.071	0.061	0.062	0.07	mA
Third	0.057	0.061	0.059	0.06	0.061	0.06	mA
Fifth	0.0048	0.0052	0.0049	0.005	0.0051	0.005	mA

Table B.14: Resistive Current Components: YWH samples

Components	Sample 1	Sample 2	Sample 3	Sample 4	Sample 5	Ave.Value	Unit
Fund.	0.239	0.237	0.25	0.238	0.241	0.24	mA
Third	0.173	0.161	0.158	0.156	0.153	0.16	mA
Fifth	0.062	0.071	0.06	0.057	0.055	0.061	mA

Table B.15: Resistive Current Components: RLW samples

Components	Sample 1	Sample 2	Sample 3	Sample 4	Sample 5	Ave.Value	Unit
Fund.	0.03	0.036	0.042	0.044	0.049	0.04	mA
Third	0.0026	0.0025	0.0031	0.0039	0.0029	0.003	mA
Fifth	0.0016	0.0015	0.0016	0.0019	0.0019	0.0017	mA

Table B.16: Resistive Current Components: RLH samples

Components	Sample 1	Sample 2	Sample 3	Sample 4	Sample 5	Ave.Value	Unit
Fund.	0.34	0.36	0.38	0.37	0.35	0.36	mA
Third	0.26	0.28	0.3	0.29	0.27	0.28	mA
Fifth	0.2	0.21	0.19	0.21	0.22	0.21	mA

Appendix C

Times to degradation

The times to degradation, the percentage cumulative degradation and the logarithmic values assigned to the BEW, BEH, YWW, YWH, RLW and RLH samples are given:

TABLE C.1: Times to degradation for BEW Samples

$t_m(minutes)$	t_i (hours)	$F(i,n)$ (%)	x_i	y_i
1	100.5	0.93	-4.6731	4.61
1	100.5	2.59	-3.6404	4.615
1	100.5	4.25	-3.1366	4.61
2	201.1	5.91	-2.7982	5.3
2	201.1	7.57	-2.5419	5.3
2	201.1	9.23	-2.3347	5.3
3	301.6	10.89	-2.1602	5.71
6	603.2	12.55	-2.0091	6.4
6	603.2	14.21	-1.8756	6.4
6	603.2	15.87	-1.7556	6.4
7	703.7	17.53	-1.6464	6.56
7	703.7	19.19	-1.5461	6.56
8	804.3	20.85	-1.4532	6.69
13	1307	22.51	-1.3664	7.18
14	1407	24.17	-1.2849	7.25
14	1408	25.83	-1.2079	7.25
15	1508	27.49	-1.1349	7.32
15	1508	29.15	-1.0654	7.32
16	1609	30.81	-0.99882	7.38
17	1709	32.47	-0.93497	7.44
17	1709	34.12	-0.87387	7.44
19	1910	35.78	-0.81451	7.55
20	2011	37.44	-0.75706	7.61
23	2312	40.76	-0.64708	7.75
28	2815	42.42	-0.59422	7.94
34	3418	44.83	-0.51961	8.14

Applying equation (2.5) yields the correlation factor for BEW varistor components:

$$\eta\,(x_i, y_i) = \frac{(-4.6731+44.4721)\cdot(4.61-179.65)+...+(-0.51961+44.4721)\cdot(8.14-179.65)}{\sqrt{\left[(-4.6731+44.4721)^2+...+(-0.51961+44.4721)^2\right]\cdot\left[(4.61-179.65)^2+...+(8.14-179.65)^2\right]}}$$

$\eta\,(x_i, y_i) = 0.955857$ which is higher than the critical coefficient value (See figure 2.1).

Equation (2.6) enables the determination of the shape parameter for BEW samples:

$$\beta = \frac{(-4.6731+44.4721)^2+...+(-0.51961+44.4721)^2}{[(-4.6731+44.4721)\cdot(4.61-179.65)]+...+[(-0.51961+44.4721)\cdot(8.14-179.65)]}$$

$\beta = 0.97961$

The scale parameter is calculated using equation (2.7):

$$\theta = \exp\left[179.65 - \frac{[(-4.6731+44.4721)\cdot(4.61-179.65)]+...+[(-0.51961+44.4721)\cdot(8.14-179.65)]}{(-4.6731+44.4721)^2+...+(-0.51961+44.4721)^2}\cdot(-44.4721)\right]$$

$\theta = 4167.6$ hours.

For BEH samples:

Applying equation (2.5) yields the correlation factor:

$$\eta\,(x_i, y_i) = \frac{(-4.6731+1.29364)\cdot(4.61-6.73)+...+(-0.68882+1.29364)\cdot(8.011-6.73)}{\sqrt{\left[(-4.6731+1.29364)^2+...+(-0.68882+1.29364)^2\right]\cdot\left[(4.61-6.73)^2+...+(8.011-6.73)^2\right]}}$$

$\eta\,(x_i, y_i) = 0.958317$ which is higher than the critical coefficient value (See figure 2.1).

Equation (2.6) enables the determination of the shape parameter for BEH samples:

$$\beta = \frac{(-4.6731+1.29364)^2+...+(-0.68882+1.29364)^2}{[(-4.6731+1.29364)\cdot(4.61-6.73)]+...+[(-0.68882+1.29364)\cdot(8.011-6.73)]}$$

$\beta = 1.0929$

The scale parameter is calculated using equation (2.7):

$$\theta = \exp\left[6.73 - \frac{[(-4.6731+1.29364)\cdot(4.61-6.73)]+...+[(-0.68882+1.29364)\cdot(8.011-6.73)]}{(-4.6731+1.29364)^2+...+(-0.68882+1.29364)^2}\cdot(-1.29364)\right]$$

$\theta = 2746.5$ hours.

Applying equation (2.5) yields the correlation factor for YWW varistor components:

$$\eta\,(x_i, y_i) = \frac{(-4.6731+1.31044)\cdot(4.61-6.107127)+...+(-0.1142+1.31044)\cdot(7.606-6.107127)}{\sqrt{\left[(-4.6731+1.31044)^2+...+(-0.1142+1.31044)^2\right]\cdot\left[(4.61-6.107127)^2+...+(7.606-6.107127)^2\right]}}$$

TABLE C.2: Times to degradation for BEH Samples

$t_m(minutes)$	t_i (hours)	$F(i,n)$ (%)	x_i	y_i
1	100.5	0.93	-4.6731	4.610158
1	100.5	2.59	-3.6404	4.610158
1	100.5	4.25	-3.1366	4.610158
2	201.1	5.91	-2.7982	5.306782
2	201.1	7.57	-2.5419	5.306782
2	201.1	9.23	-2.3347	5.306782
3	301.6	10.89	-2.1602	5.709102
3	301.6	12.55	-2.0091	5.709102
3	301.6	14.21	-1.8756	5.709102
5	502.67	15.87	-1.7556	6.219934
5	502.67	17.53	-1.6464	6.219934
5	502.67	19.19	-1.5461	6.219934
10	1005.3	20.85	-1.4532	6.913041
10	1005.3	22.51	-1.3664	6.913041
10	1005.3	24.17	-1.2849	6.913041
11	1105.9	25.83	-1.2079	7.008415
11	1105.9	27.49	-1.1349	7.008415
11	1105.9	29.15	-1.0654	7.008415
11	1105.9	30.81	-0.99882	7.008415
12	1206.4	32.47	-0.93497	7.095396
12	1206.4	34.12	-0.87387	7.095396
12	1206.4	35.78	-0.81451	7.095396
14	1407.5	37.44	-0.75706	7.249571
14	1407.5	39.10	-0.70131	7.249571
15	1508	40.76	-0.64708	7.318540
15	1508	42.42	-0.59422	7.318540
15	1508	44.83	-0.51961	7.318540
15	1508	45.74	-0.49203	7.318540
19	1910.1	47.4	-0.44246	7.554911
20	2010.7	49.06	-0.39375	7.606238
20	2010.7	50.72	-0.3458	7.606238
20	2010.7	52.38	-0.29852	7.606238
20	2010.7	54.04	-0.20557	7.606238
24	2412.8	55.7	-0.49203	7.788543
30	3016	57.36	-0.15973	8.011687
30	3016	59.02	-0.11419	8.011687
30	3016	60.68	-0.68882	8.011687

$\eta(x_i, y_i) = 0.935602$ which is higher than the critical coefficient value (See figure 2.1).

Equation (2.6) enables the determination of the shape parameter for YWW samples:

$$\beta = \frac{(-4.6731+1.31044)^2+...+(-0.1142+1.31044)^2}{[(-4.6731+1.31044)\cdot(4.61-6.107127)]+...+[(-0.11421+1.31044)\cdot(7.606-6.107127)]}$$

$\beta = 1.4578$

Table C.3: Times to degradation for YWW Samples

$t_m(minutes)$	t_i (hours)	$F(i,n)$ (%)	x_i	y_i
1	100.5	0.93	-4.6731	4.610456
1	100.5	2.59	-3.6404	4.610456
1	100.5	4.25	-3.1366	4.610456
2	201.1	5.91	-2.7982	5.303554
2	201.1	7.57	-2.5419	5.303554
2	201.1	9.23	-2.3347	5.303554
2	201.1	10.89	-2.1602	5.303554
2	201.1	12.55	-2.0091	5.303554
3	301.6	14.21	-1.8756	5.709035
3	301.6	15.87	-1.7556	5.709035
3	301.6	17.53	-1.6464	5.709035
3	301.6	19.19	-1.5461	5.709035
3	301.6	20.85	-1.4532	5.709035
3	301.6	22.51	-1.3664	5.709035
4	402.1	24.17	-1.2849	5.996701
4	402.1	25.83	-1.2079	5.996701
4	402.1	27.49	-1.1349	5.996701
5	502.63	29.15	-1.0654	6.219854
5	502.63	30.81	-0.99882	6.219854
5	502.63	32.47	-0.93497	6.219854
5	502.63	34.12	-0.87387	6.219854
5	502.63	35.78	-0.81451	6.219854
6	603.16	37.44	-0.75706	6.402183
6	603.16	39.10	-0.70131	6.402183
7	703.68	40.76	-0.64708	6.556324
7	703.68	42.42	-0.59422	6.556324
8	804.21	44.83	-0.51961	6.689860
8	804.21	45.74	-0.49203	6.689860
8	804.21	47.4	-0.44246	6.689860
9	904.73	49.06	-0.39375	6.807637
10	1005.3	50.72	-0.3458	6.913041
10	1005.3	52.38	-0.29852	6.913041
13	1306.8	54.04	-0.2518	7.175337
15	1507.9	55.7	-0.20557	7.318473
17	1708.9	57.36	-0.15973	7.443605
20	2010.5	59.02	-0.11419	7.606139

The scale parameter is calculated using equation (2.7):

$$\theta = \exp\left[6.107127 - \frac{[(-4.6731+1.31044)\cdot(4.61-6.107127)]+...+[(-0.1142+1.31044)\cdot(8.14-6.107127)]}{(-4.6731+1.31044)^2+...+(-0.1142+1.31044)^2}\cdot(-1.31044)\right]$$

$\theta = 1103.3$ hours.

For YWH samples:

Applying equation (2.5) yields the correlation factor:

$$\eta\left(x_i, y_i\right) = \frac{(-4.6731+0.96645)\cdot(4.61-6.024655)+...+(0.3933+0.96645)\cdot(7.008-6.024655)}{\sqrt{\left[(-4.6731+1.29364)^2+...+(0.3933+0.96645)^2\right]\cdot\left[(4.61-6.024655)^2+...+(7.008-6.024655)^2\right]}}$$

$\eta\left(x_i, y_i\right) = 0.951579$ which is higher than the critical coefficient value (See figure 2.1).

Equation (2.6) enables the determination of the shape parameter for YWH samples:

$$\beta = \frac{(-4.6731+0.96645)^2+...+(0.3933+0.96645)^2}{[(-4.6731+0.96645)\cdot(4.61-6.024655)]+...+[(0.3933+0.96645)\cdot(7.008-6.024655)]}$$

$\beta = 1.7141$

The scale parameter is calculated using equation (2.7):

$$\theta = \exp\left[6.73 - \frac{[(-4.6731+0.96645)\cdot(4.61-6.024655)]+...+[(0.3933+0.96645)\cdot(7.008-6.024655)]}{(-4.6731+0.96645)^2+...+(0.3933+0.96645)^2}\cdot(-0.96645)\right]$$

$\theta = 726.68$ hours.

Applying equation (2.5) yields the correlation factor for RLW varistor components:

$$\eta\left(x_i, y_i\right) = \frac{(-4.6731+1.14801)\cdot(4.61-6.280336)+...+(0.11191+1.14801)\cdot(7.31847-6.280336)}{\sqrt{\left[(-4.6731+1.14801)^2+...+(0.11191+1.14801)^2\right]\cdot\left[(4.61-6.280336)^2+...+(7.31847-6.280336)^2\right]}}$$

$\eta\left(x_i, y_i\right) = 0.969156$ which is higher than the critical coefficient value (See figure 2.1).

Equation (2.6) enables the determination of the shape parameter for RLW samples:

$$\beta = \frac{(-4.6731+1.14801)^2+...+(0.11191+1.14801)^2}{[(-4.6731+1.14801)\cdot(4.61-6.280336)]+...+[(0.11191+1.14801)\cdot(7.31847-6.280336)]}$$

$\beta = 1.63$

The scale parameter is calculated using equation (2.7):

$$\theta = \exp\left[6.280336 - \frac{[(-4.6731+1.14801)\cdot(4.61-6.280336)]+...+[(0.11191+1.14801)\cdot(8.14-6.280336)]}{(-4.6731+1.14801)^2+...+(-0.1142+1.14801)^2}\cdot(-1.14801)\right]$$

$\theta = 1079.4$ hours.

For RLH samples:

Applying equation (2.5) yields the correlation factor:

$$\eta\left(x_i, y_i\right) = \frac{(-4.6731+0.83043)\cdot(4.61-6.166468)+...+(0.3933+0.83043)\cdot(7.09531-6.1664685)}{\sqrt{\left[(-4.6731+0.83043)^2+...+(0.3933+0.83043)^2\right]\cdot\left[(4.61-6.166468)^2+...+(7.09531-6.166468)^2\right]}}$$

$\eta\left(x_i, y_i\right) = 0.974395$ which is higher than the critical coefficient value (See figure 2.1).

Equation (2.6) enables the determination of the shape parameter for RLH samples:

$$\beta = \frac{(-4.6731+0.83043)^2+...+(0.7877+0.83043)^2}{[(-4.6731+0.83043)\cdot(4.61-6.166468)]+...+[(0.7877+0.83043)\cdot(7.09531-6.166468)]}$$

$\beta = 1.75$

The scale parameter is calculated using equation (2.7):

$$\theta = \exp\left[6.166468 - \frac{[(-4.6731+0.83043)\cdot(4.61-6.166468)]+...+[(0.7877+0.83043)\cdot(7.09531-6.166468)]}{(-4.6731+0.83043)^2+...+(0.7877+0.83043)^2}\cdot(-0.83043)\right]$$

$\theta = 765.22$ hours.

Table C.4: Times to degradation for YWH Samples

$t_m(minutes)$	t_i (hours)	$F(i,n)$ (%)	x_i	y_i
1	100.5	0.93	-4.6731	4.610456
1	100.5	2.59	-3.6404	4.610456
1	100.5	4.25	-3.1366	4.610456
1	100.5	5.91	-2.7982	4.610456
2	201.1	7.57	-2.5419	5.303554
2	201.1	9.23	-2.3347	5.303554
2	201.1	10.89	-2.1602	5.303554
2	201.1	12.55	-2.0091	5.303554
2	201.1	14.21	-1.8756	5.303554
3	301.6	15.87	-1.7556	5.709035
3	301.6	17.53	-1.6464	5.709035
3	301.6	19.19	-1.5461	5.709035
3	301.6	20.85	-1.4532	5.709035
3	301.6	22.51	-1.3664	5.709035
3	301.6	24.17	-1.2849	5.709035
3	301.6	25.83	-1.2079	5.709035
3	301.6	27.49	-1.1349	5.709035
3	301.6	29.15	-1.0654	5.709035
3	301.6	30.81	-0.99882	5.709035
3	301.6	32.47	-0.93497	5.709035
3	301.6	34.12	-0.87387	5.709035
4	402.1	35.78	-0.81451	5.996701
4	402.1	37.44	-0.75706	5.996701
4	402.1	39.10	-0.70131	5.996701
4	402.1	40.76	-0.64708	5.996701
5	502.63	42.42	-0.59422	6.219854
5	502.63	44.83	-0.51961	6.219854
5	502.63	45.74	-0.49203	6.219854
5	502.63	47.4	-0.44246	6.219854
5	502.63	49.06	-0.39375	6.219854
6	603.16	50.72	-0.3458	6.402183
6	603.16	52.38	-0.29852	6.402183
6	603.16	54.04	-0.2518	6.402183
7	703.68	55.7	-0.20557	6.556324
7	703.68	57.36	-0.15973	6.556324
7	703.68	59.02	-0.11419	6.556324
7	703.68	60.68	-0.068882	6.556324
8	804.21	62.34	-0.023707	6.689860
9	904.73	64	0.02142	6.807637
9	904.73	65.66	0.066592	6.807637
10	1005.3	67.32	0.11191	6.913041
10	1005.3	68.98	0.15746	6.913041
11	1105.8	70.64	0.20338	7.008324
11	1105.8	72.3	0.24978	7.008324
11	1105.8	73.96	0.2968	7.008324
11	1105.8	75.62	0.3446	7.008324
11	1105.8	77.28	0.3933	7.008324

Table C.5: Times to degradation for RLW Samples

$t_m(minutes)$	t_i (hours)	$F(i,n)$ (%)	x_i	y_i
1	100.5	0.93	-4.6731	4.610456
1	100.5	2.59	-3.6404	4.610456
1	100.5	4.25	-3.1366	4.610456
2	201.05	5.91	-2.7982	5.303554
3	301.6	7.57	-2.5419	5.709035
3	301.6	9.23	-2.3347	5.709035
3	301.6	10.89	-2.1602	5.709035
3	301.6	12.55	-2.0091	5.709035
3	301.6	14.21	-1.8756	5.709035
4	402.1	15.87	-1.7556	5.996701
4	402.1	17.53	-1.6464	5.996701
4	402.1	19.19	-1.5461	5.996701
4	402.1	20.85	-1.4532	5.996701
4	402.1	22.51	-1.3664	5.996701
5	301.6	24.17	-1.2849	6.219854
5	301.6	25.83	-1.2079	6.219854
5	301.6	27.49	-1.1349	6.219854
5	301.6	29.15	-1.0654	6.219854
5	301.6	30.81	-0.99882	6.219854
5	301.6	32.47	-0.93497	6.219854
5	301.6	34.12	-0.87387	6.219854
5	402.1	35.78	-0.81451	6.219854
7	703.68	37.44	-0.75706	6.556324
7	703.68	39.10	-0.70131	6.556324
7	703.68	40.76	-0.64708	6.556324
7	703.68	42.42	-0.59422	6.556324
7	703.68	44.83	-0.51961	6.556324
7	703.68	45.74	-0.49203	6.556324
7	703.68	47.4	-0.44246	6.556324
8	804.21	49.06	-0.39375	6.689860
9	904.73	50.72	-0.3458	6.807637
9	904.73	52.38	-0.29852	6.807637
10	1005.3	54.04	-0.2518	6.913041
11	1105.8	55.7	-0.20557	7.008324
11	1105.8	57.36	-0.15973	7.008324
11	1105.8	59.02	-0.11419	7.008324
12	703.68	60.68	-0.068882	7.095313
12	804.21	62.34	-0.023707	7.095313
13	1306.8	64	0.02142	7.175337
14	1407.4	65.66	0.066592	7.249499
15	1507.9	67.32	0.11191	7.318473

Table C.6: Times to degradation for RLH Samples

$t_m(minutes)$	t_i (hours)	$F(i,n)$ (%)	x_i	y_i
1	100.5	0.93	-4.6731	4.610456
1	100.5	2.59	-3.6404	4.610456
1	100.5	4.25	-3.1366	4.610456
1	100.5	5.91	-2.7982	4.610456
1	100.5	7.57	-2.5419	4.610456
2	201.05	9.23	-2.3347	5.303554
2	201.05	10.89	-2.1602	5.303554
2	201.05	12.55	-2.0091	5.303554
2	201.05	14.21	-1.8756	5.303554
2	201.05	15.87	-1.7556	5.303554
2	201.05	17.53	-1.6464	5.303554
3	301.58	19.19	-1.5461	5.709035
3	301.58	20.85	-1.4532	5.709035
3	301.58	22.51	-1.3664	5.709035
4	402.1	24.17	-1.2849	5.996701
4	402.1	25.83	-1.2079	5.996701
4	402.1	27.49	-1.1349	5.996701
4	402.1	29.15	-1.0654	5.996701
4	402.1	30.81	-0.99882	5.996701
4	402.1	32.47	-0.93497	5.996701
4	402.1	34.12	-0.87387	5.996701
5	502.63	35.78	-0.81451	6.219854
5	502.63	37.44	-0.75706	6.219854
5	502.63	39.10	-0.70131	6.219854
5	502.63	40.76	-0.64708	6.219854
5	502.63	42.42	-0.59422	6.219854
5	502.63	44.83	-0.51961	6.219854
5	502.63	45.74	-0.49203	6.219854
5	502.63	47.4	-0.44246	6.219854
6	603.16	49.06	-0.39375	6.402183
6	603.16	50.72	-0.3458	6.402183
6	603.16	52.38	-0.29852	6.402183
6	603.16	54.04	-0.2518	6.402183
6	603.16	55.7	-0.20557	6.402183
6	603.16	57.36	-0.15973	6.402183
7	703.68	59.02	-0.11419	6.556324
7	703.68	60.68	-0.068882	6.556324
7	703.68	62.34	-0.023707	6.556324
7	703.68	64	0.02142	6.556324
7	703.68	65.66	0.066592	6.556324
8	804.21	67.32	0.11191	6.689860
8	804.21	68.98	0.15746	6.689860

Table C.7: Times to degradation for RLH Samples(Continued)

$t_m(minutes)$	t_i (hours)	$F(i,n)$ (%)	x_i	y_i
9	904.73	70.64	0.20338	6.807637
9	904.73	72.3	0.24978	6.807637
9	904.73	73.96	0.2968	6.807637
9	904.73	75.62	0.3446	6.807637
10	1507.9	77.28	0.3933	6.913041
10	1507.9	78.94	0.4433	6.913041
10	1507.9	80.6	0.4946	6.913041
10	1507.9	82.26	0.5477	6.913041
10	1507.9	83.92	0.603	6.913041
11	1507.9	85.58	0.6609	7.008324
11	1507.9	87.24	0.7222	7.008324
11	1507.9	88.9	0.7877	7.008324
12	1507.9	90.56	0.8588	7.095313
12	1507.9	92.22	0.93751	7.095313

Appendix D

Chi-Square Distribution Table

Calculation of the test stastic of the hypothesis testing:

BE Samples:

$$z = -2\ln\frac{\prod_{i=200}^{4500}\left\{\frac{\beta_1}{\theta_1}\cdot\left(\frac{t-\gamma}{\theta_1}\right)^{\beta_1-1}\exp\left[-\left(\frac{t-\gamma}{\theta_1}\right)^{\beta_1}\right]\right\}}{\prod_{i=200}^{4500}\left\{\frac{\beta_2}{\theta_2}\cdot\left(\frac{t-\gamma}{\theta_2}\right)^{\beta_2-1}\exp\left[-\left(\frac{t-\gamma}{\theta_2}\right)^{\beta_2}\right]\right\}} \geq \chi^2_{0.01}$$

$$z = \frac{\left(2.46\times10^{-4}\times0.91\right)\times...\times\left(2.35\times10^{-4}\times0.36\right)}{(3.33\times10^{-4}\times0.85)\times...\times(4.16\times10^{-4}\times0.17)}$$

$z = 2.1460 < 6.635$ (See figure 92).

YW Samples:

$$z = -2\ln\frac{\prod_{i=200}^{1200}\left\{\frac{\beta_1}{\theta_1}\cdot\left(\frac{t-\gamma}{\theta_1}\right)^{\beta_1-1}\exp\left[-\left(\frac{t-\gamma}{\theta_1}\right)^{\beta_1}\right]\right\}}{\prod_{i=200}^{1200}\left\{\frac{\beta_2}{\theta_2}\cdot\left(\frac{t-\gamma}{\theta_2}\right)^{\beta_2-1}\exp\left[-\left(\frac{t-\gamma}{\theta_2}\right)^{\beta_2}\right]\right\}} \geq \chi^2_{0.01}$$

$$z = \frac{\left(4.37\times10^{-4}\times0.96\right)\times...\times\left(1.32\times10^{-3}\times0.63\right)}{(5.73\times10^{-4}\times0.91)\times...\times(3.16\times10^{-3}\times0.34)}$$

$z = 0.63976 < 6.635$ (See figure 92).

RL Samples:

$$z = -2\ln\frac{\prod_{i=200}^{1400}\left\{\frac{\beta_1}{\theta_1}\cdot\left(\frac{t-\gamma}{\theta_1}\right)^{\beta_1-1}\exp\left[-\left(\frac{t-\gamma}{\theta_1}\right)^{\beta_1}\right]\right\}}{\prod_{i=200}^{1400}\left\{\frac{\beta_2}{\theta_2}\cdot\left(\frac{t-\gamma}{\theta_2}\right)^{\beta_2-1}\exp\left[-\left(\frac{t-\gamma}{\theta_2}\right)^{\beta_2}\right]\right\}} \geq \chi^2_{0.01}$$

$$z = \frac{\left(4.37\times10^{-4}\times0.86\right)\times...\times\left(1.43\times10^{-3}\times0.14\right)}{(5.73\times10^{-4}\times0.79)\times...\times(3.56\times10^{-3}\times0.05)}$$

$z =$ - 1.2855 < 6.635 (See figure 92).

Chi-Square Distribution Table

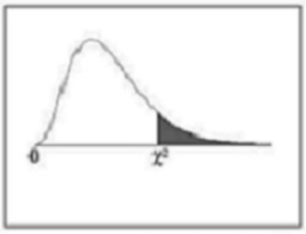

The shaded area is equal to α for $\chi^2 = \chi^2_\alpha$.

df	$\chi^2_{.995}$	$\chi^2_{.990}$	$\chi^2_{.975}$	$\chi^2_{.950}$	$\chi^2_{.900}$	$\chi^2_{.100}$	$\chi^2_{.050}$	$\chi^2_{.025}$	$\chi^2_{.010}$	$\chi^2_{.005}$
1	0.000	0.000	0.001	0.004	0.016	2.706	3.841	5.024	6.635	7.879
2	0.010	0.020	0.051	0.103	0.211	4.605	5.991	7.378	9.210	10.597
3	0.072	0.115	0.216	0.352	0.584	6.251	7.815	9.348	11.345	12.838
4	0.207	0.297	0.484	0.711	1.064	7.779	9.488	11.143	13.277	14.860
5	0.412	0.554	0.831	1.145	1.610	9.236	11.070	12.833	15.086	16.750
6	0.676	0.872	1.237	1.635	2.204	10.645	12.592	14.449	16.812	18.548
7	0.989	1.239	1.690	2.167	2.833	12.017	14.067	16.013	18.475	20.278
8	1.344	1.646	2.180	2.733	3.490	13.362	15.507	17.535	20.090	21.955
9	1.735	2.088	2.700	3.325	4.168	14.684	16.919	19.023	21.666	23.589
10	2.156	2.558	3.247	3.940	4.865	15.987	18.307	20.483	23.209	25.188
11	2.603	3.053	3.816	4.575	5.578	17.275	19.675	21.920	24.725	26.757
12	3.074	3.571	4.404	5.226	6.304	18.549	21.026	23.337	26.217	28.300
13	3.565	4.107	5.009	5.892	7.042	19.812	22.362	24.736	27.688	29.819
14	4.075	4.660	5.629	6.571	7.790	21.064	23.685	26.119	29.141	31.319
15	4.601	5.229	6.262	7.261	8.547	22.307	24.996	27.488	30.578	32.801
16	5.142	5.812	6.908	7.962	9.312	23.542	26.296	28.845	32.000	34.267
17	5.697	6.408	7.564	8.672	10.085	24.769	27.587	30.191	33.409	35.718
18	6.265	7.015	8.231	9.390	10.865	25.989	28.869	31.526	34.805	37.156
19	6.844	7.633	8.907	10.117	11.651	27.204	30.144	32.852	36.191	38.582
20	7.434	8.260	9.591	10.851	12.443	28.412	31.410	34.170	37.566	39.997
21	8.034	8.897	10.283	11.591	13.240	29.615	32.671	35.479	38.932	41.401
22	8.643	9.542	10.982	12.338	14.041	30.813	33.924	36.781	40.289	42.796
23	9.260	10.196	11.689	13.091	14.848	32.007	35.172	38.076	41.638	44.181
24	9.886	10.856	12.401	13.848	15.659	33.196	36.415	39.364	42.980	45.559
25	10.520	11.524	13.120	14.611	16.473	34.382	37.652	40.646	44.314	46.928
26	11.160	12.198	13.844	15.379	17.292	35.563	38.885	41.923	45.642	48.290
27	11.808	12.879	14.573	16.151	18.114	36.741	40.113	43.195	46.963	49.645
28	12.461	13.565	15.308	16.928	18.939	37.916	41.337	44.461	48.278	50.993
29	13.121	14.256	16.047	17.708	19.768	39.087	42.557	45.722	49.588	52.336
30	13.787	14.953	16.791	18.493	20.599	40.256	43.773	46.979	50.892	53.672
40	20.707	22.164	24.433	26.509	29.051	51.805	55.758	59.342	63.691	66.766
50	27.991	29.707	32.357	34.764	37.689	63.167	67.505	71.420	76.154	79.490
60	35.534	37.485	40.482	43.188	46.459	74.397	79.082	83.298	88.379	91.952
70	43.275	45.442	48.758	51.739	55.329	85.527	90.531	95.023	100.425	104.215
80	51.172	53.540	57.153	60.391	64.278	96.578	101.879	106.629	112.329	116.321
90	59.196	61.754	65.647	69.126	73.291	107.565	113.145	118.136	124.116	128.299
100	67.328	70.065	74.222	77.929	82.358	118.498	124.342	129.561	135.807	140.169

FIGURE D.1: Chi-Square Table [73]

Bibliography

[1] G. D' Antona, C. Muscas, and S. Sulis. Harmonic source estimation: a new approach for the localisation of non- linear loads. *Proceedings of the 13th International Conference on Harmonics and Quality of Power, Wollongong, Australia*, October 2008.

[2] D. Serfontein and A. Rens. The validation of single point measurements for the localisation of multiple harmonic sources. *Proceedings of the 14th International Conference on Harmonics and Quality of Power, Bergamo, Italy*, September 2010.

[3] M. Balci and M. Hocaoglu. On the validity of harmonic source detection methods and indices. *Proceedings of the 14th International Conference on Harmonics and Quality of Power, Bergamo, Italy*, September 2010.

[4] R. Herrera, P. Salmeron, and S. Litran. Assessment of harmonic distortion sources in power networks with capacitor banks. *Proceedings of the 11th International Conference on Renewable Energies and Power Quality, Las Palmas de Gran Canary, Spain*, April 2011.

[5] C.Nahm. Pulse aging behaviour of zno-pr6o11-coo-cr2o3-dy2o3 varistor ceramics with sintering time. *Ceramics international*, 37(6):1409–1414, May 2011.

[6] W. Sun, Y. Li, D. Zeng, R. Cai, and Z. Meng G. Yang. Investigation of voltage-current characteristics of zno varistors under 8/20 microsecond impulse current. *The IEEE Power Engineering and Automation Conference, Wuhan, China*, September 2011.

[7] Z. Nanfa, K. Guoyao, and G. Yaping. Long duration impulse withstand capability of spd. *The Asia-Pacific International Symposium on Electromagnetic Compatibility, Beijing, China*, April 2010.

[8] J. Rossman, J. Nelson, and M. Droke. Reliability and failure of porcelain high-voltage surge arresters. *International Conference on High Voltage Engineering and Application, New Orleans, USA*, October 2010.

[9] K. Eda, A. Iga, and M. Matsuoka. Degradation mechanism of non-ohmic zinc oxide ceramics. *Journal of Applied Physics*, 1(5):2678–2684, January 1980.

[10] C.de Salles, M. L. Martinez, and A.A. de Queiroz. Ageing of metal oxide varitors due to surges. *Proceedings of the International Symposium on Lightning Protection (XI SIPDA), Fortaleza, Brazil*, October 2011.

[11] R.A. Sargent, G. L. Dunlop, and M. Darveniza. Effects of multiple impulse currents on the microstructure and electrical properties of metal oxide varistors. *IEEE Transactions on Electrical Insulation*, 6(3):586–592, June 1992.

[12] P.Osmokrovic, B. Loncar, S. Stankovic, and S.Vasic. Aging of the over-voltage protection elements caused by over-voltages. *Microelectronics Reliability*, 12(12): 1959–1966, December 2002.

[13] M.Wang, K.Hu, B.Y. Zhao, and N.F. Zhang. Degradation phenomena due to humidity in low voltage zno varistors. *Ceramics International*, 11(2):151–154, November 2007.

[14] V. Larsen and K. Lien. In-service testing and diagnosis of gapless metal oxide surge arresters. *Proceedings of the 9th International Symposium on Lightning Protection, Foz do iguacu, Brazil*, November 2007.

[15] A.Vasic, M. Vujisic, K. Stankovic, and P.Osmokrovic. Aging of overvoltage protection elements caused by past activations. *Journal of Microelectronics, Electronic Components and Materials*, 42(3):197–204, October 2012.

[16] Epcos Data Book. Siov metal oxide varistors. pages 51–52, 2008. URL http://www.epcos.com.

[17] T. Saha and K. Madira. Modeling metal oxide surge arrester for the modern polarization based diagnostics. *IEEE Transactions on Dielectrics and Electrical Insulation*, 12(6):1249–1258, December 2005.

[18] C. Nahm. Aging characteristics of zno–pro1.83-based semiconducting varistors for surge protection reliability. *Microelectronics Reliability*, 54(11):2417–2422, November 2014.

[19] N. Tsukamoto. Study of degradation by impulse having 4/10lls and 8/20lls waveform for movs (metal oxide varistors). *2014 International Conference on Lightning Protection (ICLP), Shanghai, China*, October 2014.

[20] D.Zhou, C.Zhang, and S.Gong. Degradation phenomena due to dc bias in low-voltage zno varistors. *Materials Science and Engineering: B*, 1-3(99):412–415, May 2003.

[21] T.Gupta. Application of zinc oxide varistors. *Journal of American Ceramics Society*, 73(7):1817–1840, September 1990.

[22] M.Trontelj, D. Kolar, and V. Krasevec. Influence of additives on varistor microstructure, in advances in ceramics. *Journal of American Ceramic Society*, 7(7):107–116, September 1983.

[23] T.Gupta, W.Carlson, M. Yan, and A. Houer. Influence of additives on varistor microstructure, in advances in ceramics. *Journal of American Ceramic Society*, 7 (7):30–40, September 1983.

[24] C. Nahm. Microstructure, electrical properties, and aging behavior of zno–pr6o11–coo–cr2o3–y2o3–er2o3 varistor ceramics. *Ceramics International*, 37 (8):3049–3054, December 2011.

[25] H. Cui, Q.Wang, and Y. Tu. Thermally stimulated current characteristics of aged zno varistors under different applied voltage ratios. *Proceedings of the Asia-Pacific Power and Energy Engineering Conference (APPEEC),Wuhan,China*, March 2011.

[26] M.Wang, Q.Tang, and C.Yao. Electrical properties and ac degradation characteristics of low voltage zno varistors doped with nd2o3. *Ceramics International*, 36(3): 1095–1099, January 2010.

[27] J. He, J. Liu, J. Hu, and W. Long. Ac ageing characteristics of y2o3-doped zno varistors with high voltage gradient. *Materials Letters*, 65(17-18):2595–2597, September 2011.

[28] M. Khederzadeh. Impact of mov operation on power quality in transmission lines compensated by tcsc. *Transmission and distribution conference and exposition, Chicago, USA*, April 2008.

[29] J. Woodworth. Field testing of arresters. *ArresterFacts-002*, 2011. URL http://www.arresterworks.com.

[30] V. Hinrichsen. Monitoring of high voltage metal oxide surge arresters. *6th International Conference on Electrical Insulation, Bilbao, Spain*, October 1997.

[31] X. Yan, Y. Wen, and X. Yi. Study on the resistive leakage current characteristic of mov surge arresters. *Proceedings of the Asia-Pacific IEEE/PES Transmission and Distribution Conference and Exhibition,Yokohama, Japan*, October 2002.

[32] M.Jaroszewski, P. Kostyla, and K. Wieczorek. Effect of voltage harmonics content on arrester diagnostic result. *Proceedings of the International Conference on Solid Dielectrics (ICSD 2004), Toulouse, France*, July 2004.

[33] C. Karawita and M.Raghuveer. Leakage current based assessment of degradation of mosa using an alternative technique. *Annual Report of the Conference on Electrical Insulation and Dielectric Phenomena (CEIDP'05)*, pages 199–201, October 2005.

[34] Z.Abdul-Malek, N.Yusof, and M. Yousof. Field experience on surge arrester condition monitoring – modified shifted current method. *Proceedings of the 45th Universities Power Engineering Conference (UPEC 2010), Cardiff, United Kingdom*, September 2010.

[35] M. Khodsuz, M. Mirzaie, and S. Seyyedbarzegar. Metal oxide surge arrester condition monitoring based on analysis of leakage current components. *International Journal of Electrical Power and Energy Systems*, 12(6):188–193, November 2014.

[36] E. Shulzhenko, M. Rock, M. Birle, and C. Leu. Applying of surge arresters in power electronic network components. *Proceedings of the International Conference on Lightning Protection, Shanghai, China*, October 2014.

[37] IEEE Standards C62.48 TM-2005. Guide on interactions between power system disturbances and surge-protective devices. *IEEE power engineering society*, November 2005.

[38] C. Macanda and M. Cantagrel. ac power quality and surge protectors. *7th Asia-Pacific International Conference on Lightning, Chengdu, China*, November 2011.

[39] J. Woodworth. Arrester condition monitors: A state of the art review. *ArresterFacts-036*, 2012. URL http://www.arresterworks.com.

[40] P. Cygan and J.R. Laghari. A review of electrical and thermal multistress ageing models. *IEEE International Symposium on Electrical Insulation, Toronto, Canada*, June 1990.

[41] IEEE Standards 930 TM 2007. Guide for the statistical analysis of electrical insulation breakdown data. *IEEE Dielectrics and Electrical Insulation Society*, September 2007.

[42] R. Ross. Graphical methods for plotting and evaluating weibull distributed data. *IEEE International conference on properties and applications of dielectric materials, Brisbane, Australia*, July 1994.

[43] J. White. The moments of log-weibull order statistics. *Technometrics*, 11(2):373–386, February 1969.

[44] H. Yahyaoui, P. Notingher, S. Agnel, and Y. Kieffel. Proprietes dielectriques d'une resine epoxy chargee d'alumine sous l'effet du champ electrique continu et de la

temperature. *Journees JCGE'2014 - SEEDS, Jun 2014, Saint- Louis, France*, June 2014. URL http://www.hal.archives-ouvertes.fr/hal-01083915.

[45] M. R. Meshkatoddini. Statistical study of the thin metal-oxide varistor ceramics. *Australian Journal of Basic and Applied Sciences*, 5(4):751–763, January 2010.

[46] G. L. Amicucci, B. D'Elia, and P. Gentile. Mean time to failure of metal oxide varistors under lightning stress. *Proceedings of the IEEE Power Tech Conference, Bologna, Italy*, June 2003.

[47] K. Brown. Metal oxide varistor degradation. *International Association of Electrical Inspectors (IAEI) News Magazine*, April 2004.

[48] J. He, R. Zeng, Y. Tu, S. Han, and H. Cho. Aging characteristics and mechanisms of zno nonlinear varistors. *Proceedings of The 6th International Conference on Properties and Applications of Dielectric Materials, Xi'an, China*, June 2000.

[49] Z. Zheng, H. Cui, Q. Wang, S. Hen, and Y. Tu. Space charge characteristics of zno varistors after pulse degradation. *Proceedings of the Asia-Pacific Power and Energy Conference (APPEEC), Shanghai, China*, March 2012.

[50] J. He, J. Liu, J. Hu, R. Zeng, and W. Long. Non-uniform ageing behavior of individual grain boundaries in zno varistor ceramics. *Journal of the European Ceramic Society*, 31(2):1451–1456, February 2011.

[51] IEEE Standards C62.62 TM-2010. Test specifications for surge-protective devices (spds) for use on the load side of the service equipment in low-voltage (1000 v and less) ac power circuits. *IEEE power and energy society*, December 2010.

[52] J. Woodworth. Arrester reference voltage. *ArresterFacts-027*, 2011. URL http://www.arresterworks.com.

[53] IEEE Standards C62.34 1996. Performance of low-voltage surge-protective devices (secondary arresters). *IEEE Surge Protective Devices Committee of the Power Engineering Society*, December 1996.

[54] IEEE Standards C62.11 TM 2012. Standard for metal-oxide surge arresters for ac power circuits higher than 1 kv. *IEEE power and energy society*, December 2012.

[55] R. Hernandez, I. Ramrez, R. Saldivar, and G. Montoya. Analysis of accelerated ageing of non-ceramic insulation equipments. *IET Generation, Transmission and Distribution*, 6(1):59–68, January 2012.

[56] Nabertherm GmbH. High temperature laboratory furnace. *Operating Manual*, 2011. URL http://www.nabertherm.com.

[57] Lapp Cables Group. Operating instructions. *High Temperature Cables*, 2013. URL http://www.lappkabel.co.za.

[58] IEEE Power Standards Coordinating Committee. Guide for applying harmonic limits on power systems. *IEEE Standards P519.1^{TM}/D12*, November 2012.

[59] T. Halim, K. Muthusamy, S.W. Lam, and S.Y. Chia. Review and classification of reliability statistical models exhibiting failure-free life characteristic. *40th International Conference on Computers and Industrial Engineering, 2010*, July 2010.

[60] P.D. O'Connor and A. Kleyner. Practical reliability engineering, john wiley & sons. pages 87–92, 2011.

[61] A. J. Dobson, J. Annette, and A. Barnett. An introduction to generalized linear models, crc press. pages 81–82, 2008.

[62] M. Kayid, I. A. Ahmad, S. Izadkhah, and A. M. Abouammoh. Further results involving the mean time to failure order, and the decreasing mean time to failure class. *IEEE Transactions on Reliability*, 62(3):670–678, September 2013.

[63] Y. Liu, W. Tang, and R. Zhao. Reliability and mean time to failure of unrepairable systems with fuzzy random lifetimes. *IEEE Transactions on Fuzzy Systems*, 15(5): 1009–1026, October 2007.

[64] G. G Brown and H. C. Rutemiller. Evaluation of prob of x higher than y when both x and y are three-parameter weibull distributions. *IEEE Transactions on Reliability*, R.22(2):78–82, June 1973.

[65] Z. Nanfa, X. Jianhu, S. Zhen, and D. Liuhua. A deep insight into zno nonlinear resistor. *IEEE Transactions on Power Electronics*, October 2014.

[66] D. Wei, L. Weidong, F. Zhiyang, and C. Jian. The network-model on-line monitoring system of zno surge arresters in 500kv substation. *IEEE IEEE/PES Transmission and Distribution Conference and Exhibition: Asia and Pacific, Dalian, China*, April 2005.

[67] J.D. Glover, M.S. Sarma, and T.J. Overbye. Power systems analysis and design, 4th ed. cengage learning, united states of america. pages 232–233, 2005.

[68] Z. Bing, K.J. Karimi, and J. Sun. Input impedance modeling and analysis of line-commutated rectifiers. *IEEE Transactions on Power Electronics*, 24(10):2338–2346, October 2009.

[69] K.A. Stroud and D.J. Booth. Advanced engineering mathematics, palgrave macmillan. pages 232–233, 2011.

[70] J. Bird. Electrical circuit theory and technology 5th ed. routledge, united kingdom. pages 193–195, 2014.

[71] F. Iliasa, D. Cristian, L. Popa, and D. Vatau. A few aspects concerning the thermal connection of zno based varistors. *IEEE Universities Power Engineering Conference, Cardiff, Wales, United Kingdom*, 31 August - 03 September 2010.

[72] S. Li, J. Li, W. Liu, J. Lin, J. He, and P. Cheng. Advances in zno varistors in china during the past 30 years - fundamentals, processing, and applications. *IEEE Electrical Insulation Magazine*, 31(4):35–44, August 2015.

[73] Chi-square distribution table. *Chi-Square Table*, Last access 2015. URL http://www.statistics.com/chi-square.